Scanning Microscopy

Volume 6 | Number 1 Article 2

1-25-1992

Cathodoluminescence Applied to the Microcharacterization of Mineral Materials: A Present Status in Experimentation and Interpretation

G. Remond
Bureau de Recherches Geologiques et Minieres

F. Cesbron
Universite d'Orleans

R. Chapoulie
Universite Michel de Montaigne

D. Ohnenstetter
CNRS

C. Roques-Carmes
Ecole Nationale Superieure de Mecanique et des Microtechniques

Cathodoluminescence Applied to the Microcharacterization of Mineral Materials: A Present Status in Experimentation and Interpretation

Authors

G. Remond, F. Cesbron, R. Chapoulie, D. Ohnenstetter, C. Roques-Carmes, and M. Schvoerer

Scanning Microscopy, Vol. 6, No. 1, 1992 (Pages 23-68) 0891-7035/92$5.00+.00
Scanning Microscopy International, Chicago (AMF O'Hare), IL 60666 USA

CATHODOLUMINESCENCE APPLIED TO THE MICROCHARACTERIZATION OF MINERAL MATERIALS: A PRESENT STATUS IN EXPERIMENTATION AND INTERPRETATION

G. REMOND* (1), F. CESBRON (2), R. CHAPOULIE (3), D. OHNENSTETTER (4), C. ROQUES-CARMES (5), M. SCHVOERER (3).

(l) Bureau de Recherches Geologiques et Minieres, Departement Geologie, ORLEANS, FRANCE
(2) Universite d'Orleans, Laboratoire des Ressources et Materiaux Mineraux and LPCE-CNRS, ORLEANS, FRANCE
(3) Universite Michel de Montaigne - Bordeaux 3, Centre de Recherche Interdisciplinaire d'Archeologie Analytique, CNRS, TALENCE, FRANCE
(4) CNRS, Chimie et Synthese des Mineraux, ORLEANS, FRANCE
(5) Ecole Nationale Superieure de Mecanique et des Microtechniques, Laboratoire de Microanalyse des Surfaces, BESANCON, FRANCE

(Received for publication July 12, 1991, and in revised form January 25, 1992)

Abstract

Experimentation and interpretation of cathodoluminescence (CL) microscopy and spectroscopy applied to the microcharacterization of material minerals are reviewed. The origins of the intrinsic (host lattice) and extrinsic (impurities) luminescence emissions in crystals are briefly discussed. Merits and limitations of the available techniques are illustrated. CL emission changes as a function of the incident electron dose are illustrated for the case of natural quartz and sphalerite (ZnS) crystals. These effects are discussed in terms of the development of bulk charging, production of heat, diffusion of impurities, and creation of lattice defects induced by the incident ionizing particles. Although CL emission is mostly extrinsic in origin there is no general rule for identifying the nature of impurities from the CL emission spectra of minerals. However there is potential for using CL spectroscopy for trace element analysis as presented for the case of minerals containing rare-earth luminescent ions. The CL emission is a signature of the crystal-chemistry properties of minerals and hence contains potential genetic information. Some of the applications of CL emissions in the geosciences are summarized.

Key words: Cathodoluminescence, intrinsic luminescence, extrinsic luminescence, defects, impurities, beam damage, charging in insulators.

* Address for correspondence:
G. REMOND
BRGM - Département Géologie
BP 6009 - 45060 ORLEANS CEDEX 2 - FRANCE

Phone: (33) 38 64 36 00

Introduction

Many common minerals display cathodoluminescence (CL), i.e, visible light emission induced by electron bombardment, and species exhibiting this property have been regularly reported in the literature. Coy-Yll (16), Nickel (90), Amieux (2), and Hagni (33) among others, have given compilations of minerals susceptible to show CL emission.

Most mineral families have members showing fairly intense CL emission. These crystals may be native elements (diamond), sulfides (mainly sphalerite, ZnS), oxides (periclase MgO, corundum Al_20_3, cassiterite SnO_2...), halides (halite NaCl, fluorite CaF_2), sulfates, vanadates, molybdates, phosphates, carbonates and silicates. The last three classes have been the most extensively studied as they form the major constituents of sedimentary and igneous rocks.

Since the beginning of the applications of the Electron Probe Micro-Analyzer (EPMA) in mineralogy, the CL properties of natural or artificial crystals were used for electron column alignement. The EPMA was thus naturally used for CL analysis in minerals.

CL detection and analysis can be performed using, either a fixed electron beam irradiation of the specimen surface or a dynamic irradiation by means of the scanning function of the EPMA and Scanning Electron Microscope (SEM). Very well documented descriptions of instrumentation for CL microscopy and spectroscopy have been given by Muir and Grant (86), Pfefferkorn et al. (95), Holt and Datta (41) and Holt and Saba (42) for SEM-CL applications. The potential of CL microscopy and spectroscopy in material sciences led to the development of sophisticated commercial equipment as discussed by Wright (140) for CL analysis with the SEM and by Marshall (76) for the case of CL attachments to optical microscopes. A bibliography on technical

aspects and applications of CL in the field of semiconductors, biology and geology has been published by Bröcker and Pfefferkorn (6) (7) and recent books by Yacobi and Holt (144) and Marshall (76) illustrate the present state of CL in synthetic and natural crystals. Barker (4) listed 424 references dealing with applications to geosciences.

This paper is an interdisciplinary review on the potential of CL microscopy and spectroscopy for the detection and the localization of defects in mineral materials. Our purpose is to emphasize the need for a rigorous experimental procedure to obtain a reliable relationship between the CL emission of a mineral, its dielectric properties and subsequently its genetic conditions. From examples taken from mineralogy, geology and solid state physics we will try to present the most important problems being still to be investigated in the fields of generation and emission mechanisms and detection of CL emission of mineral materials.

After a brief summary of the available technologies for CL microscopy and spectroscopy, the reliability of CL data will be discussed in terms of the mechanisms of dissipation of the incident energy within the solid and the intrinsic dielectric properties of the materials. The relationship between the CL properties of minerals and the presence of point defects will be discussed emphasizing the role of impurities. Possibilities of CL analysis to complement X-ray spectrometry with the EPMA and SEM for the identification and the localization of impurities within minerals will be discussed.

Owing to their electronic configuration, rare-earth elements are particular luminogen ions characterized by narrow emission lines in their CL spectrum. By analogy with X-ray spectrometry, the development of an analytical procedure allowing a reliable identification of elements being present at trace levels will be illustrated for the particular case of zircons $Zr(SiO_4)$ which are known to contain rare-earth elements and actinides as impurities.

CL emission studies provide a signature for recognizing minerals having the same crystal-chemistry properties, i.e., the same dielectric properties as discussed by Czernuska and Page (18) for zirconia ceramics, by Schvoerer et al. (113) for ancient ceramics and synthetic alumina and by Stoecklein (129) for mineral charges in paint.

Since the 60's, Long and Agrell (64), Sippel and Glover (123), Smith and Stenstrom (124) showed that CL can be used for rapid identification of rock-forming minerals and that structural and composition variations revealed by CL emission also contained potential genetic information. As CL in a mineral may depend on slight differences in composition, it can be used to detect changes in environmental conditions (nature, concentration and oxidation state of trace elements, temperature and salinity of solutions etc...), to describe the chronology of sucessive stages of crystallization, to trace ore deposits, to help in the identification of rare minerals, to make the distinction between natural and synthetic minerals, etc. Some examples of such applications will be presented.

Cathodoluminescence of crystals

Basis and definitions

The basic process of luminescence involves the excitation of an electron from the ground state f, to an excited state e, followed by a de-excitation process to the ground state accompanied by the emission of a photon.

During the de-excitation process, a fluorescence emission takes place if the electron returns directly to the ground state. The de-excitation process involving a metastable level m, leads to a phosphorescence mechanism. According to this mechanism the excited electron is trapped on the metastable level e —> m which does not allow further transition m —> f. The system will not change from the state m unless it receives an additional amount of energy sufficient to reach again an excited level e, with the possibility of return to the ground state f with the emission of a photon.

We will consider only the luminescence in crystals. The luminescence emission may be an intrinsic (i.e. being characteristic of the host lattice) or an extrinsic property of the crystal (i.e. to result from the presence of impurities). Detailed descriptions of the mechanisms of intrinsic and extrinsic luminescence emission are given (among others) in the book "Luminescence in crystals" by D. Curie (17) for the case of photoluminescence (PhL), electro-luminescence (EL) and CL. In addition, a review of luminescence mechanisms has been given by Leverenz (62). For the case of minerals, the two groups of theories, i.e., spectroscopic and semiconductor have been reviewed by Marfunin (68).

Intrinsic luminescence: At and near room temperature the intrinsic luminescence emission results from direct band to band recombination of electron and holes according to the decay routes marked (1) and (2) in Fig. 1. The intrinsic luminescence consists of an emission band with its maximum occurring at energy $h\nu = Eg$ where Eg is the absorption edge of the material. The intrinsic emission is produced by the inverse mechanism responsible for the absorption edge of the material and is often called the edge emission band. This is often called self-activated luminescence. The term near-band-gap radiation is also used to designate the intrinsic luminescence band, because excitons and shallow recombination centers may contribute to this

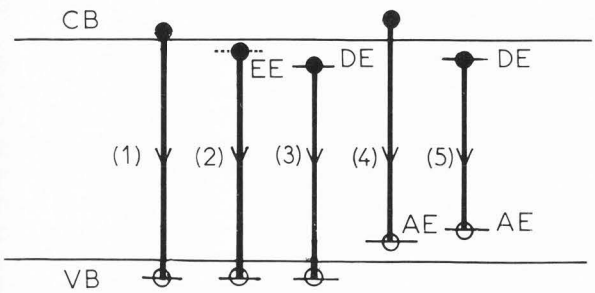

Fig. 1: Schematic diagram of radiative transitions between the conduction band (CB), the valence band (VB), exciton (EE), donor (DE) and acceptor (AE) levels in a semiconductor.

(1) interband transition, (2) exciton decay, (3) Lambe-Klick model, (4) Schon-Klassens model and (5) Prener-Williams model.

emission. Excitons are mobile uncharged quanta of crystal excitation. Both free excitons and excitons bound to an impurity may follow transitions according to the decay routes (I) and (2) in Fig. 1. Traditionally, the band scheme used for luminescence in semiconductors is transposed to the case of materials having a large band gap. The use of such a scheme is thus arbitrary because experimental data on the intrinsic emission of large band gap crystals are difficult to obtain with the available technologies. In silicates the band gap is about 10 eV and direct band to band recombination of charges would lead to emissions whose energies are not detectable with the equipment usually used for CL studies applied to the geosciences. Luminescence of intrinsic origin is used to designate emission involving lattice defects as charge recombination centers. Because of the large band gap of the insulating silicate minerals, the intrinsic luminescence can only take place in the presence of major lattice perturbation. Crystal lattice parameter changes, creation of vacancies may result from impurities and/or from transient or permanent lattice defects induced by ionizing radiations as summarized by Duraud et al. (22).

Extrinsic luminescence: In minerals the luminescence property is mostly the result of the presence of luminescence-activating ions such as transition metals, rare-earth elements or actinide ions. The energy level diagrams of ions **in a crystal field** form the basis for representing both optical absorption and luminescence spectra as schematically illustrated in Fig. 2 for the case of Cr^{3+} ions in Al_2O_3 crystals. Under excitation by the incident energy the ions with incompletely filled shells pass from the ground to the excited state leading to an absorption band in the optical spectrum. The luminescence emission results from a de-excitation process of the excited state.

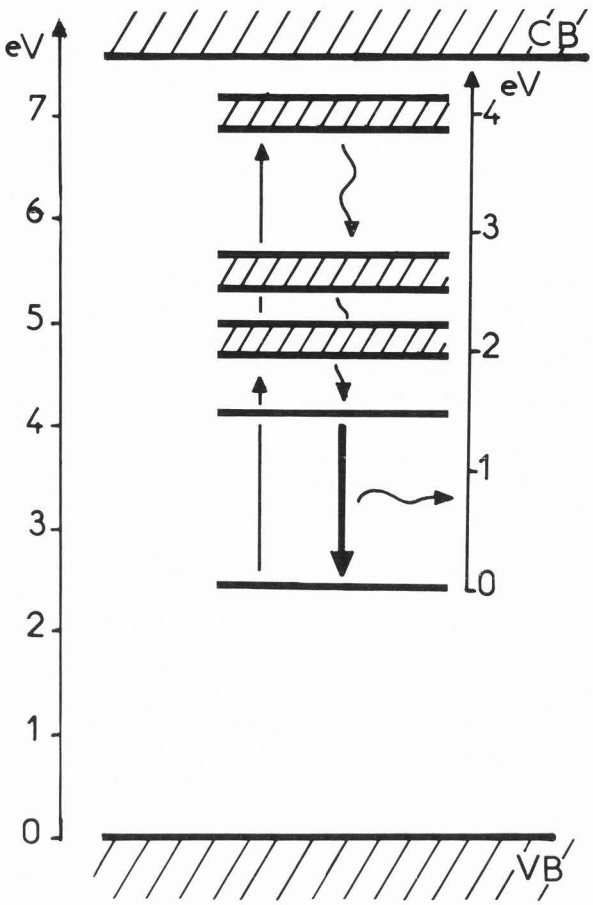

Fig. 2: Ion activator energy levels in a band scheme for the characteristic luminescence emission of Cr^{3+} ions in an Al_2O_3 host crystal. Excitation and emission occur as a result of transitions between the ion activator levels without participation of conduction and valence bands (from ref.(68)).

For the case of an Al_2O_3 crystal containing Cr^{3+} ion impurity (Fig. 2) the excitation and the luminescence emission are the result of transitions between the luminescent ion levels without participation of valence and conduction bands. Such a scheme is appropriate to describe the luminescence property of many minerals in which the same levels and bands describe optical absorption and luminescence spectra of ions and crystals. However the scheme in Fig. 2 cannot describe the possible simultaneous properties of luminescence and photoconductivity which can be observed in many semiconductor materials such as those of the ZnS type.

Concepts based on the band theory of semiconductors are necessary for interpreting luminescence involving the internal ionization of ionic

impurities i.e. the transfer of electrons from the valence band to the conduction band (and/or through ionization of the activator) and transfer to the other ions or defects in the crystal.

As an example, while the luminescence of ZnS crystals associated with Mn^{2+} is described according to a spectroscopic scheme similar to that in Fig. 2, the luminescence of the same host ZnS crystals containing Cr^{2+} ions is explained on the basis of an electron-hole recombination scheme. The excitation raises a valence electron into the conduction band. The electron is trapped from the conduction band by the Cr^{2+} ion leading to the formation of a Cr^{+} center and the luminescence occurs from the Cr^{+} to valence band recombination mechanism.

The electron-hole recombination via defect levels involve several mechanisms as discussed among others by Shionoya (116) and Curie (17) for the case of luminescence of lattices of the ZnS type. The major processes for electron-hole recombination for semiconductors are summarized in Fig. 1.

Extrinsic luminescence arises from electron transitions on shallow or deep localized energy states located within the forbidden band gap in the energy diagram of crystals. Extrinsic luminescence may result from radiative electron-hole recombination according to the decay routes (3), (4) and (5) in Figure 1. These levels are associated with donor-acceptor centers. The shallow levels exhibiting a large capture probability for conduction electrons are electron traps (normally unoccupied) or donor levels (normally occupied). Similarly, deep levels act as hole traps or acceptor. The energy levels associated with point defects result from the presence of impurities and crystal lattice defects in the crystal. These imperfections, responsible for the extrinsic luminescence, are called activators. In some instances, two activators must be simultaneously present to provoke the luminescence emission. The secondary activator is called a coactivator when its presence is necessary to create a luminescence center with the activator, i.e., to create an acceptor-donor pair for electrical charge recombination. The secondary activator is a sensitizer when its presence is necessary to transfer the excitation energy to the activator (sensitized luminescence) by resonance or migrating exciton mechanisms. Recombination centers are luminescent centers when they lead to radiative transitions or killer centers when they lead to non-radiative transitions. Crystals exhibiting luminescence involving electron movement through the conduction band are known as photoconductor materials, while luminescence in non-photoconductor material results from the de-excitation of excited levels of luminogen ions without any necessity to raise electrons into the conduction band. The unoccupied shallow levels with a large capture probability for conduction electrons constitute electron traps responsible for the phosphorescence mechanism.

There are competitive probabilities between radiative and non-radiative transitions occurring on the recombination centers in a similar way for transitions occurring on core levels during electron bombardment. Radiative transitions resulting from electron-hole recombination on core levels lead to the emission of X-ray photons, the non-radiative transition leading to the Auger electron emission mechanism. Similarly, for transitions involving energy levels located within the forbidden band gap the radiative mechanisms are accompanied by luminescence emission while the non-radiative process of the luminescence mechanism leads to the ejection of an exoelectron according to an Auger process.

Fig. 3 illustrates the analogy between radiative or non-radiative transitions involving core level de-excitation with X-ray photon or Auger electron emissions, and radiative or non-radiative transitions involving electron traps and luminescent centers leading to emission of luminous photons or exoelectrons. The recombination kinetics depends on the density of defects which naturally exist in the crystal and will also depend on the mechanisms of dissipation of the incident energy within the crystal.

As a consequence of multiple mechanisms of energy transfer of the excitation energy to the luminescence centers, the luminescence spectrum of a crystal containing several luminescent ions may be not the sum of the luminescence spectra of the same crystal containing separately each individual luminescence-activating ions. This is in contrast to the case for the X-ray spectrum of a specimen, which is the sum of the X-ray spectrum of each element contained within the compound. Thus, the mechanisms of luminescence in crystals lead to complex spectra consisting of many bands and/or narrow peaks whose wavelengths and intensities depend on the entire crystallographic properties of the mineral (i.e, nature, chemical environment and concentration of the ions) rather than only on the qualitative nature of the luminescence-activating ions.

The cathodoluminescence process

The terminology cathodoluminescence (CL) is used to designate the luminescence emission induced by electron bombardment of the specimen. Besides the role of the incident electrons all other forms of energy resulting from the incident energy dissipation will contribute to the emission process.

Electrons and X-ray photons: Elastic and inelastic scattering of the incident electrons within the target will lead to the production of backscattered electrons (change in the trajectory without any energy loss) and secondary electrons resulting from energy

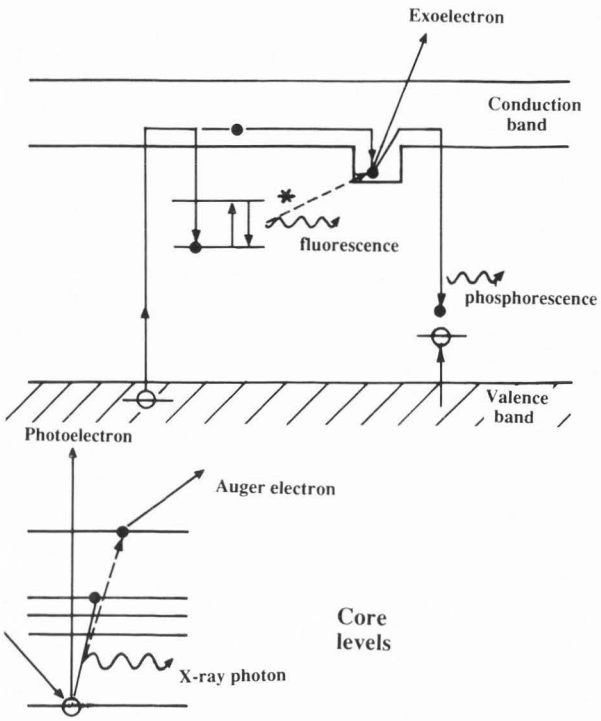

Fig. 3: Analogies between radiative and non-radiative transitions resulting from electron-hole recombination on core levels (X-ray and Auger electron emissions) or on point defect levels (luminescence and exoelectron emissions).

loss of the incident electrons. The inelastic scattering process leads to the production of X-ray photons or Auger electrons. Electrons and X-ray photons may both contribute to the creation of electron-hole pairs which recombine on the luminescent centers with radiative transitions leading to luminous photon emission.

Thermal effect: Most of the energy of the electron beam is converted to heat. The production of heat in the target during analysis with the EPMA was considered by Castaing (12) who calculated that for a 30 kV potential, a current of about 0.5 μA and a ≈ 1 μm beam diameter the temperature rise in copper would be 18 °C. According to Myhajlenko et al. (87) for a 30 kV-10 μA electron beam 3 μm in diameter on a Si substrate, the steady-state maximum temperature rise should be 150 °K and 30 °K for initial substrate temperature of 300 °K and 100 °K respectively.

The best known beam damage observed during EPMA analysis is the decrease of the Na and K X-ray intensities at longer irradiation times when analyzing glasses (92) and to a lesser extent silicate crystals. Studying silver bearing natural sulfides Remond et al. (103) showed that higher Ag concentrations occurred at the periphery than at the center of the electron beam spot. Local heating can be dissipated along the surface and into the depth. Heating during electron bombardment may cause beam damage leading to surface concentration enhancement of some ions as a result of a thermodynamically driven segregation from the bulk to the surface. However the thermal effect is not the unique possible mechanism and both thermal and electrical field enhanced diffusion may occur simultaneously.

Surface and volume charging effects: Electrical charges are built-up at the surface of insulating materials exposed to the electron beam irradiation. These charges may recombine or be trapped at defects leading to a local charge distribution which can cause phenomena such as deflection and instability of the incident beam, dielectric breakdown in the sample, and electromigration of mobile ions.

Preventing charging during electron bombardment is generally done by deposition of a thin conductive layer on the surface of the insulating materials. Cazaux (13) expressed the creation of electrical fields in insulators in terms of classical electrostatics considering the case of an incident beam normal to the sample. Assuming a uniform trapped charge distribution inside a cylinder, Cazaux (13) showed that surface coating will lead to cancellation of the surface radial component of the electrical field and will consequently prevent the incident beam from moving away from its initial position. However, a strong capacitor effect at the interface between the surface metal and the dielectric substrate may subsist leading to beam damage.

In minerals, the temperature increase from the electron beam is probably high due to their poor thermal conductivity. However, it is difficult to accurately measure the temperature increase which can be sufficient to provoke the loss of some species by evaporation or by electron stimulated desorption combined with field enhanced diffusion mechanisms (91) .

Cathodoluminescence emission may be the sum of different luminescence mechanisms resulting from electron excitation (**cathodoluminescence in the strict sense**), X-ray photons generated within the target (**roetgenoluminescence**, or radio-luminescence), electrical field created by trapped charges in insulators (**electroluminescence**) and thermal effects leading to two competitive phenomena, e.g., **thermal quenching** and **thermoluminescence**. Quantum rules can be modified or cease to be satisfied as a function of the temperature increase leading to modifications and attenuation of the intensity of the emission bands. Reciprocally,

temperature increases may lead to thermo-luminescence during electron bombardment (due to release of trapped electrons).

As a function of the energy and intensity of the incident electron beam and the dielectric properties of the luminescent crystal, each of the available energies released within the crystal are able to (a) modify the relative emission intensities in the different emission bands, (b) modify the relative probabilities of radiative and non-radiative recombination and (c) modify the filling of electron traps.

The cathodoluminescence intensity

According to Yacobi and Holt (144) the observed CL intensity can be expressed as :

$$I_{CL} = f_D f_A f_R \eta \frac{G i_b}{e} \qquad [1]$$

where f_D is a constant factor accounting for instrumental factors (detection solid angle, collection and transmissive efficiency of the detection system...) f_A is the absorption factor, f_R is a factor accounting for internal reflection loss of CL intensity, η is the radiative recombination efficiency (ratio of the radiative recombination rate to the total recombination rate), i_b is the incident electron beam current, e the electronic charge and G is the generation factor, i.e., the number of electron-hole pairs generated per incident electron.

Similarly with the intensity of an X-ray peak induced by electron bombardment, the intensity of a CL emission band is the product of three terms expressing i) the generation of CL photons within the solid, resulting from electron-solid interactions, ii) the emission of CL photons resulting from generated photon-solid interactions, and iii) the experimental and instrumental parameters.

CL photon generation : According to Yacobi and Holt (144) the generation factor G, is given by :

$$G = \frac{E_b}{\varepsilon_i}(1 - \gamma_e) \qquad [2]$$

where E_b is the electron beam energy, ε_i the ionization energy, i.e., the amount of energy needed for the formation of an electron-hole pair, and γ_e is the fractional energy loss due to the backscattered electrons.

$$\gamma_e = \frac{N_e}{N_b} \cdot \frac{E_{AV}}{E_b} \qquad [3]$$

where N_e is the **total** number of elastically and inelastically backscattered electrons ($\approx$50 eV < E < E_b) per second, N_b is the number of incident **beam** electrons per second of energy E_b and E_{AV} is the average energy per emitted electron.

Equation [2] is of a particular importance because ε_i has been found to be a constant for any given material, independent of the incident energy and as reported by Yacobi and Holt (144) :

$$\varepsilon_i = 3\, E_g \qquad [4]$$

where E_g is the width of the forbidden gap in the electronic energy band structure of the material.

Equation [2] is analogous to that proposed by Ishikawa et al. (47) expressing the number of photons created n, per incident electron with energy E_b:

$$n = \frac{E_b}{\varepsilon}(1 - \eta_e) \qquad [5]$$

were ε is the mean energy to create one CL photon and η_e is the backscatter electron coefficient as used in data processing with the SEM and EPMA:

$$\eta_e = \frac{N_e}{N_b} \qquad [6]$$

While ε_i in equation [2] is a constant characteristic of the material, the quantity ε, in equation [5] depends on how much of the beam energy goes into producing photons which depends not only on the concentration of the luminescent ions but also on the non-luminescent impurity concentration, the density of dislocations and other non-radiative recombination centers and the surface recombination properties of the sample.

The number of generated photons is proportionnal to the number of electron-hole pairs created by the incident energy weighted by the radiative recombination coefficient η. The total CL intensity created in the specimen per incident electron, I_{sp}, is thus:

$$I_{sp} = \eta\,(1 - \eta_e)\frac{E_p}{\varepsilon_i} \qquad [7]$$

In fact, the number of photons generated in the specimen is a function of depth below the surface because the number of electron-hole pairs depends on the incident energy dissipation which is a function of depth. Thus, equation [7] can be expressed as:

$$I_{sp} = \int_0^\infty I_{CL}(z)\, dz \qquad [8]$$

where $I_{CL}(z)$ describes the distribution of CL photons as a function of depth in the specimen.

CL photon emission: The generated photons are absorbed along the length of the photon path in the interior of the material before reaching the specimen surface. The absorption correction factor f_A is the ratio between the CL intensity created in the specimen and the intensity observed at an angle θ to the surface I_{obs} (CL) so that:

$$f_A = \frac{I_{obs}\,(CL)}{I_{sp}\,(CL)} = \frac{\int_0^\infty I_{CL}\,(z)\,\exp\,(-\mu\,z\,\mathrm{cosec}\,\theta)\,dz}{\int_0^\infty I_{CL}\,(z)\,dz} \qquad [9]$$

where μ is the absorption coefficient of the specimen for the analyzed CL wavelength.

The interaction between the CL photons and the specimen is not simply absorption because for the visible CL wavelengths and the refractive index of minerals, internal reflections may occur. Although luminescence is generated isotropically, only the small fraction inside a cone of semi-angle θ_c will escape, θ_c being the critical angle of total internal reflection at the specimen surface-vacuum interface. The fraction f_R of the total generated signal leaving homogenous targets has been discussed by Reimer (100). The critical angle θ_c which depends on the refractive index of the material defines the lateral resolution of the CL emission which consequently will vary from a specimen to another at constant irradiation conditions. For polycrystalline specimens the situation is much more complex because internal reflections will occur on all crystallographic planes randomly orientated in the analyzed volume.

The dependence of the measured CL intensity upon absorption and internal reflection may lead to contrast changes being difficult to distinguish from the variations in the spatial distribution of the recombination centers.

The CL yield is proportional to the radiative recombination efficiency which, for a given crystal, will vary as a function of the temperature increase and the electrical field created within the target, i.e., as a function of the dielectric property of the crystal.

The intensity of the CL emission is thus the product of many factors making difficult the interpretation of both the CL emission spectra and the contrast of CL images.

CL intensity as a function of the excitation conditions: Equations [1] and [7] show that the number of generated CL photons is proportional in a first approximation to the specimen current $i_{sp} \approx i_b\,(1 - \eta_e)$ where η_e is the electron backscatter coefficient. This approximation is only valid if $\gamma_e \approx \eta_e$,i.e., when the number of inelastically backscattered electrons is low with respect to that of elastically backscattered electrons, a situation which depends on the incident energy. From the study of commercial phosphors and semiconductors, the dependence intensity on voltage or primary electron energy was found to follow a power law relation $(E_b - E_0)^q$ where $1 \le q \le 2$ and E_0 is called the "dead voltage". This excitation threshold results from a "dead layer" at the specimen surface where the charge recombination mechanisms lead to mostly non-radiative transitions indicating that the radiative recombination efficiency is a function $\eta(z)$ of the depth below the surface.

In terms of the excitation conditions, the CL intensity generated in the specimen $I_{sp}(CL)$ and that observed at the specimen surface $I_{obs}(CL)$ can be rewritten as:

$$I_{sp}\,(CL) = i_{sp}\,(E_b - E_0)^q \qquad [10]$$

and :

$$I_{obs}(CL) = i_{sp}\,(E_b - E_0)^q\,F(E_b, n, k) \qquad [11]$$

where $F(E_b, n, k)$ is the net correction factor for optical losses including absorption f_A and multiple internal reflection f_R effects

The function $F(E_b, n, k)$ depends on the optical constants of the material (refractive index n and extinction coefficient k) and the incident energy E_b which determines the depth of the electron penetration and consequently the thickness of matter in which the absorption takes place.

Increasing the accelerating voltage leads to an increase of the emitting volume creating two competitive mechanisms between the number of generated photons and the absorption factor. Consequently, the observed CL intensity is expected to exhibit a maximum for the particular value, E_p, of the incident energy satisfying the equation:

$$\frac{d\,I_{obs}\,(CL)}{d\,E_b} = \frac{d}{d\,E_b}\,(E_b - E_0)^q\,F(E_b, n, k) = 0 \qquad [12]$$

An equation similar to equation [12] exists for the case of X-ray photons induced under electron bombardment with the EPMA. Such a relation has been used by Kyser (54) to obtain an indirect determination of the mass absorption coefficient for soft X-rays. The method has been applied by Remond et al. (104) to determine the most probable mass absorption coefficient among the published values which frequently exhibit large discrepancies.

In semiconductors, the variations of CL intensity as a function of the beam conditions have been intensively investigated (see among other Holt (39), Kyser and Wittry (55) and Yacobi and Holt (144).

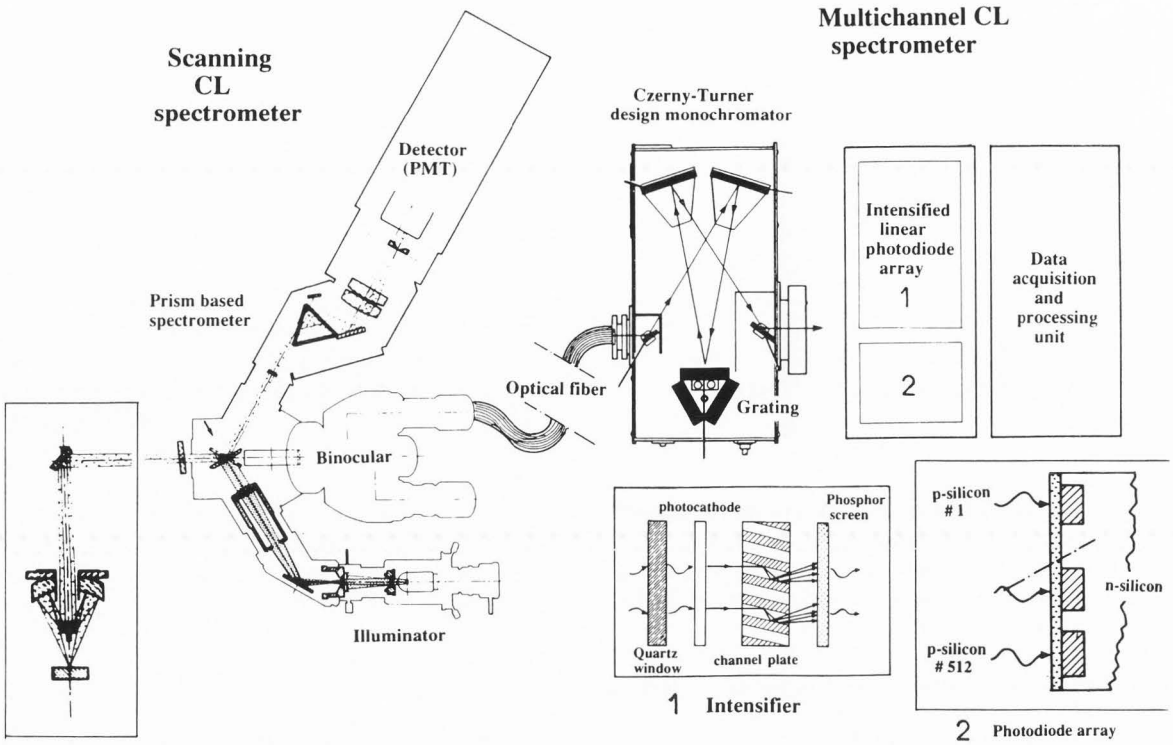

Fig. 4: Set-up to an EPMA of a **scanning** prism based CL spectrometer and a **multichannel** CL spectrometer using a grating and an intensified linear photodiode array (see insert 1 for the intensifier and insert 2 for the photodiode array). The optical microscope of the EPMA is used as a CL collector.

In minerals, Coy-Yll (16) showed that the CL intensity linearly increased with the electron beam current before reaching a plateau. The particular beam current corresponding to saturation of the CL emission varies from one mineral to another. Coy-Yll (16) showed that the CL intensity can be expressed as:

$$I_{CL} = K\, i_b^m \qquad [13]$$

where K and m are constants depending upon the mineral and the incident energy. In addition, Remond (102) showed that for some minerals the total CL intensity and the spectral CL emission at constant beam power varied as a function of the electron beam diameter and irradiation time. The dissipated energies within the specimen provoke the ionization of the atoms. The number of electron-hole pairs created in the specimen is proportional to the incident dose rate, i.e., the product of the beam voltage with the incident current per unit area (beam spot) at the specimen surface. At constant beam energy, the number of electron-hole pairs will increase with the beam current. The number of generated CL photons will linearly increase with the beam current before reaching a plateau indicating a saturation effect. The saturation effect results from capture of some of the released electrons by electron traps leading to self-absorption of the generated photons. The phenomenon is accentuated by the temperature increase during the irradiation time. A fraction of the total excitation dose, i.e., the dose rate multiplied by the irradiation time remains stored in the specimen as a result of charges trapped on metastable levels. This absorbed (or accumulated) dose is released by applying a temperature increase to release the charges from traps.

For insulating materials such as minerals in which CL is mostly extrinsic in origin, it is impossible to obtain a unique expression for the CL intensity as a function of the excitation conditions. The observed CL intensity is not simply proportional to the number of charge carriers created during electron bombardment because temperature increase, bulk charging and production of X-ray photons will selectively modify the radiative and non-radiative transition probabilities as a function of the experimental factors and the dielectric properties of the specimen.

For all the reasons mentioned above the dependence of CL intensity on the excitation can be summarized by the following expression:

$$I_{CL} = f(i_b, d, t)\ (V - V_0)^q \qquad [14]$$

where d is the beam diameter, t the irradiation time, V_0 the dead voltage and $1 \leq q \leq 2$.

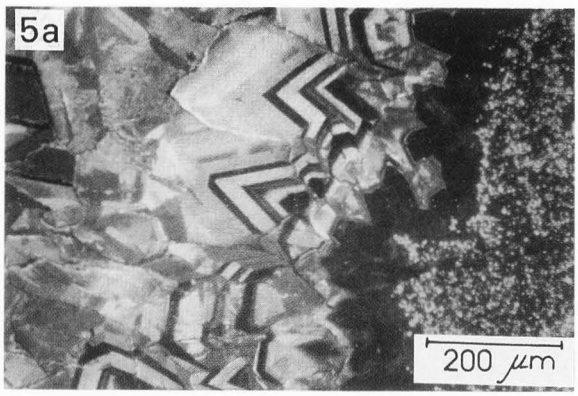

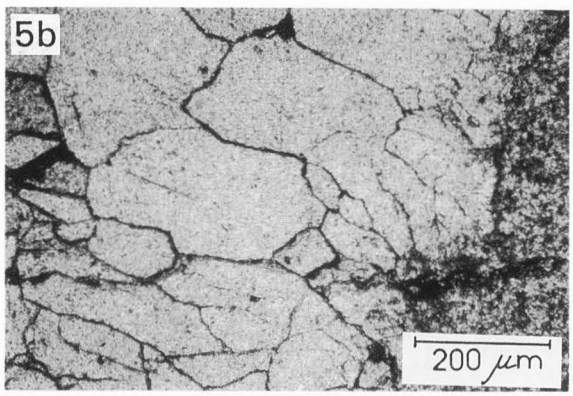

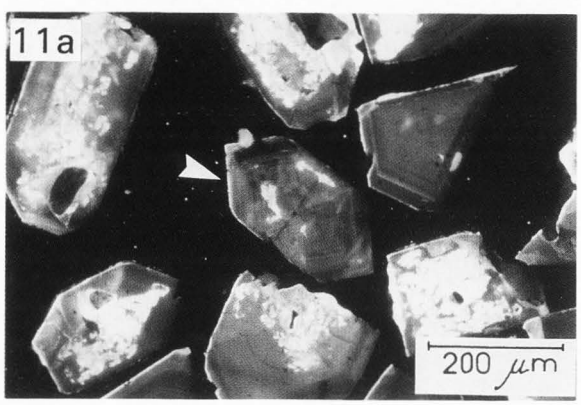

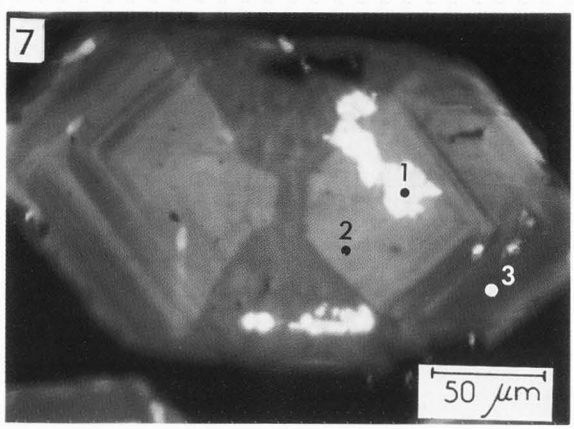

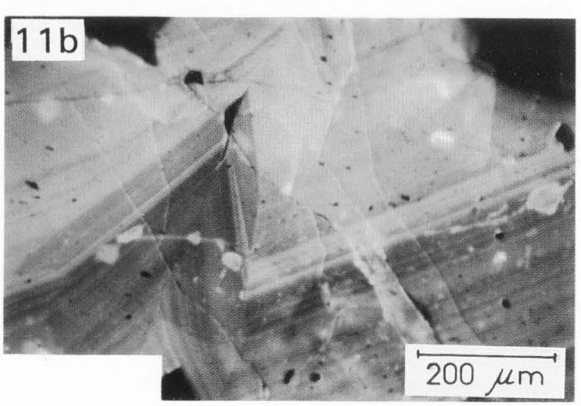

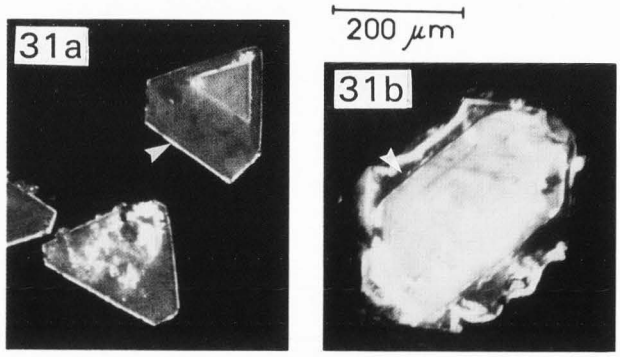

Fig. 5: Cathodoluminescence microscopy (a) and transmitted light photograph (b) using a cold cathode electron gun attachement to an optical microscope. The area in (a) exhibiting an orange CL color corresponds to carbonate, the oscillatory zoning areas correspond to quartz (from ref.(60)).

Fig. 11: Cathodoluminescence microscopy by means of a cold cathode electron gun attachment, revealing two populations of natural zircons ($Zr(SiO_4)$) exhibiting a blue (a) and a yellow-green (b) CL color respectively (uncoated specimen). The zircon grain marked by an arrow corresponds to that shown in Fig. 7.

Fig. 7: Cathodoluminescence image of a zircon ($Zr(SiO_4)$) grain recorded by placing a photographic plate in front of the eyepiece of the EPMA (carbon coated specimen).

Fig. 31: CL images (cold cathode electron gun) of (a) Dy^{3+}-doped synthetic zircon (arrow) and (b) undoped zircon. The synthetic zircons developped around a natural seed characterized by an intense blue CL emission.

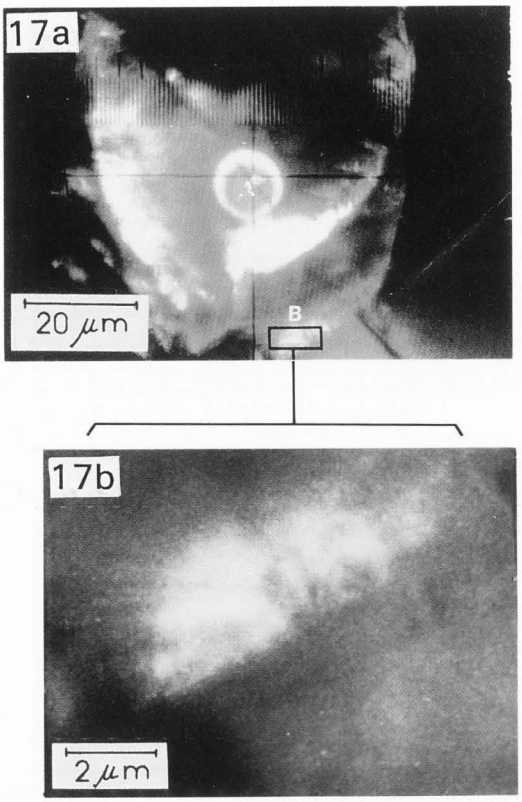

Fig. 17: Remote cathodoluminescence in a natural sphalerite (ZnS) crystal recorded by a photographic plate in front of the eyepiece of the microscope of the EPMA. (a) CL emission propagation at long distances from the beam spot (20 μm in diameter) located at point A. (b) photographic enlargement of the area B in (a) showing the CL produced in B by the electron beam incident at point A.

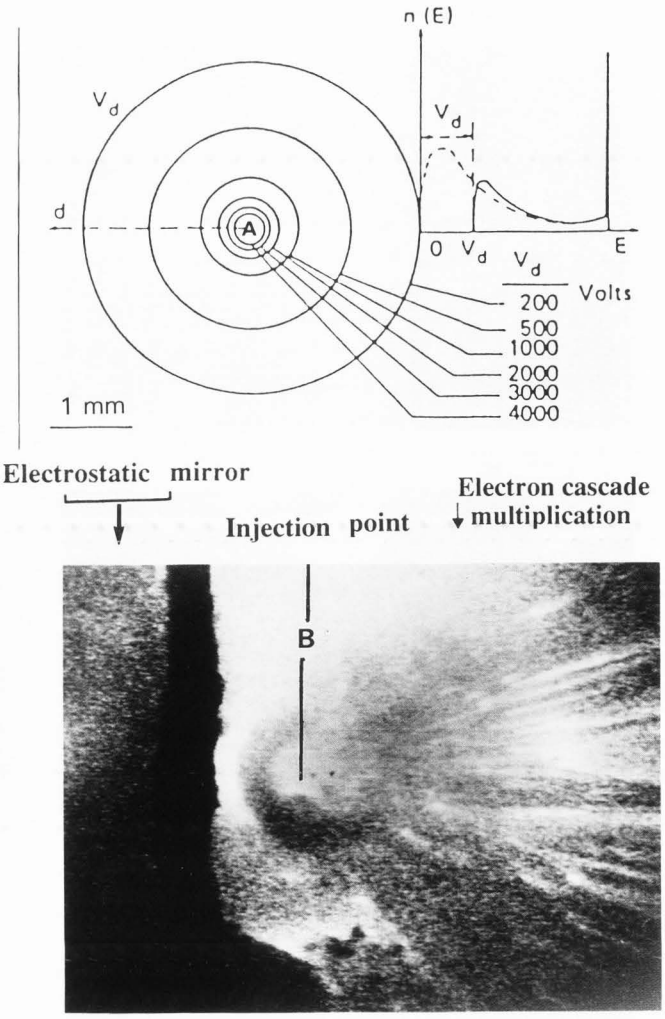

Fig. 18: Remote electron cascade multiplication in an amorphous SiO_2 induced by an electrical field according to Vigouroux et al. (136) (a) surface equipotential lines Vd as a function of the distance d from the electron beam incident at point A. (b) secondary electron multiplication cascade at distances from the injection point in B at the surface of the electrostatic mirror induced by the negative charge created in A.

Note the analogy between the electron multiplication cascade and the remote CL emission shown in Fig. 17.

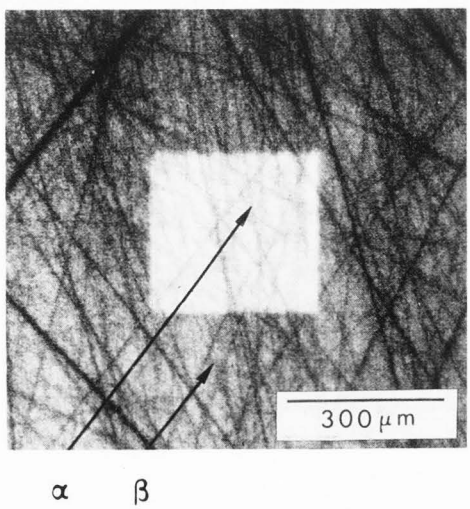

Fig. 19: Variations of the total visible CL intensity as a function of electron dose within an artificial zinc sulfide crystal. The full β area is first observed before to reduce the dimensions of the scanned area (α region). The time this region is exposed to irradiation is lengthened before the initial region is again observed. The region marked α has been exposed for 500 s to a 25 keV/10 nA electron beam. The region marked β has been exposed for 10 s to the beam (from Remond et al. (102) (107)).

Instrumentation

Cathodoluminescence microscopy

Cathodoluminescence by means of a fixed electron beam: Two types of electron sources are used, based either on a heated filament or a cold cathode electron gun.

EPMA's are intensively used for CL microscopy. For this purpose, a fixed unfocused incident beam, a few hundreds of microns in diameter, is used to bombard the surface of the specimen and the emitted light is recorded on a photographic plate in front of the eyepiece of the optical microscope of the EPMA.

In order to make CL microscopy easy for petrological applications and to provide simultaneous transmitted and polarized light examination of the luminescent areas, CL devices can be attached to the stages of conventional optical microscopes. Le Poole et al. (61) designed a luminescence microscope based on an electron optical system similar to that of the EPMA, i.e, using a heated W filament and focusing lenses. A highly sensitivity CL microscope has been developed by Ramseyer et al. (98) in order to detect weak and short-lived luminescence in minerals.

Commercial CL microscope attachments (CMA) are derived from the equipment designed by Sippel (120) based on the use of a cold cathode electron gun and vacuum chamber attached to an optical microscope. Commercial CMA are equipped either with a cold cathode electron gun oblique with respect to the specimen surface or with a horizontal electron gun, the beam being deflected by magnets onto the specimen surface. For a detailed description and the operating conditions of these types of equipment see for example Marshall (75) (76).

The most important difference between the equipment using a heated W filament or a cold cathode electron gun lies in the vacuum within the specimen chamber. For the equipment using thermal emission, the vacuum ranges between 10^{-5} an 10^{-6} Torr. With cold cathode electron guns the vacuum is $\approx 10^{-2}$ Torr in order to ionize the residual gas. Some electrical charges in the discharge may reach the specimen and neutralize the static charge created at the surface by modifying the secondary electron yield of the specimen (58). Thus, by the use of a cold cathode electron gun, conductive coatings of the minerals are not necessary as they are when using SEM or EPMA techniques.

Cathodoluminescence by means of scanning beam technique: Using the scanning beam facility of SEM and EPMA equipments, CL microscopy can be performed to image the local variations of the CL intensity. Being usually related to the presence of small amounts of impurities, CL imaging in minerals can be combined with secondary and backscattered electron signals emitted at the electron beam spot to reinforce the contrast due to small local composition changes.

Combination of panchromatic CL imaging with other SEM images can be used as a guide for further investigations on the observed specimen heterogeneities. Such combined CL / backscattered electron imaging and trace element analysis have been illustrated by Henry and Toney (37). Besides the contribution to the identification and localization of trace elements, CL imaging may be a help in the illustration of crystallographic changes as illustrated by Czernuska and Page (18). These authors showed that CL microscopy can be used for studying phase distribution and deformation structures in zirconia ceramics. The CL images can be compared with the secondary or backscattered electron and X-ray images as illustrated by Remond et al. (102) (105) to reveal heterogeneities within cassiterite (SnO_2) crystals which were apparently homogeneous as shown by optical and SEM examination. For CL examination these authors simply used a photomultiplier tube (PMT) as a detector, the front window of the PMT being directly placed in the vacuum of the specimen chamber.

In order to improve the collection efficiency of the emitted photons, several optical collectors have been developed using either lenses or mirrors. The collector can be located to one side or above the sample. An optical lens based collector has been developed by Semo (114) (115). This equipment is used as an interface between the vacuum where CL photons are produced and the air where they are detected. Similar optical collectors are now commercialized by SEM manufacturers or simply built in SEM laboratories.

The built-in two spherical-mirror microscope attached to the EPMA can be used to direct the CL flux either to the eyepiece of the microscope or to a detector for panchromatic or monochromatic selected CL image recording. Usually, SEM's are not equipped with optical devices allowing direct optical observation of the specimen during electron bombardment. For CL microscopy (or spectroscopy) by means of the SEM, light collectors have been developed as discussed in Yacobi and Holt (144). A parabolic mirror placed immediatly above the specimen surface can be used to increase the collection efficiency. The specimen is placed at the focus point of the mirror and the light is reflected towards the detector. However, more recent equipment consists of a semi-ellipsoidal mirror placed a short distance above the specimen surface. The first focus point corresponds to the light source at the electron beam impact, the detector being located at the second focus point. A set of external manipulators allows the adjustment of

the mirror position and the system is retractable to make easy the use of the SEM for secondary and backscattered electron imaging. CL collection devices using two semi-ellipsoidal mirrors have been used by Hörl and Roschger (43) for studying biological materials characterized by a very weak CL emission. The first semi-ellipsoidal mirror is placed above the specimen which is placed at the first focus point. The second focus point is common to a second semi-ellipsoidal mirror placed symmetrically to the first one with respect to the specimen surface. The exit window is located at the second focus point of the second ellipsoidal mirror. A two-mirror assembly has also been used by Trigg (132) for the study of CL properties of optical materials. The geometrical arrangement used by Trigg (132) consists of a semi-ellipsoidal mirror located immediatly beneath and co-axial with the final lens of the SEM. The collected CL light by the ellipsoidal mirror is reflected by a plane mirror located below the specimen and the CL beam is focused out of the SEM through a silica window. These arrangements avoid the use of a light pipe to direct the luminous photons from the mirror to the detector and have a large solid angle for focusing the photons on the detector.

The available CL collectors (light pipe, optical system using lenses or mirrors) are usually combined with a PMT as a detector. Rather than PMT, silicon photodiodes operated at room temperature have also been used (143). Silicon and germanium photodiodes are more particularly suitable for the detection of long wavelengths ($\lambda > 1$ μm) such as for the case of semi-conductors (15). The amplified photomultiplier output controls the video signal of the SEM cathode-ray-tube (CRT) display. The detection mode provides panchromatic CL images illustrating the variations of both the intensity and the wavelength of the CL emission convoluted by the response function of the detector assembly.

False color CL imaging has also been obtained using signal processing through the multichannel analyzer of an X-ray energy dispersive spectrometer attached to the SEM. Different methods for cathodoluminescence color imaging and color coding have been described by Saparin and Obyden (111). As discussed by Buschbeck and Hörl (8), color CL images using scanning electron beam techniques and a color monitor have been obtained with three interference filters and three detection channels corresponding to the red, the blue and the green respectively. Applications of digital acquisition and processing of CL color images in mineralogy have been recently discussed by Steele (128) and by Wright and Kearsley (142). Le Nindre et al.(60) also showed that CL images obtained by means of a CL microscope attachment can be digitized and quantitatively processed.

Cathodoluminescence spectrometry

As for the case of X-ray spectrometry, CL spectra can be obtained using either a sequential or a simultaneous detection mode.

The two basic parts of the CL spectrometer are the grating or prism monochromator and the detector successively. Gratings are characterized by a high wavelength resolution and a linear scattering accompanied in turn by an important loss in intensity since only a small fraction of the diffracted light can reach the detector. Prisms have a high transmission but the spectral resolution is lower than that obtained with gratings.

A CL spectrometer has been developed by Semo (114) (115). The system consists of a flint prism, a condenser lens and a PMT as a detector. Originally, the system was developed to be fitted to a SEM column by means of an optical lens based collector. A similar version of the spectrometer was commercialized as a CL attachment to the EPMA. The two spherical mirrors of the optical microscope of the EPMA are used as CL collector (Fig. 4). A rotating mirror is used to alternatively observe the luminescent area through the eyepiece of the microscope and to analyze the CL intensity variations as a function of wavelength. Such a spectrometer allows a sequential analysis of the CL emission, the analyzed wavelength being selected by moving the slit in the focal plane of the optical condenser lens placed behind the monochromator. One merit of such equipment lies in the high transmission of the prism. A disavantage of the spectrometer is its non linear response function of the analyzed wavelength vs the slit position.

An optical multichannel analyzer (OMA) for simultaneous detection of CL emission spectra has been decribed by Löhnert et al. (63). The CL emission collected by a semi-ellipsoidal mirror is focused on the entrance slit of a grating monochromator operated under vacuum with a detector consisting of a vidicon camera equipped with a Silicon Intensified Target (SIT) consisting of ≈ 1000 x 1000 silicon diodes coupled with an integrated image intensifier stage. The camera video signal is processed into a multichannel analyzer before being displayed.

Intensified linear photodiode arrays (LPDA) have been used as efficient detectors in multichannel analysis of optical signals in photoluminescence and Raman spectroscopies and their potential use for cathodoluminescence spectral analysis with SEM techniques has been pointed out by Jones and Landon (51). An intensified photodiode array based CL spectrometer linked by an optical fiber to the eyepiece of the optical microscope of the EPMA is schematically illustrated in Fig. 4. The CL spectrometer consists of a grating monochromator, the exit slit of which is removed, permitting a laterally dispersed spectrum to irradiate the detector. The

Table 1 : **Available equipment for CL analysis**

Light collector	Transfer of light	Mono-chromators	Detectors
lenses, spherical mirror, (built in EPMA) parabolic or semi-ellipsoidal mirror (SEM attachment)	lenses, mirrors, light pipe or optical fiber	filters, prisms or gratings	photomultiplier tube or photodiodes

detector head shown in Fig. 4 consists of a proximity focused image intensifier type consisting of a quartz window placed in front of a photocathode, an accelerating grid, a micro-channel plate and a luminescent screen. The electrons released from the photocathode by the incident luminous photons are accelerated and directed towards a micro-channel plate providing a gain in the number of electrons. These electrons interact with a phosphor screen producing luminous photons which are in turn detected by the LPDA unit consisting of 1024 or 512 silicon diodes. Wavelength information is determined by the position of the diode within the array, the height of the pulse collected at each diode being proportional to the amount of light falling on the corresponding array element. All diodes are simultaneously illuminated and read sequentially leading to a simultaneous detection mode of the emitted photons. The integration time is the same for each diode and is adjustable from a few milliseconds to several seconds depending upon the intensity of the analyzed luminescent emission.

The CL intensity is generally low and the detected signals are noisy. The use of a "lock-in" amplifier leads to a significant improvement in the signal-to-noise ratio. The detection mode for a "lock-in" amplification requires a modulated light input. This may be achieved by optical chopping at the detector input or by using an electron beam brightness modulation.

Beam modulation also leads to time resolved analysis of the CL emission.

Using either cold cathode or thermoelectronic electron guns, CL analyses of minerals are usually performed at room temperature. The interpretation of CL data as well as the emission efficiency,should be greatly improved by studying CL properties at low temperature as is done for the case of biological specimens emitting very weak CL intensity and being easily damaged by electron irradiation. The advantages of low temperature CL analysis have been discussed by Warwick (138) and Holt (40) among others.

As summarized in Table 1, a variety of components are available to develop specific attachments to EPMA, SEM and optical microscopes for the detection and the analysis of the CL emission. All of these components can be combined with other in a variety of fashions in order to obtain an optimized detection efficiency as a function of the nature of the CL application.

In this study we used a multichannel CL spectrometer manufactured by the Tracor Northern Company. It consists of a grating monochromator (3 gratings available), an intensified linear photodiode array (512 diodes) linked by an optical fiber to the EPMA (CAMECA, MS46 type) installed at the Ecole Nationale Superieure de Mecanique des Microtechniques (ENSMM) in Besançon (France). The transmission efficiency of the optical fiber and the spectrometer allows us to analyze wavelengths ranging from 250 nm to 900 nm. Owing, to the glassy optical components placed on the CL emission path in the EPMA, only the wavelength domain ranging from 400 nm to 700 nm was analyzed in practice.

To evaluate the overall efficiency of the available CL detection systems we also used the equipment installed at the Centre de Recherche Interdisciplinaire d'Archeologie Analytique (CRIAA) at the University of Bordeaux 3 (France). This equipment consists of a spectrometer of the sequential type attached to a JEOL 820 scanning electron microscope. The light collector was a retractable semi-ellipsoidal mirror manufactured by the Oxford

Instrument Company. The output of the collector was linked by an optical fiber to a 1200 grooves/millimeter (gr/mm) grating monochromator. The analyzed wavelength range was 250 nm - 700 nm.

For CL microscopy we used a cold cathode electron gun attachment manufactured by the Technosyn Company and installed at the Bureau de Recherches Geologiques et Minieres in Orleans (France). Direct photographic recording through the eyepiece of the optical microscope of an EPMA was also performed.

Experimentation

Complementarity of the technologies used

Fixed or scanning beam irradiation are two complementary techniques for CL microscopy. Color CL images using either the unfocused beam of the EPMA or the CL device attached to an optical microscope can be used only for qualitative observation of textures that are not revealed by other microscopic techniques. An example of CL structures in a specimen containing quartz and carbonate minerals is shown in Fig. 5 (color plate) for comparison with the optical observation using transmitted light microscopy. Both photographs in Fig. 5a and 5b were recorded by means of a microscope equipped with a cold cathode electron gun allowing both CL and optical examination.

Commercial photographic films have a broad response function allowing the recording of CL images with a broad color domain of the visible spectrum as illustrated for the case of the CL emission of the specimen in Fig. 5. The orange CL emission corresponds to carbonate and the area exhibiting CL zoning corresponds to quartz.

Panchromatic CL images with the SEM generally reveal the same structures as observed by using CL recording with static beam irradiation (Fig. 5 and 6).

However, the PMT used as a CL detector with the SEM has a sharper response function to photon energies than that of a color photographic plate. It is common to use PMT having the same photocathode for CL and secondary electron detectors. Most of the photocathodes are of the S20 type with a maximum sensitivity in the blue region and a very low efficiency in the red part of the visible spectrum. High contrast in panchromatic CL imaging may occur when the spectral CL emissions within the analyzed areas exhibit broad emission bands with maximum intensity at very different wavelengths. The effect of the photocathode response function on the contrast of a panchromatic CL image is shown in Fig. 6 corresponding to the same area as that shown on the color photograph in Fig. 5a. The marked contrast in the panchromatic CL-SEM image resulted from the lower efficiency of the photomultiplier for the orange color of carbonate compared to the white quartz CL emission.

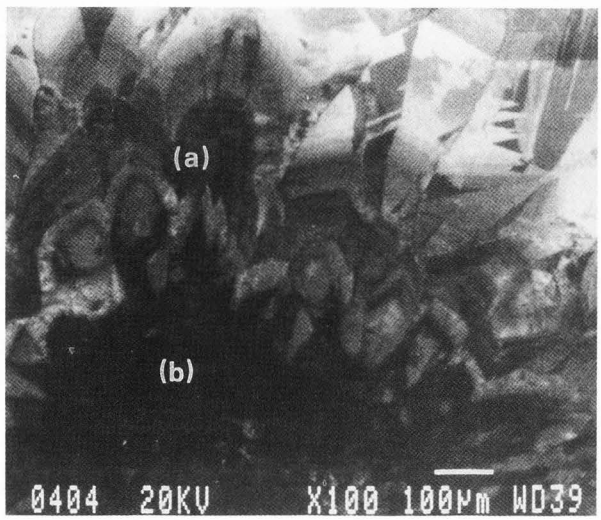

Fig. 6: Panchromatic scanning CL microscopy of the specimen shown in Fig. 5 (color plate). Note the sharp contrast between the quartz (a) and the carbonate (b) resulting from the response function of the detector from the blue (a) to the orange-red (b).

The contrast in a panchromatic CL image can be improved by using digital acquisition and processing procedures commonly available with modern SEMs and EPMAs. Image reconstruction can be used in order to reveal details within areas exhibiting high difference in signal levels. An approach could consist of recording and summing three images corresponding to the three fundamental colors selected by interferential filters. The beam energy and beam current can be adjusted in order to improve the signal to noise ratio and the detection efficiency for each of the three successive images. Thus, the CL image is the sum of three optimized images to compensate for the response of the detector as a function of wavelengths.

To illustrate the complementarity of the available spectrometers, the CL spectra of a natural zircon were recorded using sequential and simultaneous detection respectively. Spectra corresponding to the three areas marked on the color CL image in Fig. 7 (color plate) of a natural zircon ($Zr(SiO_4)$) are shown in Fig. 8 using the scanning spectrometer equipped with a 1200 grooves/millimeter (gr/mm) and a PMT as a detector. The entrance and exit slits of the spectrometer were opened to their maximum width in order to have a high detection sensitivity for a rapid qualitative survey and for CL mapping at selected wavelengths. The spectra

Figs. 5, 7, 11 and 31 are on color plate page 31.

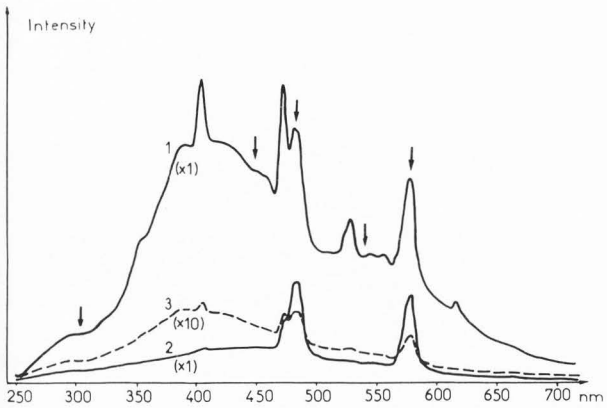

Fig. 8: CL emission spectra of natural zircon corresponding to the three locations (beam spot ≈ 1 μm) marked on the CL image in Fig. 7 (color plate). Spectra were recorded with a scanning grating (1200 grooves/mm) based CL spectrometer. Entrance and exit slits were widely opened. (Arrows show the wavelengths selected for monochromatic CL images in Fig. 13).

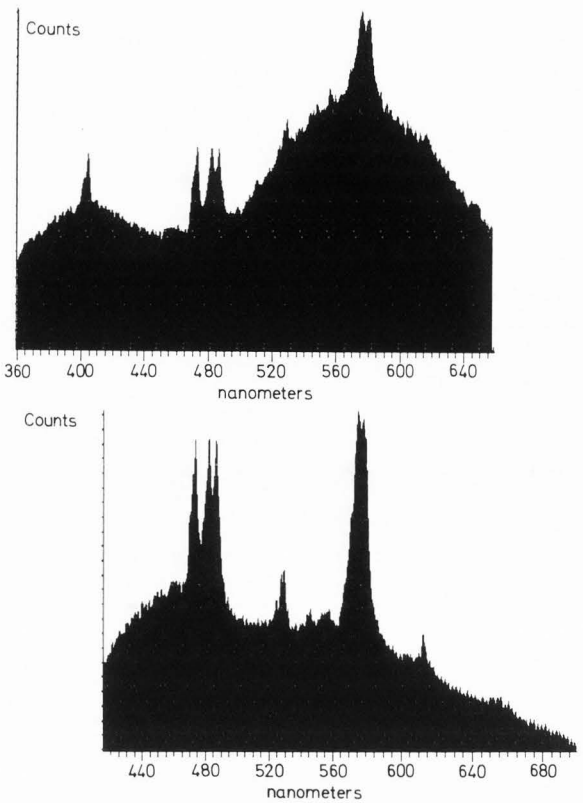

Fig. 9: CL emission spectra measured by means of the multichannel CL spectrometer equipped with a 150 grooves/mm grating and a linear photodiode array (300 nm spectral coverage). The two analyzed wavelength domains corresponding to two distinct areas within a zircon grain were obtained by changing the grating position between the two successive measurements.

in Fig. 8 were recorded at a rate of 50 nm per minute over a wavelength domain from 250 nm to 700 nm. The total data acquisition time was ≈ 10 minutes. As shown in Fig. 8 narrow CL peaks are superimposed on broad emission bands whose intensities changed as a function of the analyzed location within the zircon crystal.

The sequential acquisition procedure was compared to the simultaneous detection mode by using a grating monochromator coupled to a photodiode array (512 diodes at 0.025 mm spacing). Accounting for the length of the photodiode array (12.5 mm) the width of the analyzed spectral domain and the spectral dispersion changed as a function of the grating used. The spectrometer was linked by an optical fibre bundle to the eyepiece of the optical microscope of an EPMA (Fig. 4). The CL emission spectra shown in Fig. 9 were obtained with a 150 gr/mm grating providing a 300 nm spectral coverage and a 24 nm/mm spectral dispersion. The photodiode intensifier was moderately powered and the data acquisition time was only 20 seconds. The two spectra in Fig. 9 correspond to two different areas within the zircon specimen and were obtained by changing the grating position to select two wavelength ranges of 300 nm width.

All spectra were obtained with a 20 keV electron beam energy. The beam intensity was ≈ 300 nA when using CL spectrometers attached to the EPMA. When using the CL spectrometer attached to the SEM equipped with a semi-ellipsoidal mirror collector, a lower beam intensity was used. The difference in the electron beam conditions was due to the different collection efficiency of the two optical collectors. In the present study, the spectrometer coupled to the photodiode array detector was simply linked by an optical fiber to the microscope of the EPMA. Preliminary experiments showed that an increase by a factor of ≈ 20 in the sensitivity can be obtained by removing the semi-transparent window used to illuminate and observe the specimen simultaneously. The absorption by the lenses and semi-transparent windows along the optical path leads to low detection efficiency of short wavelength occurring in the blue region of the visible spectrum with respect to the efficiency of the system equipped with the ellipsoidal mirror placed at a very short distance of the specimen surface.

The spectra in Fig. 8 and Fig. 9 were not corrected for the response function of the detection units. Significant changes in the CL intensity, the shape and the wavelength position of the emission bands may occur when comparing raw CL spectra with data corrected for the response function of the

spectrometer. Some examples illustrating the effect of the instrumental response on the reliability of CL spectra can be found in Yacobi and Holt (144). Broad emission bands undergo larger correction effects than do narrower bands. Thus, the presence of narrow CL peaks can be used for comparing the respective merits of the scanning and multichannel CL spectrometers.

Using a scanning monochromator, the resolution can be improved by reducing the width of the entrance and exit slits of the spectrometer. The gain in resolution by reducing the slit widths is shown in Fig. 10 for the case of the scanning spectrometer equipped with a 1200 gr/mm grating.

By reducing the slit width, the peak centered at 472 nm was resolved into a triplet. However, increasing the wavelength resolution by adjusting the slit width is obviously accompanied by an important decrease in the measured intensity. With zircon a mineral that often shows intense CL, that is not a problem. However, when examining low-intensity minerals such as quartz it can be.

For the case of a photodiode-array based spectrometer, the absence of mechanical parts makes the reproducibility and accuracy of wavelength readings greater than those of any mechanically scanned spectrometer. A photodiode array has a constant length, the change in the spectral coverage and the spectral resolution is obtained by using several gratings of different gr/mm values. Increasing the number of gr/mn will increase the reciprocal linear spectral dispersion (nm/mm) but consequently decrease the spectral range incident on the photodiode array. Thus, successive recordings corresponding to different positions of the grating are necessary to split the full spectrum into several partial high resolution spectra. The spatial resolution of the diode array spectrometer is one diode wide. The theoretical spectral resolution is equal to the product of the reciprocal linear dispersion (nm/mm) of the grating by the width of the diode (0.025 mm). Thus, the expected spectral resolution should be 0.6 nm and 0.3 nm for the 150 gr/mm and 300 gr/mm gratings respectively. In practice, the spectral resolution is worse than the predicted value by a factor of about 2. This discrepancy results from the aperture response function of the array (51). As shown in Fig. 4 the LPDA consists of p-type bars in an n-type silicon substrate. Each diode integrates the energy from the p-silicon area and of each of the adjacent n-silicon areas. The signal does not originate from a single diode but from an aperture area whose size is equal to the diode spacing (51). The resolution we measured as the full-width at half-maximum of the 546 .1 nm line of Hg was 1 nm and ≈ 0.6 nm respectively.

The spectral resolution obtained with the 300 gr/mm grating coupled to the photodiode array

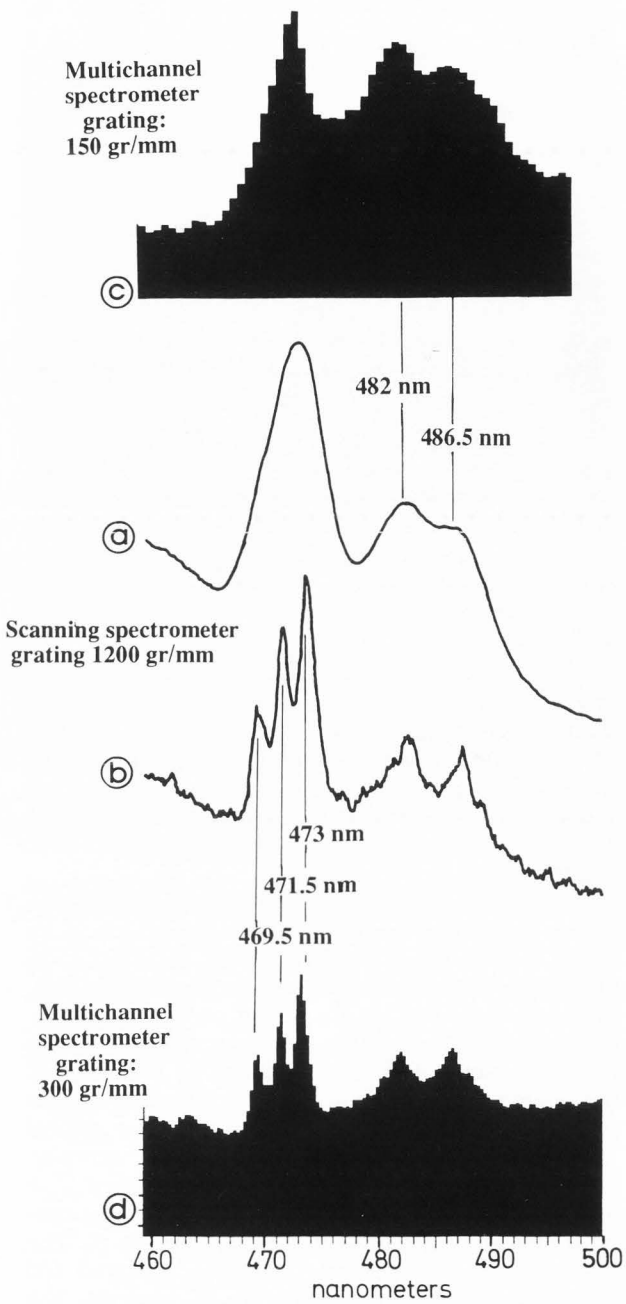

Fig. 10: Comparative wavelength resolution obtained using a **scanning** (a) (b) and a **multichannel** (c) (d) CL spectrometers. The **scanning** spectrometer was equipped with a 1200 grooves/mm grating. The entrance and exit slits were widely opened in (a) and narrowed in (b). The **multichannel** spectrometer was equipped with a 150 grooves/mm grating in (c) and a 300 grooves/mm grating in (d).

was sufficient to identify all the features found using the scanning grating monochromator coupled with a photomultiplier (Fig. 10b and 10d). Data in Fig. 10d were obtained by using a 300 gr/mm ruled grating and show that the peak centered at 472 nm consists of several sharp features similar to Fig. 10b.

It is noticeable that the gain in resolution obtained by increasing the spectral dispersion of the grating coupled with the intensified photodiode array is accompanied by a lower loss of sensitivity than that obtained by reducing the width of the slits of the scanning grating monochromator. In addition, it is possible to adjust the power of the intensified LPDA to increase the sensitivity of detection without increasing the electron beam intensity, i.e., without creating beam damage.

The overall efficiency of CL detection is the net result of many instrumental factors (solid angle of the light collector, transmission of the fiber optics and monochromator devices, sensitivity of the detectors...) and all possible combinations of the available components summarized in Table 1 lead to complementary rather than competitive techniques for CL studies with the use of EPMA or SEM.

Contribution of CL spectroscopy to the interpretation of CL images

Selected wavelength CL imaging: Owing to the numerous parameters leading to CL changes, color photographic recording provides only **qualitative** information and panchromatic CL images at **selected wavelengths** may be preferred for a better understanding of the relationship between the CL emission and the properties of the specimen.

Examples of CL microscopy are illustrated for the case of natural zircons. As shown in Fig. 11 (color plate), CL images obtained with a cold cathode electron gun attachment, shows two populations of zircons based on their blue (Fig. 11a) or yellow-green (Fig. 11b) CL color respectively. CL images revealed heterogeneities and of particular interest was the zircon crystal (marked by an arrow in Fig. 11a) exhibiting unusual sector zoning similar to that already observed by Hoffman and Long (38). The X-ray images in Fig. 12 showed that yttrium (Y) and dysprosium (Dy) exhibited a heterogeneous distribution settling some of the boundaries shown on the CL image in Fig. 7 (color plate). However, the variations in Y and Dy concentrations were not sufficient to reveal sector zoning shown by CL microscopy. By analogy with X-ray mapping, selected wavelength CL images were then recorded using the scanning CL spectrometer attached to the SEM. The monochromatic CL images in Fig. 13 at 482 nm and 578 nm correspond to the maximum intensity of narrow CL peaks shown on spectra in Fig. 8 and the

Figs. 5, 7, 11 and 31 are on color plate page 31.

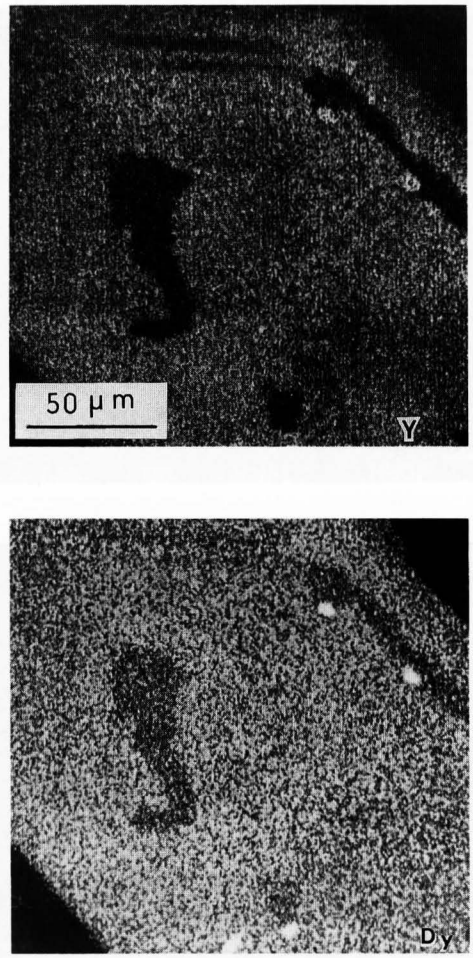

Fig. 12: X-ray maps illustrating the relationship between the CL emission and the spatial distribution of Y and Dy impurities within the zircon grain shown in Fig. 7 (color plate).

images at 313.5 nm, 450 nm and 531 nm correspond to intensities associated with broad CL emission bands. The differences in contrast shown on the monochromatic CL images as a function of the analyzed wavelengths indicate that several mechanisms involving several luminescent centers are probably responsible for the CL intensity changes shown on the CL color images in Fig. 7 and Fig. 11.

Although the dominant color was slightly different, the same features showing the sector zoning and bright patches were observed under the unfocused electron beam of the EPMA (Fig. 7). From the photographic CL images it is difficult to conclude whether the observed variations resulted from local changes in CL color or only from changes in luminosity. It is thus, necessary to quantify the observed colors.

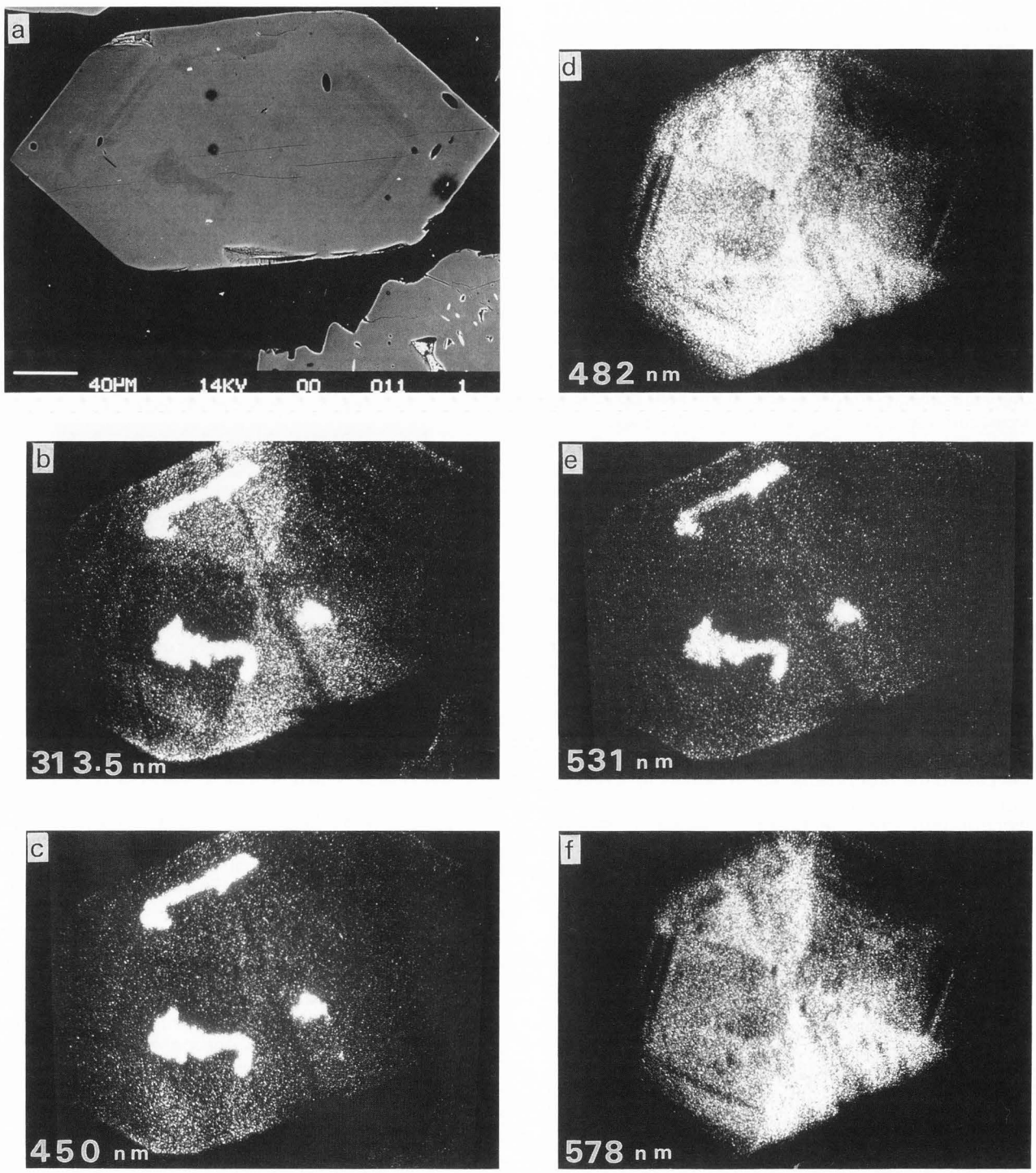

Fig. 13: Backscattered electron image (a) (atomic number contrast) and monochromatic CL image at 313.5 nm (b), 450 nm (c), 482 nm (d), 531 nm (e) and 578 nm (f). Note that images (d) and (f) correspond to the maximum intensity of narrow CL peaks and that images (b), (c) and (e) correspond to the intensity of broad CL emission bands shown in CL spectra in Fig. 8.

Calibration of CL observations: The observed color of the CL obtained by direct viewing recording on a photographic plate must be used carefully when comparing several CL images. For long exposure times (≈ several minutes) the sensitivity of the photographic plate loses its nominal response function as a function of wavelengths. Consequently, the CL distribution may be progressively shifted towards a dominant color on the photographic plate.

In addition, color changes during long exposure time may result from selective absorption of the CL emission by the surface contamination layer which develops under high electron beam intensities. With a CL optical microscope operated with residual gas in the specimen chamber and the cold cathode electron gun, experience has shown that the quartz or glass window placed between the specimen and the objective lens may turn brown resulting from contamination. The contamination product can be rapidly deposited when the observed specimen consists of small mineral grains embedded in plastic. This can be avoided by frequently cleanning the window.

In order to make comparable several CL observations, quantitative information must be derived from the CL emission spectra accounting for the response function of the detector (human eye or photographic plate).

To fully specify the perception of a beam of light, e.g., the CL emission of a specimen observed through an optical device or recorded on a photographic plate, it is necessary to take into consideration the following characteristics: i) the color associated with the dominant wavelength (λ_D) of the emission, ii) the saturation of the color (or excitation purity) which is the extent to wich the color is pure and iii) the brightness or luminous intensity. Many text books describe the available procedures for quantitative measurements of color (see Wright (141) among others). Only the use of the chromaticity diagram according to the agreements from the Commission Internationale de l'Eclairage (CIE) will be summarized. Quantitative expression of color of rocks and minerals has been discussed by Cervelle and Malezieux (14) based on the response function of the eye, the spectral distribution of the incident light and the reflectance (diffuse or specular) of the specimen. The procedure can be extended to the case of the CL emission.

Let $I^*_{CL}(\lambda)$, be the CL emission spectrum measured within the wavelength domain 400 nm-700 nm corresponding to the sensitivity thresholds of the human eye. $I^*_{CL}(\lambda)$ is the CL intensity emitted at the specimen surface **corrected for the response function of the spectrometer used**.

Let $\overline{x_\lambda}, \overline{y_\lambda}$ and $\overline{z_\lambda}$, be three sensitivity response factors for the eye corresponding to red, green and blue respectively.

Three stimulus values X,Y and Z can be calculated for each of the red, green and blue regions according to:

$$(X, Y, Z) = \int_\lambda (\overline{x_\lambda}, \overline{y_\lambda}, \overline{z_\lambda})\, I^*_{CL}(\lambda)\, d\lambda \qquad [15]$$

The three stimuli (equation [15]) are used to calculate the corresponding chromaticity coordinates x, y and z of the color according to:

$$x = \frac{X}{X+Y+Z},\ y = \frac{Y}{X+Y+Z} \text{ and } z = \frac{Z}{X+Y+Z} \qquad [16]$$

$$\text{with } x + y + z = 1 \qquad [17]$$

In practice, the analyzed wavelength domain is divided into intervals of equal widths (typically 10 nm) and the CL intensities are measured. The $\overline{x_\lambda}, \overline{y_\lambda}$ and $\overline{z_\lambda}$ values relative to the same wavelength intervals are derived from tables (141). The three stimuli X, Y and Z are thus calculated according to equation [15] using a summation of products rather than integration.

According to equation [17] only two coordinates, x and y, are used to define the color. The set of (x, y) values are expressed according to:

$$x = \frac{\Sigma\, (\overline{x_\lambda}\, I^*_{CL}(\lambda))}{\Sigma\, (\overline{x_\lambda}\, I^*_{CL}(\lambda)) + \Sigma\, (\overline{y_\lambda}\, I^*_{CL}(\lambda)) + \Sigma\, (\overline{z_\lambda}\, I^*_{CL}(\lambda))}$$

$$y = \frac{\Sigma\, (\overline{y_\lambda}\, I^*_{CL}(\lambda))}{\Sigma\, (\overline{x_\lambda}\, I^*_{CL}(\lambda)) + \Sigma\, (\overline{y_\lambda}\, I^*_{CL}(\lambda)) + \Sigma\, (\overline{z_\lambda}\, I^*_{CL}(\lambda))} \qquad [18]$$

Once the chromaticity coordinates (x,y) are known, the color of the object M, is defined by its position (x,y) in a chromaticity chart as shown in Fig. 14. This chart, consists of a curved, horseshoe-shaped line graduated from violet (400 nm) to red (700 nm). The diagonal line connecting 400 nm and 700 nm contains purple and magenta colors resulting from the combination of red and violet components.

The set of chromaticity coordinates (x,y) provides a physical representation of the observation of the CL color. An easier and more suggestive description of the color is the use of the notions of the dominant wavelength and purity respectively. These two parameters are commonly used to quantify the color of and object illuminated with a light source exhibiting a spectral distribution $S(\lambda)$ (14) (141).

According to the set of equations [18] the illuminant $S(\lambda)$, is defined by the point $S(x_0, y_0)$ in the chromaticity chart. The observed color of the object (M(x,y)) is influenced by the nature of the incident illuminant $S(x_0, y_0)$. As shown in Fig. 14, the line passing from (x_0, y_0) through (x,y) intercepts the spectrum locus at a wavelength λ_D which is the **dominant wavelenqth**, i.e., the equivalent wavelength representing the color of the object. The **purity** p_e is defined as the ratio of the distance SM to the distance $S\lambda_D$ or:

$$p_e = \frac{x - x_0}{x(\lambda_D) - x_0} \text{ or } p_e = \frac{y - y_0}{y(\lambda_D) - y_0} \qquad [19]$$

When observing the CL emission there is no external illumination source and the observed CL color is defined by the (x,y) chromaticity coordinates which only depend on the spectral distribution $I^*_{CL}(\lambda)$ of the emission and the response function of the observer eye. For practical use it is however helpfull to use the dominant wavelength and purity parameters by combining the (x,y) chromaticity coordinates of the CL source with those (x_0, y_0) of a **white** reference light source. Applications of the quantitative color measurements to CL emissions have been illustrated by El Ali (23) studying CL properties of carbonates.

Possible artifacts

Artifacts may arise from spurious luminescence signals induced by backscattered electrons reaching some luminescent components within the specimen chamber. When the front window of the PMT was placed in the vacuum of the SEM for panchromatic CL emission, Remond and al. (106) showed that backscattered electrons induced luminescence of the glass window. Signals resulting from the luminescence of the analyzed minerals and of the detector window are detected simultaneously. For the case of a single crystal, the amount of impurities responsible for the CL emission is too low to provoke a sufficient atomic number variation to be detected on the backscattered electron image. Thus, the spurious luminescence of the PMT window is constant and acts as an offset to the CL intensity variations observed at the surface of the mineral. For the case of specimens containing several phases of different atomic number, the fluorescence of the front window of the detector will reflect the backscatter coefficient changes within the analyzed areas and the observed CL image will be equivalent to the sum of the .true CL image plus the backscattered electron image. Consequently, non-luminescent minerals can appear luminescent. It is thus important to verify that

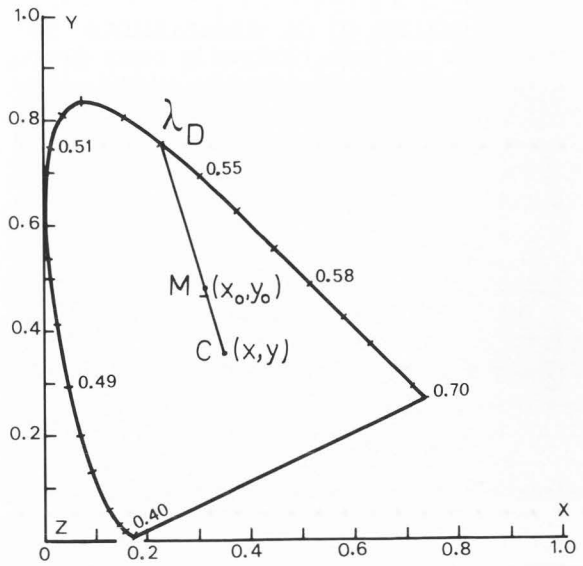

Fig 14: Chromaticity chart according to the Commission Internationale de l'Eclairage (CIE), (x_0,y_0) and (x,y) are the chromaticity coordinates of a reference white source and the CL emission respectively, λ_D is the dominant wavelength, i.e., the color of the observed CL.

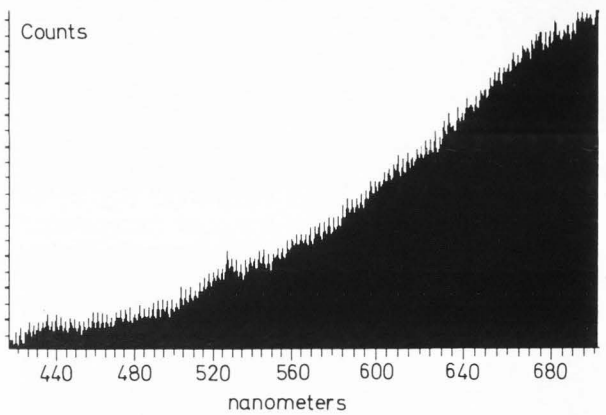

Fig. 15: Light resulting from the W filament of the electron gun measured after reflection on a Ag coated Cu target, using the multichannel CL spectrometer. The data acquisition time and the power of the intensifier were increased with respect to the normal conditions used for CL spectra acquisition of minerals.

any window which can be exposed to backscattered electrons within the specimen chamber consists of non-luminescent materials.

Another source of spurious light is the electron gun filament. A polished, Ag coated, pure copper specimen was used to measure the possible contribution of that extra light to the CL signal. The material studied has no CL property so that the

measured spectrum shown in Fig. 15 corresponds to the light originating from the filament after reflection at the surface of the metallic specimen. The intensity of this spurious light was very low and the gain of the intensifier was set much higher than was used for the analysis of CL emission observed at the surface of minerals. In addition, the reflectance of minerals is generally much lower than that of the Ag coated copper specimen so we conclude that the contribution of the filament light to the CL intensity was negligible.

Light reflection by a metallic mirror will lead to optical phase changes between the incident and reflected CL rays. However optical phase differences leading to interference will result from multiple reflection and transmission of the CL rays through any semi-transparent mirror placed in the optical path of the CL detection unit. The polychromatic CL emission of a mineral may be selectively affected by passing through any semi-transparent material leading in turn to a change in the observed color resulting from interference between the successively reflected and transmitted rays. Such phenomena may occur when using the optical microscope of the EMPA.

The CL emission spectrum of a synthetic diamond was recorded through the semi-transparent mirror of the optical device of the EPMA. The spectrum exhibited small features suggesting the existence of possible interfering peaks superimposed on a broad emission band. However this hypothesis was disproved since the same features still existed in the spectrum recorded after the semi-transparent mirror was removed. The change was that the CL intensity was increased with respect to that measured through the semi-transparent window. In addition, the low transmission efficiency within the blue region of the spectrum resulted from absorption by the glass windows placed along the optical path of the EPMA.

Relationship between the CL emission and the dielectric properties of minerals

CL microscopy and spectroscopy related to the presence of defects

It is well-known that CL microscopy can reveal heterogeneities which are not shown either by optical microscopy or by scanning electron microscopy. An example of a potential of CL microscopy has been illustrated in the present paper by comparing CL and transmitted light photographs of a quartz specimen (see Fig. 5 on color plate).

The relationship between the CL emission and the distribution of defects is shown in Fig. 16 comparing CL images with an X-ray topography image according to the Lang method of a natural quartz specimen. The specimen was a thin slice ($\approx$ 5 millimeters in thickness) cut perpendicularly to the c axis of a quartz crystal. As shown in Fig. 16a a narrow monochromatic X-ray beam collimated by a slit (f_1) impinges on the specimen at location (A). The specimen is orientated in such a way that the (hkl) planes are in Bragg position for the incident wavelength. The diffracted beams from the crystal are selected by a slit (f_2) and detected on a photographic plate (PP). The specimen is mechanically translated in front of the incident X-ray beam. As shown in Fig. 16b, a high density of dislocations is apparent. The sharp dark parallel lines of different orientations correspond to interference fringes. The CL images in Fig. 16c correspond to areas marked in Fig. 16b. Comparisons between the X-ray topography and CL images are difficult owing to the in-depth difference characteristic of these modes of observation. Transmission X-ray topography illustrates the distribution of defects within the bulk while the CL emission originates from only a few microns below the specimen surface. However, the CL images in Fig. 16c show that the dislocations are not luminescent and that the quartz has heterogeneous CL properties.

A discussion on the role of dislocations in the CL properties of semiconductors can be found in Yacobi and Holt (144). In minerals, there does not appear to be a single relationship between the CL emission and the type of dislocations based on transmission electron microscopy work. Several mechanisms leading to CL emission at dislocations have been investigated by Yamamoto (145) among others and the most probable mechanism was attributed to donor-acceptor pairs along the dislocation core.

Besides the intrinsic luminescence, the CL emission in minerals is generally an extrinsic property resulting from the presence of recombination centers or luminescence-activating ions associated with impurities. Correlations between CL images and the spatial distribution of impurities analyzed by means of X-ray spectrometry with the EPMA and by secondary ion mass spectrometry with the ion microprobe have been reported by Remond (101) (102). Before commenting on the role of impurities and on the use of CL emission as a possible analytical approach for identifying elements present at trace levels in minerals, we will briefly discuss the dependence of CL properties upon the excitation conditions.

Illustration of bulk charging

As indicated by equation [14] the CL emission is a complex function of the intensity and diameter of the incident electron beam. Ramseyer et al. (97) showed that an increase of the CL emission of quartz was obtained by evaporation of a conductive

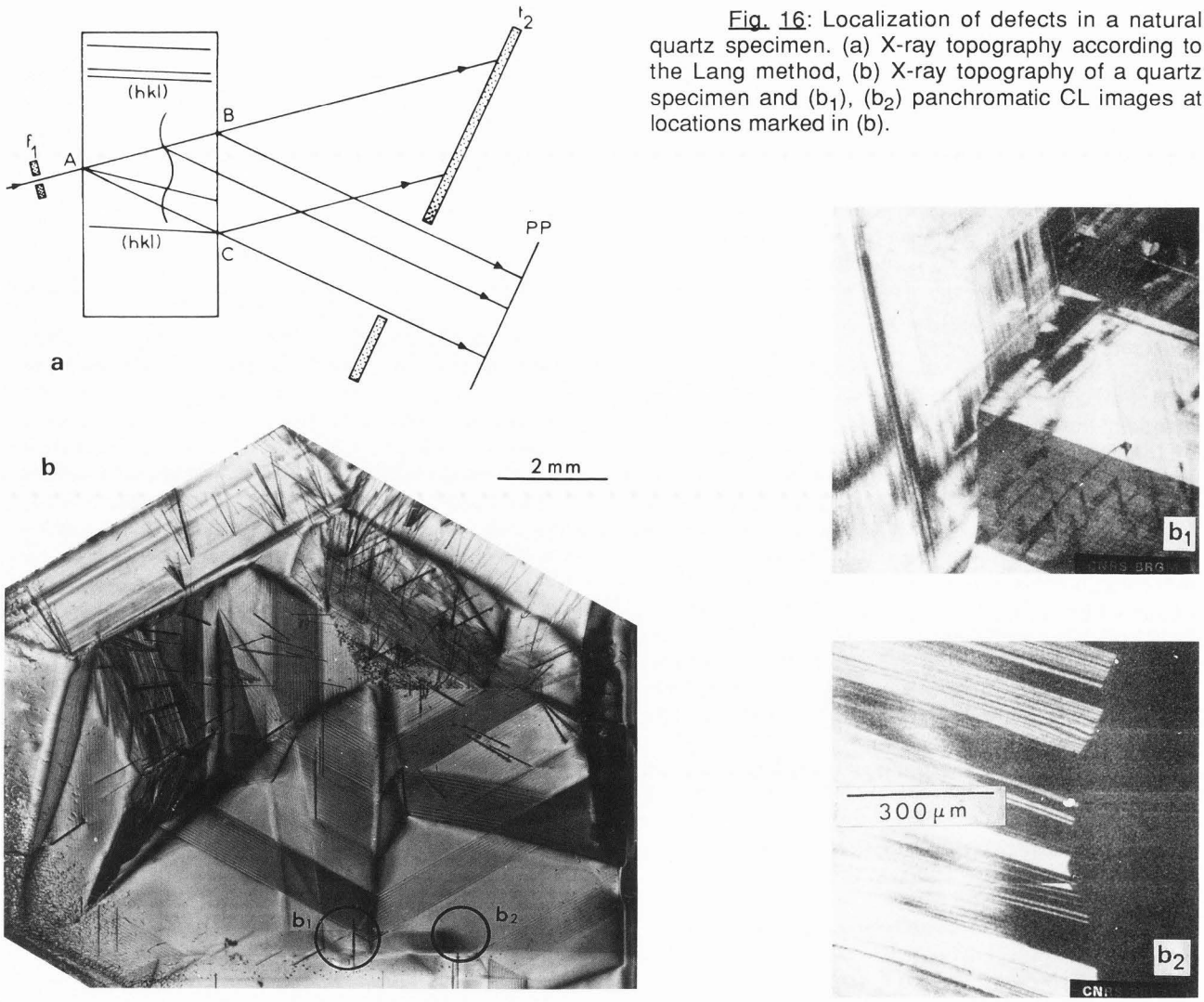

Fig. 16: Localization of defects in a natural quartz specimen. (a) X-ray topography according to the Lang method, (b) X-ray topography of a quartz specimen and (b_1), (b_2) panchromatic CL images at locations marked in (b).

aluminum layer onto the thin section surface. According to these authors the metal coating not only prevents surface charging but also acts as a mirror reflecting the CL intensity which is observed by transmission through the thin section. Besides a mirror effect induced by the surface metallic layer, the increase in CL intensity may also result from an electrical field enhanced CL intensity. According to Cazaux (13) a strong capacitor effect exists at the interface between the metallic surface film and the insulating substrate; the sign of the electrical field created within the insulator depends upon the energy of the incident electrons and the diameter of the beam.

The possible effect of CL property changes induced by bulk charging will be illustrated for the case of sphalerite crystals.

The variation of the interior field as a function of the incident beam diameter offers a possible explanation to the behavior of the CL emission of some natural sphalerite (ZnS) crystals as reported by Remond (102). This author showed that for the case of a natural sphalerite crystal containing Cu and Ga as major impurities, the relative intensity of the blue and the red emission bands varied with the diameter and the current of the incident electron beam. The larger the beam size or the higher the incident beam current at a constant spot diameter, the more intense was the red emission band with respect to that of the blue band. These variations are consistent with data reported by Mattler and Ceva (79) studying the **electroluminescence** of synthetic zinc sulfide crystals. These authors showed that the intensity of the blue and green emission bands in ZnS (Cu) phosphors exhibited parallel linear decreases as a function of the accelerating voltage. In contrast, for

zinc sulfide phosphors with several activators, the different emission bands exhibited different variations as a function of the applied voltage. As an example, in ZnS (Cu, Mn), the electroluminescence emission band associated with Cu predominates at low voltages and that due to Mn predominates at high voltages.

In a second experiment an approximately 20 μm electron beam diameter was used to illuminate a sphalerite crystal whose CL emission was observed and recorded on a photographic plate placed in front of the eyepiece of the EPMA. As shown in Fig. 17, a very intense luminescent ring developed around the beam spot and the blue-green CL intensity was also visible at distances greater than several tens of nanometers from it.

The propagation of CL far from the beam spot at the specimen surface may result from internal reflection of the generated photons within the bulk on differently orientated crystallographic planes below the surface. By placing mask disks on top of an InP specimen, Warwick (137) showed evidence for CL emission directed away from the beam spot after being reflected inside the specimen. For the case of Fig. 17 internal reflections on differently oriented subsurface planes would probably lead to more linear contours of the CL pattern than those observed. During electron bombardment, the X-ray photons generated within the specimen may contribute to the production of visible CL photons (Roentgeno-luminescence). However, the CL photons are emitted at distances from the beam spot which are too large with respect to the X-ray path length through the matrix. The possible effect of remote CL emission induced by an internal electrical field was therefore investigated.

An original method for revealing heterogeneities on an insulating surface has been proposed by Vigouroux et al.(135) (136) based on an electron multiplication cascade inside the insulator placed in an electrical field. According to the experiments by Vigouroux et al. (135) (136) a charge was implanted at the surface of a glass sample irradiated by a 20 keV electron beam creating a mirror effect. The electrical field was given by the negative charge created at the point marked A in Fig. 18a. The surface of the specimen was then bombarded at point B being at potential V_B due to the charge created at location A. The secondary electron image of the whole area containing the A and B spots in Fig. 18b showed that electrons are emitted far from the B spot. According to Vigouroux et al.(135) (136) the observed contrast and remote emission resulted from electron-hole pair recombinations at point defects. In presence of an electrical field, the electrons injected into the conduction band are accelerated and acquire enough energy to ionize the valence electrons of atoms on their trajectories and a cascade multiplication of electrons then arises.

The contrasts shown on the secondary electron image in Fig. 18b are remarkably similar to those observed on the CL image in Fig. 17b which is an elargement of a portion of the CL image in Fig. 17a. The area shown in Fig. 17b is located several tens of nanometers from the injection beam spot and intense CL rays are observed similar to the intense secondary electron rays in Fig. 18.

The remote CL emission in Fig. 17 is also very consistent with electroluminescent lines in ZnS (Cu) crystals as shown by Fischer (25). This author showed that within Cu-doped ZnS crystals placed in a strong electrical field a network of electroluminescent striations or lines following certain crystal orientations were observed. Thus, the analogy with the electron multiplication cascade in an insulator according to Vigouroux (135) (136) and the electroluminescence image reported by Fischer (25) suggests that the remote CL emission shown in Fig. 17 resulted from an electroluminescence mechanism involving the three following steps: i) ionization of donor levels, ii) acceleration of electrons raised into the conduction band and iii) ejection of electrons initially in centers due to impact of an accelerated electron.

Examples of beam damage

Cathodoluminescence color and intensity changes as a function of the excitation conditions will be illustrated for the case of zinc sulfide and quartz crystals successively.

Zinc sulfide crystals: Cathodoluminescence intensity enhancement during electron beam irradiation is shown in Fig. 19 for the case of a synthetic ZnS crystal. The region marked α in Fig. 19 has been exposed ten minutes more to the electron beam than the region marked β on the panchromatic CL image obtained with the SEM. Spectral analysis showed that the CL emission consisted of two bands in the blue and red regions respectively. The increase of the total CL intensity shown in Fig. 19 appeared to be the result of an increase of the intensity of the blue band and a decrease of the red one simultaneously. The local increase of CL intensity within the area that had received the higher electron dose was **permanent** even after the specimen was exposed to air before new CL examination. The observations in Fig. 19 are similar to those in Fig. 20 corresponding to an infrared CL image of ion implanted Si showing a bright patch from electron beam annealing according to Myhajlenko et al.(87).

Synthetic and natural quartz crystals: Time dependence of CL intensity has also been observed in some quartz specimens. Recently Ramseyer et al. (98) and Ramseyer and Mullis (99) distinguished between short-lived and long lived quartz luminescence. The first CL emission type refers to

Figs. 17, 18 and 19 are on color plate page 32.

quartz exhibiting a fast decrease of the CL intensity during the first tens of seconds of electron irradiation while the long-lived CL emission refers to emission whose intensity remains stable for a long period of time of electron bombardment.

As shown in Fig. 21, total CL intensity changes were also observed at the surface of a quartz specimen after prolonged examination at high magnification and turning to a lower magnification (102) (107). The CL intensity remained constant during of short period of electron bombardment, then rapidly increased (Fig. 21a) and then decreased to complete extinction (Fig. 21b).

The darkening of the area exposed to the highest electron dose (Fig. 21b) probably resulted from an electronic damage rather than from contamination, i.e., the formation of carbon or hydrocarbon-polymer films as a result of electron bombardment of adsorbed vacuum pump oil molecules.

The first reason to support a preferential beam damage for the case of Fig. 21 rather than a contamination effect is that the time taken to produce irradiation effects on CL intensity is only seconds or few minutes which is much shorter than that to build up any significant contaminant films. Wilson et al. (139) presented evidence for this speed of response difference in electron beam induced current (EBIC) images. In addition, no darkening effect was observed on the secondary electron image after the CL darkening in Fig. 20b had occurred. The second reason supporting an electron beam induced damage is that only quartz specimens which exhibited thermoluminescence from room temperature up to $\approx$ 300 °C also exhibited a short CL intensity enhancement before to decrease as in Fig. 21b. The positive correlation between specimens exhibiting thermoluminescence and CL variations as a function of electron dose suggests that the CL constrat changes shown in Fig. 21 are the consequence of a trap filling mechanism followed by a release of trapped electrons.

Although the temperature increase may contribute to the observed CL variations, electrical field induced by bulk charging probably play an important role in the mechanisms leading to charge redistribution during the electron bombardment.

The emission spectra from quartz vary considerably from samples of different origins and exhibit several closely spaced overlapping emission bands. Luminescence studies of undoped and doped quartz specimens showed that the most often observed emission bands are centered around 295 nm (4.2 eV) 380 nm (3.2 eV), within the domains ranging from 440 nm (2.8 eV) to 470 nm (2.6 eV) and from 510 nm (2.4 eV) to 570 nm (2.2 eV) and 650 nm (1.9 eV).

As shown in Fig. 22, only CL emission bands occuring at wavelengths greater than $\approx$ 400 nm were detected with the equipment used. All the CL emission bands we observed from a natural quartz specimen analyzed at room temperature (Fig. 22) were found to be consistent with the values reported above. Using the multichannel CL spectrometer equipped with the LPDA detector the intensities of the emission bands were studied as a function of the incident electron dose, i.e., as a function of the irradiation time at constant incident beam fluence. The spectra in Fig. 22 were sequentially recorded with a data acquisition time of 20 s per spectrum. The first acquired spectrum in Fig. 22 shows a broad continuous distribution with a maximum intensity at $\approx$ 630 nm (1.97 eV). The asymmetry of this emission band suggests the presence of two other bands of weaker amplitude centered around $\approx$ 550 nm (2.2 eV) and 470 nm (2.6 eV) respectively. The second spectrum in Fig. 22 obtained after 200 s electron irradiation shows an increase of the intensity of the three emission bands while the red emission band became narrower making more clearly visible the presence of the band centered at 530 nm (2.3 eV). Extending the beam irradiation up to 500 s led to a modification of the CL emission distribution as shown on the third spectrum in Fig. 22 revealing a strong increase of emission bands occuring within the blue and the green part of the visible spectrum.

The CL band positions we observed for this quartz specimen are consistent with most of the values reported in the literature for the case of amorphous and crystalline SiO_2. The peak at 380 nm (3.3 eV) often reported was not measured with the equipment used which exhibited a low detection efficiency at short wavelengths. Although not analyzed in our experiments, the emission band at 380 nm has been shown to vary as a function of the electron dose. Studying the CL emission of undoped and Ge-doped quartz specimens, Luff and Townsend (65) showed that at room temperature the intensity of the 380 nm emission band first increased before decreasing with the electron dose. This result is similar to the variations observed in Fig. 21 as a function of the irradiation time. Alonso et al.(1) showed that intense electron irradiation eliminates the 380 nm emission band induced by X-ray photons. Kristianpoller (53) showed that the photoluminescence peak measured at 370 nm and 440 nm exhibited thermal quenching between liquid nitrogen temperature and room temperature but that both emission bands showed an increase in intensity near room temperature as we observed for the case of the emission band at $\approx$ 470 nm on the CL emission spectrum of the natural quartz specimen (Fig. 22). Luff and Townsend (65) showed that for CL experiments carried out at room temperature the intensity of the band at $\approx$ 650 nm increased with the electron dose as we observed while the band at 470 nm decreased with dose which is opposite to our

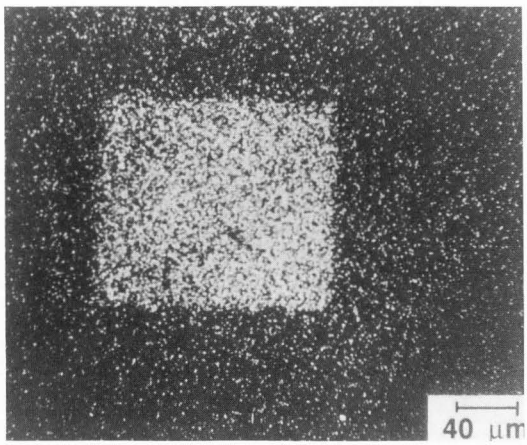

Fig. 20: Infrared CL micrograph of ion implanted Si showing a bright patch resulting from electron beam annealing (from Myhajlenko et al.(87)).

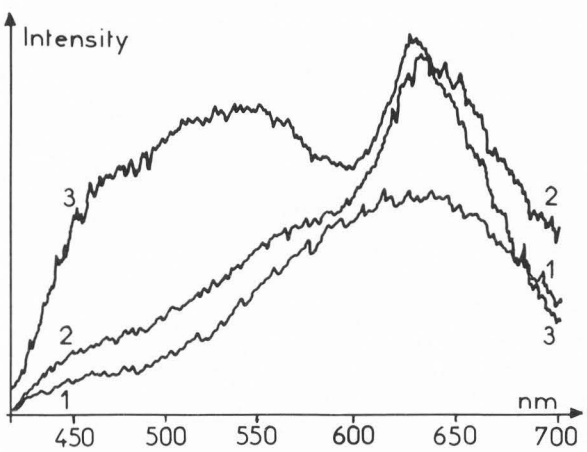

Fig. 22: CL emission of a natural quartz specimen as a function of the incident electron dose. Incident energy 20 keV, beam intensity 300 nA, beam spot 20 µm, acquisition time 20 s per spectrum. (1) 20 seconds, (2) 200 seconds and (3) 500 seconds beam irradiation.

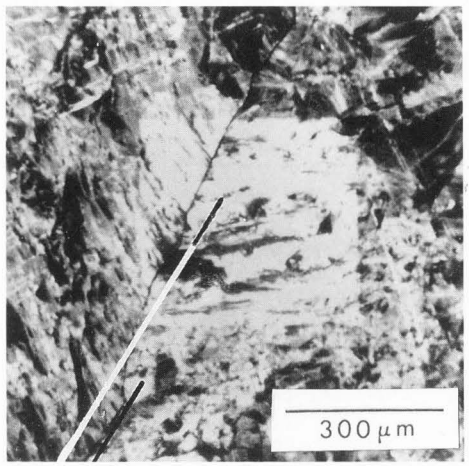

α β

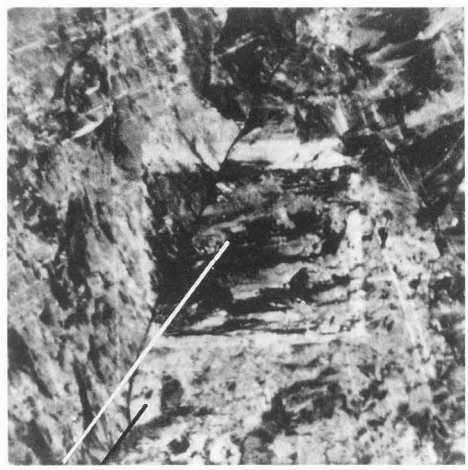

α β

Fig. 21: Variations of the total visible CL intensity as a function of electron dose within a natural quartz specimen. The region α in (a) has been exposed for 60 s more than the β region to a 25 keV/10 nA electron beam. The region α in (b) has been exposed ≈ 500 s more than the β region to the beam (from Remond et al. (107)).

observations. According to Luff and Townsend (61) the decrease with dose of the 470 nm emission band seems due solely to the temperature dependence of the competition between radiative and non-radiative decay routes within the emitting centres. In his experiments, Kristianpoller (53) recorded photoluminescence emission while heating the specimen from 80 °K to 500 °K so that the increase in intensity of the 440 nm band with electron dose was probably the sum of photo and thermoluminescence. However, Ramseyer et Mullis (99) showed that the blue short-lived cathodoluminescence in quartz, which was destroyed during electron bombardment, can be restored by heating the quartz specimen up to 500 °C for one day. Thus, the short-lived cathodoluminescence corresponds to an opposite mechanism to that of thermoluminescence. Although pure thermal quenching or stimulating effects cannot be definitely eliminated, modifications of the filling of traps and beam damage including bond breaking and impurity diffusion, are possible mechanisms for explaining the CL property changes as previously suggested by Remond et al. (107).

The defects responsible for the luminescence emission may be intrinsic (lattice) or extrinsic (impurities) in origin. As discussed in a review paper by Mc Keever (67) for the case of amorphous and crystalline SiO_2 the origins of the luminescence induced by a variety of incident energies are very complex and no unique explanation has emerged at present from theoretical and experimental studies. The emission band occurring at 380 nm seems to be related to trace impurities leading to a mechanism of electron recombination with a hole located at an impurity defect such as an Al-alkali center according to Alonso et al (l) or a growth defect according to the study of Luff and Townsend (65) on the CL emission of Ge-doped crystalline quartz. The emission band at ≈ 650 nm has been correlated with the presence of impurities such as Na^+, H^+ or OH^-. However, Luff and Townsend (65) associated this CL emission band with oxygen vacancies. As reported by Siegel and Marrone (119) the formation of the photo-luminescence band at 650 nm has been shown to develop after exposure of the quartz specimen to a ^{60}Co source and the emission was interpreted as the effect of dangling non-bridging oxygen ions **generated by the ionizing radiation**.

The blue emission band, commonly observed in all quartz and silicate minerals has been intensively studied. The band position of the blue luminescence lies between ≈ 440 nm and ≈ 490 nm depending upon the experimental conditions. Siegel (118) showed that the blue luminescence emission of crystalline quartz and silica induced by a 2 MeV electron pulse consists of a broad band in the region 460 nm - 480 nm (2.7 eV - 2.6 eV). This emission was explained as the result of the relaxation of an exciton formed during the electron beam pulse. The exciton was believed to be an electron-hole pair localized at a Si-O bond.

According to Guzzi et al (32) the blue photoemission band for all forms of SiO_2 should consist of three components with energy ≈ 4.2 eV, 3.1 eV and 2.7 eV related to defects of intrinsic origin. More particularly the emission band at 3.1 eV (≈ 400 nm) should be due to an O_2^- intrinsic defect. Nassau and Prescott (88) showed that an $(Al^{3+})^0$ center, i.e., a substitional Al^{3+} ion which has trapped a hole, could be associated with the emission band at 480 nm (2.55 eV). The same center should be also associated with emission bands at 620 nm (1.85 eV) and 355 nm (2.85 eV). Studying Ge-doped quartz, Luff and Townsend (65) associated the CL emission band occuring in the domain 510 nm - 570 nm (2.4 eV - 2.2 eV) with the decay of a self-trapped exciton following the Ge bond breaking. Recent studies by Fisher et al. (26), Tanimura et al. (130) and Itoh et al. (48) (49) showed that the blue emission band induced by electron pulse is a composite of two bands centered at 440 nm (2.8 eV) and 490 nm (2.5 eV) respectively and those authors demonstrated conclusively that these emissions are associated with the decay of self-trapped excitons. Studies of transient optical absorption revealed that **metastable centers are formed after generation of electron-hole pairs by the incident electron pulse**. The formation of the metastable center is accompanied by a large volume change indicating strong atomic rearrangement. The metastable centers are annihilated by emitting the blue luminescence. According to Itoh et al. (49) the 2.8 eV emission band is intrinsic (lattice) in origin while the 2.5 eV emission band is associated with impurities. The similarity of spectra for undoped and Ge-doped quartz led Fisher et al. (26) to the conclusion that the center associated with the 2.5 eV emission band should be similar to that associated with the 2.8 eV band but with one of the Si atoms replaced by Ge. The proposed mechanism for the complex blue CL emission of crystalline quartz is the decay of a self-trapped exciton. The existing models of self-trapped excitons have been discussed by Itoh et al. (48) (49) and Tanimura et al. (130) for the case of amorphous and crystalline SiO_2. According to these authors the most probable center, intrinsic in origin, associated with the 2.8 eV (440 nm) band should be a self-trapped exciton.

Cathodoluminescence spectroscopy as a possible analytical tool for studying trace elements in crystals

A strategy for trace element analysis

Cathodoluminescence microscopy has been shown to provide a rapid method for revealing the spatial distribution of defects, some of them being associated with the presence of impurities within minerals. However, CL spectroscopy as an analytical tool for the identification of impurities in minerals is not always feasible. While a unique relation exists between the wavelength (energy) of X-ray photons and the elements present in the target, no such unique relation exists between the CL emission peak or band energies and the nature of the impurities involved in the CL emission mechanisms. In addition, the CL emission is dependent on the mechanisms of the incident energy dissipation and on the dielectric properties of the crystals.

The example concerning alumina crystals studied by Schvoerer et al.(113) will be used to illustrate a possible analytical procedure leading to the identification of trace elements within a crystal by the use of its CL emission spectrum.

The CL spectrum in Fig. 23 illustrates a typical complex emission involving several mechanisms leading to the development of narrow and broad emission bands.

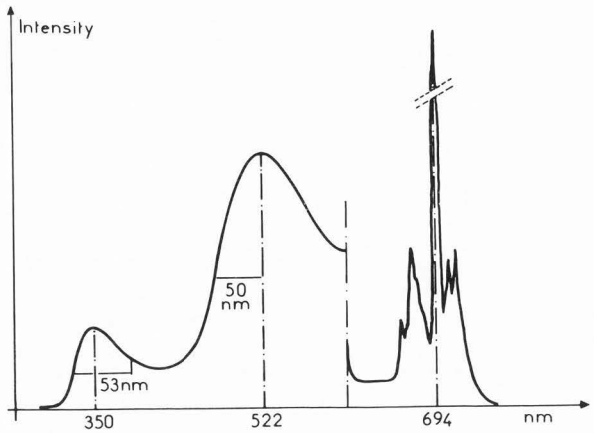

Fig. 23: CL emission of an α alumina crystal (from Schvoerer et al. (113)).

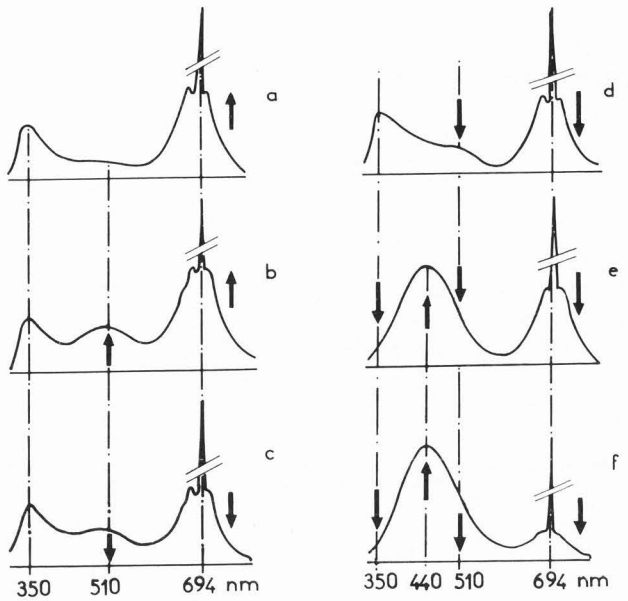

Fig. 24: CL emission spectra of Ti doped α alumina as a function of the Ti concentration. Figures (a) to (f) correspond to 10 ppm, 30 ppm, 100 ppm, 150 ppm, 600 ppm and 1500 ppm titanium successively. Note that both intensity of the the Cr^{3+} emission line (694 nm) and the emission bands at 410 nm and 510 nm associated with Ti changed with the Ti concentration (from Schvoerer et al. (113)).

An abundant literature exists on the role of Cr^{3+} ions in oxides and more particularly in alumina (see Fig. 1). These data suggest that Cr impurities could be the luminescent ions associated with the multiple narrow peaks occuring near ≈ 694 nm in Fig. 23. However, no assumption can be made from the experimental data to identify the nature of the defects associated with the bands centered near 350 nm and 510 nm.

In the absence of any general theoretical framework for relating CL spectra to crystal impurities, empirical approaches are mainly used and involve two steps. The first step consists of using non-destructive analytical techniques in order to have a spatially resolved analysis of the impurity contents within the material. The second step in the interpretation of the CL spectra is to identify among the detected impurities those which can play a role in the observed luminescence property. The identification of these elements must be used as a guide for preparing doped synthetic compounds under controlled conditions. Such an approach allowed Schvoerer et al. (113) to confirm that the Cr^{3+} ions were associated with the narrow emission peaks and that the emission band centered at ≈ 510 nm resulted from the presence of Ti^{3+} ions. However a complete understanding of the CL emission spectra can only be achieved by varying both the qualitative and the quantitative composition of synthetic compounds. Schvoerer et al. (113) showed that the relative intensity of the emission bands changed as a function of the impurity concentrations and that the existence of the broad band centered at ≈ 440 nm occurred only for Ti concentrations greater than a threshold of ≈ 600 ppm. According to Powell et al. (96) the emission band at 440 nm may result from Ti^{4+} ions.

The analytical approach illustrated by Schvoerer et al. (113) for the use of CL emission as an analytical tool is only applicable to materials containing only a small number of impurities or to industrial materials which acquired a particular property by adding known impurity(ies). In such situations it is possible to obtain a sufficient number of doped crystals with a specific impurity to draw a calibration curve of the CL features as a function of the concentration of the luminescent ions. The concept of using CL emission spectroscopy for quantitative analysis of a particular ion incorporated within a particular matrix has been discussed by Larach (56) for the case of Eu in Y_2O_3 and by Larach et al. (57) for Tm in ZnS.

In minerals, the situation is much more complex because a variety of trace elements can be found simultaneously in various sites within the host structure. An abundant literature relates the role of impurities in the luminescence spectra of synthetic zinc sulfide crystals (see for example S. Shionoya, (116)). It was thus tempting to directly use these empirical and theoretical data for the identification and the localization of trace elements in natural sphalerite (ZnS) minerals. Goni and Remond (29) and Remond (102) tried to derive the nature of impurities

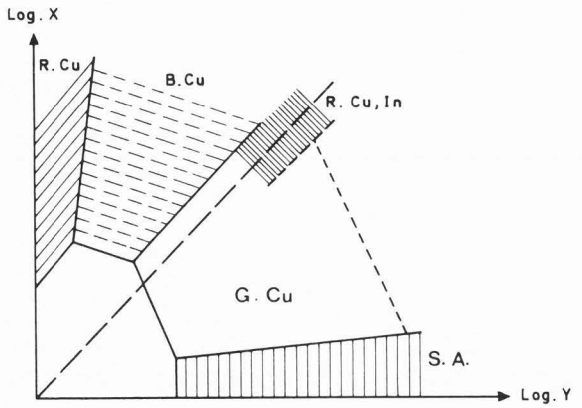

Fig. 25: Photoluminescence of synthetic zinc sulfide crystals as a function of the concentrations of the activators (X) and coactivators (Y). S.A., self activated luminescence (Zn vacancies), G:Cu green emission band associated with Cu as an activator, B:Cu blue emission band induced by Cu, R:Cu red emission band resulting from high Cu activator concentrations and R:Cu, In red emission band resulting from the presence of Cu as activator and In as coactivator (from Van Gool (133)).

in natural ZnS minerals by comparing their CL properties with the data available in the literature. These comparisons were made difficult because of (a) the crystallographic difference between the synthetic crystal giving the available CL data (wurtzite ZnS form) and the natural mineral (ZnS sphalerite), (b) the change in CL as a function of the incident electron dose leading to small shifts and variations in the relative intensities of the CL emission bands with respect to the available data concerning the photoluminescence (UV irradiation) of ZnS crystals, (c) the large variety of impurities which can be found in the natural minerals, and (d) the spectral dependence of CL associated with a given activator upon its concentration and the presence of other impurities acting as coactivators. Besides the quenching effect, high concentrations of an impurity or the presence of simultaneous impurities may lead to a modification of both the intensity and the spectral distribution of the CL emission making hazardous any relationship between the observed CL emission spectra and the impurities present in the crystal. The complexity in CL emission spectra interpretation is illustrated by the diagram in Fig. 25 from Van Gool (133) expressing the relationship between the luminescence and the concentration of the activators (Cu, Ag or Au) and coactivators (Al, Sc, Ga or In) in ZnS. As shown in Fig. 25 copper which is one of the most important activators in ZnS may induce four types of luminescence bands: the green G:Cu, the blue B:Cu, the red R:Cu, the red R:Cu,In emission bands accompanying the blue self-activated (SA) emission band.

The observed color of CL was not sufficient to directly identify the nature of the impurities but was used by Remond (102) as a guide for optimizing the experimental conditions for the analysis of impurities within natural sphalerite minerals using the EPMA. Similarly, using X-ray spectrometry and secondary ion mass spectrometry Remond (101) studied the variations of CL in cassiterite crystals (SnO_2) as a function of the distribution of the impurities, mainly Fe, Ti, Nb and W. However, the coincidence between the trace element distribution shown by comparing X-ray and ion images with CL images did not allow him to conclude that the detected impurities were the activators of the observed luminescence emissions. The empirical relationship between CL and impurities in cassiterite crystals was only used as a guide for trace element analysis.

Impurities with incomplete electronic shells (manganese and other transition metals and rare-earth ions) may exhibit characteristic luminescence spectra making possible their use for analytical purposes. Such possibilities are discussed and illustrated for the case of rare-earth element bearing minerals.

Specific problems of rare-earth luminescent ions

Characteristic CL spectra of rare-earth bearing minerals: The general representation of the electron configuration of rare-earth (RE) ions is $1s^2$ $2s^2$ $2p^6$ $3s^2$ $3p^6$ $3d^{10}$ $4s^2$ $4p^6$ $4d^{10}$ $4f^k$ $5s^2$ $5p^6$ $5d^1$ $6s^2$. The sole 5d electron only exists for Ce (Z = 58), Gd (Z = 64) and Lu (Z = 71). The $5s^2$ $5p^6$ electrons form two completely filled shells shielding deeper unpaired $4f^k$ electrons which are responsible for the optical absorption, electron paramagnetic resonance, luminescence emission and magnetic properties of (RE) elements.

The luminescence of rare-earth ions $(RE)^{n+}$ in solids results from a de-excitation process of the $(RE)^{2+}$ and $(RE)^{3+}$ ions. The emission spectra are associated with two types of transitions, i.e, f —> f and f —> d respectively. For the case of $(RE)^{2+}$ the f —> d and f —> f transitions lie close to each other. In $(RE)^{3+}$ luminescent ion spectra the f —> d transitions occur in the UV region and the f —> f transitions lead to line spectra consisting of narrow and weak lines. Because of the shielding effect of the $5s^2$ $5p^6$ electrons the f —> f transitions are moderately affected by the action of the crystal field so that only slight displacements of the emission lines are observed from one crystal to another. This situation is summarized in Fig. 26 showing the CL peak positions for some (RE) luminogen ions in several minerals (69) (70) and (73).

CL emission spectra were used by Roeder et al. (108) for identifying (RE) elements in apatite minerals originating from carbonatites, pegmatites

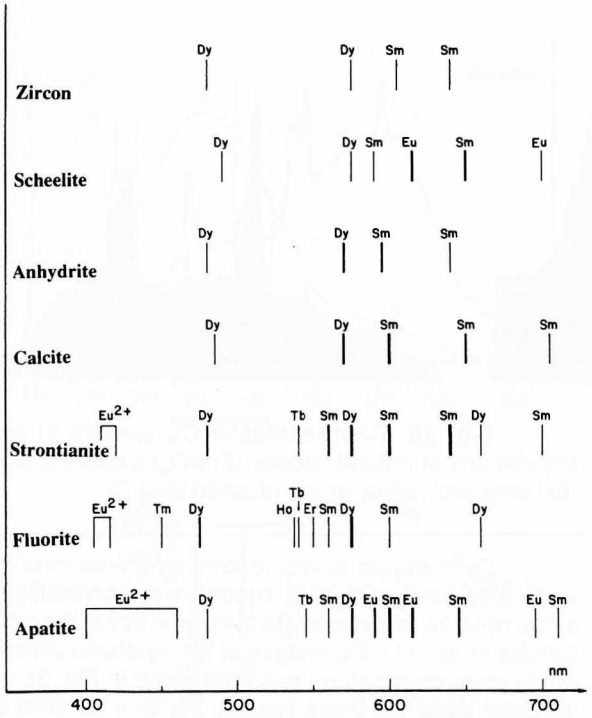

Fig. 26: Wavelength position of CL emission peaks associated with the presence of $(RE)^{3+}$ and Eu^{2+} luminescent ions in some minerals. (Data compiled from ref (70) (71) (73) (108)).

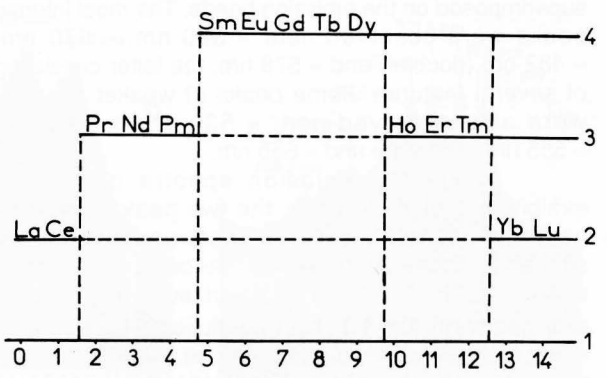

Fig. 27: CL emission properties of rare-earth ions (l) number of 4 f electrons, (2) broad emission bands, (3) narrow emission peaks when present at trace levels and (4) narrow emission lines when present as major constituents or trace elements in solids. (from Monod-Herzen (84)).

and granites. The CL spectra exhibited emission bands which were assigned to the presence of Sm^{3+}, Dy^{3+}, Tb^{3+}, Eu^{3+}, Eu^{2+} and Mn^{2+} by comparing CL properties of the natural minerals with those of synthetic doped crystals. Mason and Mariano (77) used CL emission to study (RE) bearing synthetic calcites. Spectra from Sm, Tb and Dy-bearing samples consisted of narrow-band maxima resulting from their incorporation in the 3^+ oxidation state. Substitution in both the 2^+ and 3^+ states was possible for Eu.

One limitation in qualitative analysis of CL emission spectra is that not all (RE) ions will lead to narrow emission lines. As shown in Fig. 27 according to Monod-Herzen (84) only the Sm, Eu, Gd, Tb, Dy ions have CL spectra exhibiting narrow lines when these elements are either the major components or present as impurities in the minerals. The other (RE) ions lead to broad emission bands (La, Ce, Yb, Lu) or to sharp lines only if present in very small amounts (Pr, Nd, Sm, Ho, Er, Tm). In addition, quenching effects due to self-absorption and sensitized luminescence mechanisms must be considered as discussed by Van Uitert (134) and Blasse and Brill (5) for the case of the luminescence characteristic of (RE) ions. The detection of narrow luminescence lines of some $(RE)^{3+}$ luminescent ions can be made difficult due to the presence of broad emission bands resulting from the presence of $(RE)^{2+}$ ions, Mn^{2+} or all other defects in the crystal structure. Consequently, we must keep in mind that **CL emission spectra will not provide a qualitative overview of all the RE which can exist in the host structure.**

Applications to zircons: Zircon ($ZrSiO_4$) is well-known to accept (RE) elements in its structure. Ohnenstetter et al. (91) distinguished two populations of zircons based on their blue or yellow-green CL color respectively. All zircons belonging to one population exhibited the same shape of CL emission spectra and differed only from one specimen to another by changes in the intensity of the CL emission bands. Similar variations in CL intensity also existed within each crystal as previously illustrated by spectra in Fig. 8 corresponding to the three locations marked in Fig. 7 (color plate).

The spectra in Fig. 28 summarize two representative CL emission spectra of the two populations of natural zircons exhibiting a blue or a yellow-green CL color. We investigated the possibility of identifying different impurities from these CL spectra.

As shown in Fig. 28 the CL emission spectrum of a zircon characterized by a yellow-green color consisted of broad asymmetrical bands centered near ≈ 400 nm (A),500 nm (B) and 580 nm (C). For the case of zircons exhibiting a blue CL color, the three bands marked (A), (B) and (C) in Fig. 28 were also observed. Two bands centered near 290 nm (D) and 350 nm (E) were also measured. The relative intensities of these emission bands varied as a function

of the analyzed areas. Narrow peaks were superimposed on the emission bands. The most intense peaks were observed near ≈ 390 nm, ≈ 470 nm, ≈ 482 nm (doublet) and ≈ 578 nm, the latter consisting of several features. Some peaks of weaker intensity were also observed near ≈ 530 nm, ≈ 545 nm, ≈ 555 nm, ≈ 615 nm and ≈ 655 nm.

In the CL emission spectra of zircons exhibiting a blue CL color, the two peaks occurring near 485 nm and between 570 nm and 580 nm are similar to those reported for the case of minerals containing Dy^{3+} ions as summarized in Fig. 29. As also shown in Fig. 29, high resolution CL emission spectra showed that the peak at ≈ 485 nm is a doublet consisting of two lines centered at 482 nm and 486.5 nm. Likewise, the peak ranging from 570 nm to 580 nm consists of at least seven narrow lines. These fine structures are consistent with the high resolution spectra shown in Fig. 29 according to Marfunin (68). The group of lines at 482 nm and 486.5 nm correspond to transitions of the type $4\ F_{9/2} \longrightarrow 6\ H_{15/2}$ and the multiplets near 578 nm correspond to $4\ F_{9/2} \longrightarrow 6\ H_{13/2}$ transitions within the Dy^{3+} ions. Transitions from the $4\ F_{9/2}$ level to the $6\ H_{11/2}$ level lead to luminescence emission near 660 nm. As shown in Fig. 29 a weak emission band was found to be present on the CL emission spectrum of a zircon emitting a blue CL color and may correspond to the $4\ F_{9/2} \longrightarrow 6\ H_{11/2}$ transitions within Dy^{3+} ions.

Comparisons in Fig. 29 between our experimental spectra and those obtained by Marfunin (68) and data from Mariano (71) suggested Dy^{3+} ions to be a possible candidate acting as luminescent ions associated with the peaks occuring near 482 nm, 578 nm and 660 nm. In order to support this hypothesis a Dy_2O_3 single crystal was analyzed. The specimen was a synthetic crystal prepared at the Ecole Nationale Superieure de Chimie de Paris, using the Verneuil crystal growth method (59). The Dy^{3+} ion is known to be a luminescent ion when present either as a major or a minor constituent in a solid. As expected the CL emission spectrum of the Dy_2O_3 crystal (Fig. 30) exhibited two groups of lines near 482 nm and 578 nm. However, as shown in Fig. 30 for the case of the Dy_2O_3 crystal, these peaks were found to be sharper than those occurring at the same wavelengths in the CL spectrum of the natural zircon. In addition, no fine structures in the CL peaks were observed for the case of the Dy_2O_3 crystal. The difference of line features on the CL peaks probably resulted from differences in level splitting as a function of the chemical environment of the Dy^{3+} ions. These observations indicate that the choice of reference materials is less flexible for the case of CL emission spectra than for the case of X-ray spectrometry.

Figs. 5, 7, 11 and 31 are on color plate page 31.

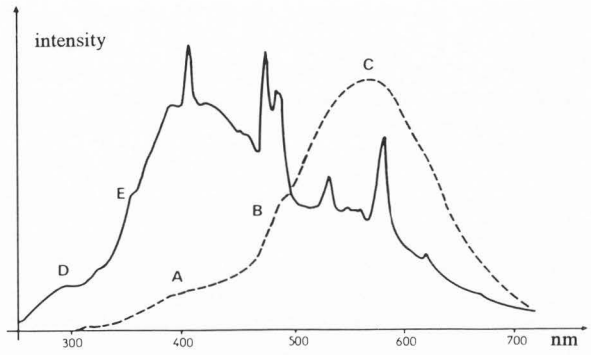

Fig. 28: Representative CL spectra of two populations of natural zircons ($ZrSiO_4$) exhibiting blue (full line) and yellow-green (dashed line) CL.

Dy^{3+}-doped and undoped synthetic zircons were also analyzed. The zircons were crystallized according to a procedure already described by Caruba et al. (11). CL images of the synthetic zircons which grew on a natural seed are given in Fig. 31 on the color plate. On these images, the blue CL color of the seed is clearly visible. The CL emission of the grown zircon are more or less visible depending upon the nature of the $(RE)^{3+}$ ion added to the medium.

CL spectra of the seed and Dy^{3+}-doped zircon overgrowth are shown in Fig. 32. The full spectra in Fig. 32a were obtained by means of the scanning CL spectrometer providing a high transmission efficiency in the short wavelength domain. Spectra in Fig. 32b were obtained with the multichannel CL spectrometer equipped with the LPDA detector. The seed exhibited a much higher intensity than that of the artificially grown doped areas. The broad continuous emission within the domain 350 nm - 650 nm was common to all CL spectra. This broad continuum seems to be the sum of several emission bands with maxima near ≈ 400 nm, ≈ 450 nm and ≈ 550 nm – 600 nm respectively. The intensity ratios of these emission bands were found to vary as a function of the analyzed locations within the zircon ring grown around the seed. Emission band occurring in the short wavelength region of the spectrum near 290 nm was only observed for the case of the natural seed emission spectrum. The emission band (A) near 400 nm in the CL emission spectrum of the undoped and Dy^{3+}-doped zircons is shifted towards ≈ 380 nm for the case of the natural seed exhibiting a blue CL color (Fig. 32). This effect may result from the presence of a band centered near ≈ 350 nm marked (E) in Fig. 28 for the case of a natural zircon. The peak to continuous emission intensity ratio was much lower for the case of the artificially doped zircon than for the natural seed. However, the positions of the

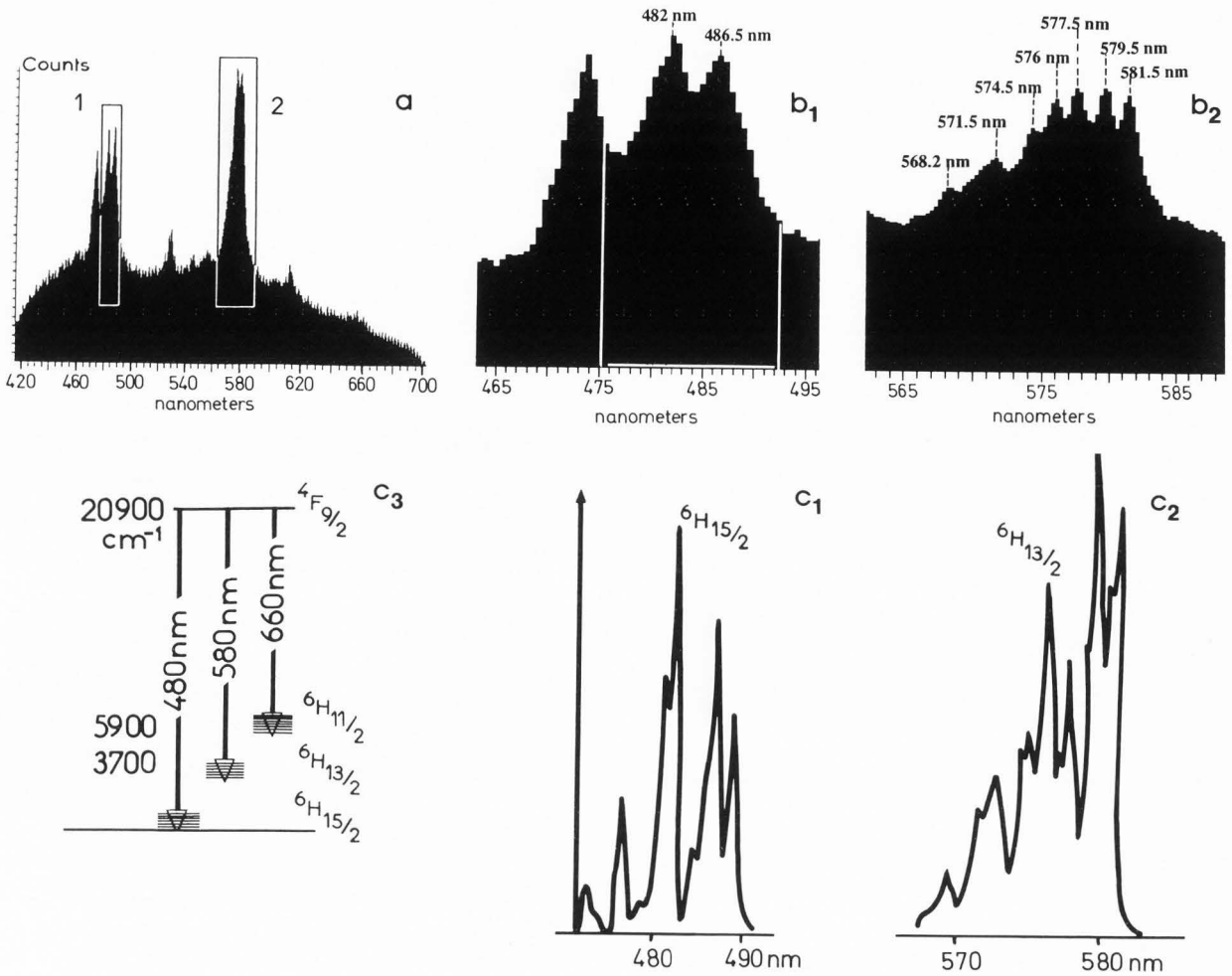

Fig. 29: Luminescence spectrum and energy level diagram for Dy^{3+} in zircon: (a) experimental spectrum using a multichannel CL spectrometer showing the existence of fine structures of CL peaks near 482 nm (b_1) and near 575 nm (b_2) and corresponding fine structures (c_1) and (c_2) of the peaks associated with the radiative transitions shown in (c_3) according to Marfunin (68).

peaks observed near 482 nm and 578 nm on the CL emission spectra (Fig. 32b) of the Dy^{3+}-doped zircon are consistent with the two groups of narrow peaks assumed to result from Dy impurities in natural zircons.

As reported by Ohnenstetter et al. (91) point chemical analyses with the EPMA showed that P, Hf, Y, Dy, Er and Yb were present as impurities within the zircons exhibiting a blue CL color. As shown in Fig. 27, Yb may induce a CL emission band while Er at trace levels may be responsible for characteristic narrow CL peaks.

The possible role of Er^{3+} ions producing some of the lines observed in the CL emission spectra of some natural zircons is suggested by studying a synthetic zircon prepared a century ago by Hautefeuille (35). The synthetic zircon was analyzed by mass spectrometry using a laser pulse to ablate a small amount of material directed into an inductively coupled plasma torch for ionization and subsequent mass analysis with a quadrupole mass spectrometer (ICP-MS). The analysis showed the presence of U, Th, Er as minor impurities with possibly Dy at very low concentration. However, no quantitative data were derived from the raw mass spectrum.

As shown in Fig. 33, very weak peaks can be observed in the CL emission spectra of the synthetic zircon originating from Hautefeuille's collection.

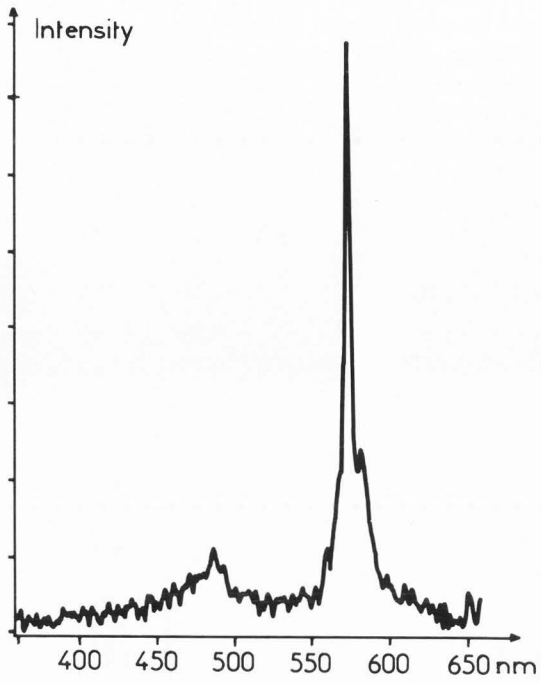

Fig. 30: CL emission spectrum of a synthetic Dy_2O_3 single crystal (**multichannel** spectrometer equipped with a 150 gr/mm grating).

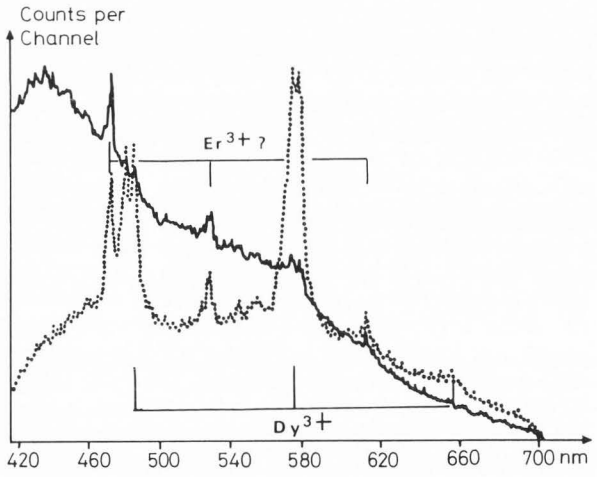

Fig. 33: CL emission spectrum of a synthetic zircon originating from the Hautefeuille's collection (135). For comparison, the CL emission spectrum of a natural zircon exhibiting a blue CL color is also shown.(····)

Fig. 34: CL spectra for several electron doses of a synthetic zircon containing U, Th, Er and Dy as impurities (Fig. 33). Spectra were recorded after 20 s, 200 s and 500 s to the electron beam (E = 20 keV, i = 300 nA, beam spot = 20 μm).

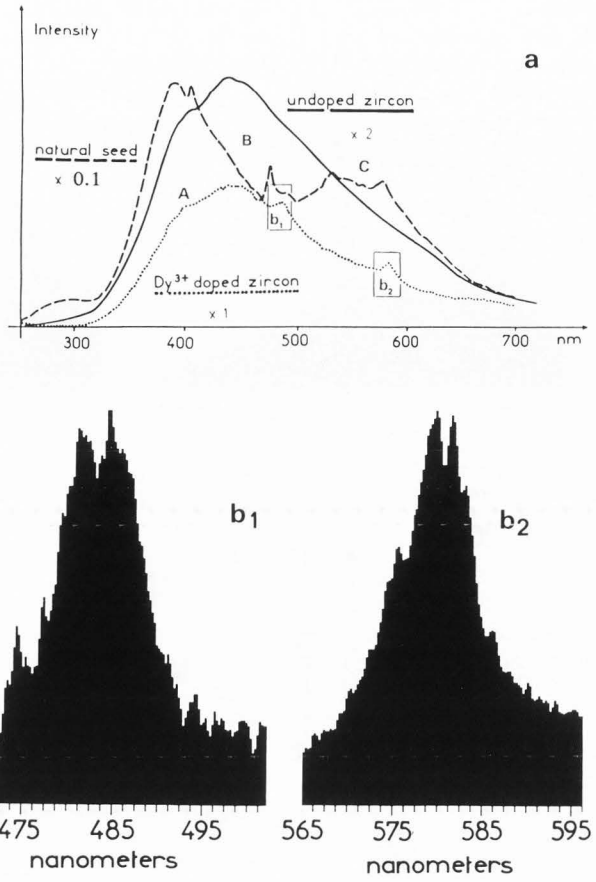

Fig. 32: CL spectra (**scanning** grating based spectrometer) of (a) the natural seed, the Dy^{3+}-doped grown zircon and the undoped synthetic zircon and (b) high resolution analysis (**multichannel** spectrometer) of the peaks centered around 482 nm and 578 nm for the case of the Dy^{3+}-doped zircon.

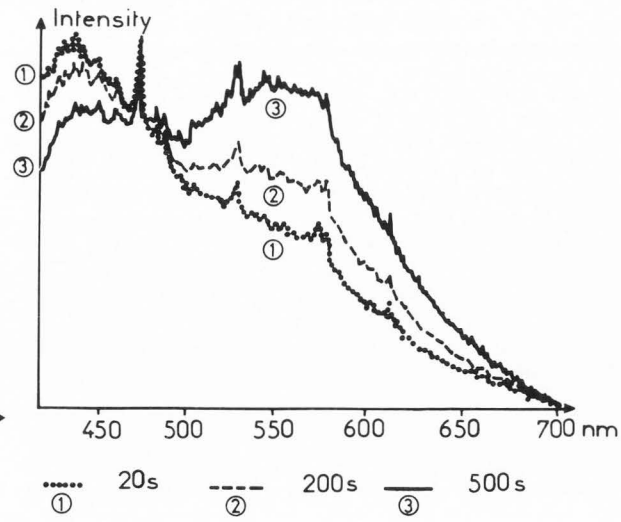

Although the narrow peaks had very weak intensities above the intense broad emission bands, the two peaks near 480 nm and 580 nm characteristic of Dy^{3+} ions can be detected. The other small features observed at 470 nm and 530 nm are also present in the CL emission spectrum of the natural zircon exhibiting a blue CL color. These two peaks occurring at 470 nm and 530 nm may tentatively be correlated with the presence of Er in both crystals. In addition, as shown in Fig. 34, the CL emission of the synthetic zircon was found to be very sensitive to the total electron dose while the CL emission spectrum of the natural zircon did not exhibit similar behavior as a function of the irradiation time.

The CL emission spectra of natural zircons exhibiting a blue CL color consists of narrow peaks superimposed on broad emission bands. The narrow peaks seems to be characteristic of $(RE)^{3+}$ ions but only those occurring near 482 nm and 578 nm can be associated with certainty with the presence of Dy^{3+} ions based on data available in the literature and CL spectra of a Dy^{3+}-doped synthetic zircon. Other heavy (RE) elements detected with the EPMA and particularly Er^{3+} may be responsible for some of the other CL narrow peaks. A narrow peak occurring at 400 nm was observed in CL spectra of zircons exhibiting a blue CL color (see Fig. 9). The luminescent ion associated with the peak at 400 nm is still unknown. Doped zircons are necessary to definitely identify the luminescent ions accompanying the Dy^{3+} ions. CL images at selected wavelengths (Fig. 13) showed different contrasts for the spatial distribution of the CL intensity associated with the narrow CL peaks or the broad emission bands respectively, indicating that the blue CL emission variations probably resulted from two contributions, i.e., an extrinsic luminescence (RE^{3+} ions) and an intrinsic luminescence (lattice defects). Four distinct emission bands were found centered near ≈ 290 nm, 350 nm, ≈ 400 nm, 450 nm and 560 nm - 580 nm. As shown in Fig. 28 the blue CL color is dominated by the very intense emission band peaking near ≈ 400 nm compared to the intensity of the emission band centered near 560-580 nm while the opposite situation is encountered for the case of zircons exhibiting a yellow-green CL color. (RE) elements are probably present in very small amounts in the zircon exhibiting a yellow-green CL emission as shown by Halden et al. (34) studying similar zircons by means of the proton microprobe (PIXE). However, the difference in the blue and yellow green CL color resulted from the difference in the intensity of the emission bands rather than from the presence or abscence of the narrow CL peaks associated with the $(RE)^{3+}$ luminescent ions.

According to Iacconi and Caruba (44) (45) (46) who studied the thermoluminescence of X-ray irradiated zircons, the band observed at 290 nm should be specific to $(OH)^-$ groups. This weak emission band was only observed for the case of zircons emitting an intense blue CL intensity and was not observed (or was too weak to be detected) in CL emission spectra of natural zircon exhibiting a yellow-green CL color nor for the case of doped or undoped synthetic zircons.

The CL spectrum in Fig. 32 for the case of an undoped synthetic zircon shows evidence for two bands A and B partly resolved, centered at 400 nm and 450 nm respectively. These two bands are common to all spectra of natural zircons (Fig. 28), the undoped and the Dy^{3+}-doped synthetic zircons (Fig. 32). According to Iacconi and Caruba (46) this emission band should be intrinsic in origin and related to SiO_4^{4-} groups. The emission band labelled B in Fig. 32 is asymmetrical with a tail on its long wavelength side. The intensity of the tail was found to vary among specimens or within the same zircon grain leading to the appearance of a band centered near 560-580 nm; this band is the most important emission structure associated with the zircon exhibiting a yellow-green CL color (band labelled C in Fig. 28). By analogy with the emission bands reported for the case of doped quartz we investigated for a possible mechanism of an intrinsic luminescence involving vacancies resulting from the incorporation of impurities. As discussed by Ohnenstetter et al.(91), EPMA analyses showed that Hf was present in all their specimens whatever their CL color. For both populations of zircons the Hf/Zr ratio varied from ≈ 0.005 to 0.018. This observation led to the conclusion than Hf may have a role in promoting or suppressing the CL emission but cannot be responsible for the change from the blue to the yellow-green color. In addition, CL microscopy showed that the higher was the Hf concentration, the lower was the CL intensity.

It is well known that zircons can easily accept yttrium as an impurity. The incorporation of yttria within zircon leads Dennen and Shields (19) to propose the tetravalent substitution between zircon and xenotime (YPO_4) which implies that Zr^{4+} is replaced by Y^{3+} in the octahedral site whereas P^{5+} replaces Si^{4+} in the tetrahedral site. As discussed by Ohnenstetter et al. (91) quantitative analyses with the EPMA showed that the Y concentration reached ≈ 2 % within zircons exhibiting a blue CL color, a value ten times greater than that encountered within the zircons characterized by a yellow-green CL color.

Ohnenstetter et al. (91) showed that for the case of the natural zircons exhibiting a blue CL color, the measured (Y + RE) atomic concentration was greater than that of P indicating that another substitution scheme must exist in addition to that proposed by Dennen and Shields (19). Caruba (10)

suggested the following expression of the zircon formula:

$$\left(Zr^{4+}_{1-\varepsilon}\,(Y+RE)^{3+}_{\varepsilon}\right)(SiO_4)_{1-x}\,(OH)_{4x-\varepsilon}\,\square_{\varepsilon} \qquad [20]$$

where $\square$ are vacancies accounting for the excess of $(Y + RE)^{3+}$ ions not compensated by P^{5+} replacing Si.

It is thus tempting to correlate the emission band centered at ≈ 350 nm with an electron recombination with holes at the vacancies resulting from $(Y + RE)^{3+}$ ions which were found to be present in zircons emitting a blue color and absent (or present in a lesser extent) in zircons exhibiting a yellow-green CL color.

Yttrium was heterogeneously distributed within the zircons and comparisons between the CL emission and EPMA data showed that the higher were the yttrium and REE concentrations, the lower was the intensity of the blue CL. The relationship between the Y and Dy concentrations and the intensity of the blue CL emission was previously illustrated by the X-ray images in Fig. 12 showing that the bright patches on the color CL images (Fig. 7 on color plate) were associated with simultaneous decreases in Y and Dy concentrations with respect to the distribution of these impurities within the sector zoning. The observed negative correlation between the Y and Dy concentrations and the intensity of the blue CL color is consistent with the data reported by Hoffman and Long (38) for the case of a zircon exhibiting an unusual sector zoning similar to that illustrated in the Fig. 7 (color plate).

Increasing the Y concentration also increases the number of lattice defects (creation of vacancies, lattice parameter changes...) which may lead to a quenching of the CL intensity. The change in CL intensity inside the sector zoning may also result from small changes in lattice expansion or from a slight misorientation of parts of the crystals probably associated with the splitting of the sectors as suggested by Hoffman and Long (38).

Besides the changes in the lattice parameters, and the creation of vacancies resulting from the presence of impurities, structural damages may be caused by the radioactive decay of uranium which is always present in zircon. Fielding (24) showed that the presence of uranium at a few ppm level is required for the formation of color centers in zircons (hyacinth) and that its distribution correlates positively with the changes in the fluorescence emission.

According to Nicholas (89) the broad photoemission band centered near 600 nm is associated with lattice defects resulting from the radioactive decay of the uranium present at trace levels rather than with U^{4+} luminescent ions which are known to be responsible for the optical absorption spectra of zircons.

Consistent with the data reported above and those obtained for the case of the zircon synthesized by Hautefeuille (35) containing U and Th as impurities (Fig. 34) the emission band occurring near ≈ 580 nm observed in all natural specimens can be tentatively associated with a mechanism involving lattice defects induced by the actinides present at concentration levels much lower than those detectable with the EPMA.

The changes in CL emission spectra of the synthetic Hautefeuille's zircon as a function of the irradiation dose (Fig. 34) are consistent with thermoluminescence emission properties of X-irradiated zircons as reported by Iacconi and Caruba (44) (45) and Kirsh and Townsend (52). As for many silicate minerals containing SiO_4^{4-} groups, a near UV emission band was found to occur in the thermoluminescence emission of zircons X-irradiated at liquid nitrogen temperature. Iacconi and Caruba (45) attributed the emission band between 340 nm and 450 nm to the thermal release of electrons and holes produced by the irradiation and then trapped on Si^{4+} and adjacent O^{2-} ions. Studying thermoluminescence emission spectra of zircons X-irradiated at room temperature, Kirsh and Townsend (52) showed that the near UV emission band becomes insignificant above 180 °C. The existence of the emission band centered near 430 nm in Fig. 34 probably results from bond breaking of the SiO_4^{4-} groups by the incident electron beam. The decrease of the intensity of this emission band as a function of the irradiation time may be tentatively attributed to a thermal increase of the zircon crystal when the electron irradiation time is prolounged. CL experiments at low temperature are necessary to support this assumption.

The increase in the intensity of the CL emission band centered near 550 nm (Fig. 34) as a function of the electron dose is similar to that observed in Fig. 22 for the case of a quartz specimen. By analogy with the results from Luff and Townsend (65) for Ge-doped quartz specimens, the behavior of the CL emission band near 550 nm shown in Fig. 34 corresponding to the Hautefeuille's synthetic zircon, may reflect an electron beam damage leading to oxygen vacancies.

Several models were proposed to explain the occurrence of $(RE)^{3+}$ spectral lines in the thermoluminescence emission spectra of zircon as discussed in Iacconi and Caruba (44) (45) and Kirsh and Townsend (52).

The luminescence of $(RE)^{3+}$ should result from the energy transfer from the emission of the SiO_4^{4-} group, the near UV emission band being partially absorbed by the $(RE)^{3+}$ ions and re-emitted as $(RE)^{3+}$ lines. A second explanation is based on a "charge - conversion model". According to this model, some of the $(RE)^{3+}$ ions are reduced during the irradiation to $(RE)^{2+}$ by capturing electrons. The holes

produced by this process are trapped. Recombinations of holes with $(RE)^{2+}$ ions occur, producing $((RE)^{3+})^*$ ions in excited energy states. The relaxation of these ions to the ground state leads to the luminescence emission. The charge - conversion model is summarized as below:

$$\left.\begin{array}{l}(RE)^{3+} \longrightarrow (RE)^{2+} \text{ hole (irradiation)} \\ \text{released hole} + (RE)^{2+} \longrightarrow ((RE)^{3+})^* \text{ (heating)} \\ ((RE)^{3+})^* \longrightarrow (RE)^{3+} + h\nu\end{array}\right] \quad [21]$$

The thermoluminescence experiments of zircon X-irradiated at room temperature carried out by Kirsh and Townsend (52) were found to be consistent with the charge - conversion model (relation [21]). This model is also apparently compatible with the CL emission spectral lines of the synthetic and natural zircons containing (RE) as impurities. As shown in Fig. 34 the height of the narrow CL emission lines remained constant while the intensity of the underlying broad emission bands varied as a function of the irradiation time. Assuming a model based on the transfer from the emission of the SiO_4^{4-} groups should lead to a simultaneous decrease of the near UV emission band and the narrow $(RE)^{3+}$ spectral lines; an effect which is not observed.

CL emission as a signature of composition and genesis of minerals

Applications of CL to carbonates

Carbonates such as calcite ($CaCO_3$) and dolomite ($CaMg(CO_3)_2$) can crystallize in a wide range of temperature. Carbonates originating from potential oil-bearing rocks can easily incorporate Mn^{2+} ions in their structure as the temperature of formation increases. Mn^{2+} being an essential luminescent ion, the luminescence property of carbonates was intensively studied. In some cases, (RE) elements, frequently associated with manganese, contribute to the CL emission. On the contrary Fe^{2+}, or possibly Fe^{3+}, is believed to behave as a quencher, though the problem is not entirely solved. One has to remember that manganese is also the main activator, responsible for the thermoluminescent properties displayed by many carbonates. Medlin (80) attributed the glow peak emission observed in calcite, dolomite, aragonite and magnesite to transition in the Mn^{2+} ion. This author also studied the quenching effect of some ions. Fe^{2+}, Co^{2+} and Ni^{2+} in low concentrations do not affect the Mn^{2+} thermoluminescence in calcite but they are quenchers in aragonite, dolomite and magnesite.

Crystal growth and zoning: Crystalline heterogeneities frequently cannot be well seen by petrographic examination and, in most studies of natural materials, X-ray topography by the Lang method is not in routine use. CL is a very convenient tool to recognize zoning during the crystal growth. In particular, overgrowths can be observed on primary crystals, based on a change in CL color, and the method has been frequently used for examining sedimentary units exhibiting a potential behavior as oil reservoirs. For instance, Sippel and Glover (123) studied the reduction of porosity in carbonate rocks by late calcite filling vacuoles and microfissures.

Identification and distribution of carbonates: All petrographers know that it is sometimes difficult under the microscope to separate calcite from dolomite; luminescence properties are then very convenient. In a carbonatite, for instance, Mn^{2+} - activated calcite usually emits a single CL band centered on 610 nm giving an orange-yellow color contrasting with the more reddish color of dolomite with its prominent emission band centered at 630 nm. Texture, distribution and evaluation of the content of one or even several carbonates in a rock is quite easily revealed by CL; in the most favorable cases, image analysis techniques can be used.

Solid solution: CL can help in determining the substitution of one element by another in a solid solution. For example, Sommer (125) (126) studied Mn^{2+} emission in the calcite - magnesite solid solution series and empirically determined the proportions of Mn^{2+} ions on Mg^{2+} or Ca^{2+} sites in dolomites. However, the interpretation of CL spectra in terms of the nature of the impurities requires the CL spectroscopy to be coupled with other techniques providing crystal-chemistry data rather thant only elemental analysis. Thus, El Ali (23) combined cathodoluminescence microscopy and spectroscopy with Electron Paramagnetic Resonance (EPR) to determine the distribution of Mn^{2+} ions in carbonates. Studying synthetic and natural calcite crystals ($CaCO_3$: Mn) at room temperature, El Ali (23) showed that the single emission broad band centered at 615 nm, associated with the Mn^{2+} ion, was correctly described by a Gaussian distribution. The CL intensity linearly increased with the Mn content going from a few tens of ppm to about 800 ppm and then reached a plateau for Mn concentrations greater than one percent due to self-quenching or concentration quenching effect (Dexter and Schulman (21)). Unfortunately, this curve has no meaning if iron is present since this element seems to be a quencher in calcite for concentrations above 150-200 ppm (ten Have and Heijnen (131)). El Ali (23) also showed that dolomite crystals were characterized by two emission bands centered at $\approx$ 513 nm and 629 nm respectively.

The emission band of lower wavelength was associated with Mn^{2+} ions substituting Ca^{2+} ions, the emission of higher wavelength resulting from Mn^{2+} substituting Mg^{2+} ions.

El Ali (23) studied the partitioning coefficient K_D of Mn^{2+} ions in the dolomite crystals by means of EPR analysis and showed that the relative intensities of the two CL emission bands were positively correlated with the K_D coefficient, i.e., the ratio of Mn^{2+} ocupancy in the Mg^{2+} site to the Mn^{2+} occupancy in the Ca^{2+} site.

Conditions of formation: If the presence of trace elements, as well as their occupancy in a crystallographic site, can be connected to other parameters such as the temperature of crystallization, salinity of solutions, pH, redox potential, etc, it may be possible to derive some information on the existing geological conditions from CL spectrum analysis.

Carpenter and Oglesby (9) and Frank et al.(27) suggested that for high oxidizing potentials, Fe being in the trivalent state and Mn in the tri- or tetravalent state, both ions cannot enter the structure of the carbonate which remains nonluminescent. For lower Eh, manganese is reduced to Mn^{2+} and can replace Ca^{2+} while Fe is still present in the trivalent state and remaining in the solution, has no quenching effect and the subsequent CL is bright. It is only for more reducing conditions that Fe^{2+} can substitute for Ca^{2+} and induce a dull CL emission.

Using EPR, Schindler and Ghose (112) and Lumsden and Llyod (66) demonstrated that in dolomite, Mn^{2+} can preferentially substitute for Ca^{2+} or Mg^{2+}. Angus et al. (3) demonstrated that the partition coefficient K_D increases with the temperature in hydrothermal dolomites, Mn^{2+} showing a preference for the Mg^{2+} site. The spectral study of CL will allow one to determine the influence of this substitution on the observed CL color. According to El Ali (23) manganese-rich hydrothermal dolomites exhibit two emission bands, e.g, I_1, at 513 nm (19,500 cm^{-1}), originating from Mn^{2+} in Ca^{2+} sites and I_2, at 629 nm (15,900 cm^{-1}), associated with Mn^{2+} in Mg^{2+} sites. Since their CL color will be a result of these two components, it will give indications of the substitution coefficient of Mn^{2+} in these sites. El Ali (23) proposed a linear relationship between the partition coefficient K_D, obtained by EPR measurements, and the ratio I_2/I_1 of intensities of the two CL emission peaks. However, instead of I_1 and I_2, it is possible to use the dominant wavelength λ_D determined in a chromaticity diagram. A shift of λ_D towards longer wavelengths (color tending toward red) is characteristic of a dolomite exhibiting a strong substitution of Mn^{2+} in the Mg^2 site and crystallized at higher temperature. Crystals formed at lower temperature display a color tending towards a green color.

A different problem is encountered for sedimentary dolomites containing low Mn^{2+} concentrations. El Ali (23) observed a partition coefficient variable with the salinity of the parent solution for the case of rapidly growing evaporitic crystals with a Ca / Mg ratio close to 1. In the Mano dolomitic series (Upper Jurassic of Aquitaine Bassin, France), the K_D coefficient decreased from bottom (K_D = 33) to top (K_D = 10) as the series evolved towards more evaporitic facies (supratidal); the dominant wavelength λ_D changed concomitantly from 587 nm to 577 nm (relative evolution of the emission band at 513 nm) as Mn^{2+} moved from the Mg^{2+} site to the Ca^{2+} site.

Fossil-bearing rocks: The fine structure of former organisms now replaced by calcite or aragonite can be revealed by CL microscopy, as also are bioclasts of small size which were more or less damaged during diagenesis. Smith and Stenstrom (124) described original cell structures of fossil crinoids and James and Klappa (50) studied the characteristics of sponges, echinoderms, etc, in reef limestones. But one of the most interesting studies was performed by Miller and Clarkson (83) who revealed the development and the internal structure of the trilobite eye even after sediment recrystallisation.

Applications of CL to silicates

Quartz: Quartz was probably the first silicate to be investigated but many mechanisms are involved and most still not completely understood. Quartz is widely studied and, its CL reveals zoning - overgrowth - and twinning patterns in addition to information about its origin and subsequent history (31). The CL emission displays several different colors according to the temperature of crystallization, the cooling rate, the episodes of deformation, the presence of activators and structural defects (134). The last two causes are probably frequently related. For instance, when Fe^{3+} replaces Si^{4+} the charge balance is restored with the substitution of O^{2-} by OH^-.

To a first approximation, detrital quartz derived from igneous and metamorphic rocks luminesces in the blue while authigenic crystals, formed at low temperature, do not luminesce or exhibit a faint dull red CL as long as they have not been subjected later to deformation and/or metamorphism. Consequently, in a sedimentary rock it is then possible to distinguish between different origins of quartz crystals. Smith and Stenstrom (124) observed this property but it was Sippel (121) who gave the first direct application to sandstone petrology, separating detrital quartz grains from surrounding authigenic quartz overgrowths and following the diagenetic events such as the

cementation and its reduction in porosity.

Many authors followed their example, among them Sibley and Blatt (117) who estimated that one third of the quartz cement in the Tuscarora Sandstone was derived from pressure solution; Ruppert et al. (110) and Ruppert (109) demonstrated that the majority of quartz in the Upper Freeport coal bed was non-luminescent and authigenic in origin while for the most part, quartz grains in the shales overlying the coal bed were luminescent and detrital in origin. Many studies have also been carried out in order to define better the relationship between colors and origins as well as geological events. Sprunt et al. (127), studying deformed quartzites, stated that blue luminescence was related to highgrade metamorphism and that the orange-red one corresponded to low-grade metamorphism. Different reasons for CL colors in quartz are mentionned in a review paper by Ruppert (109).

Zinkernagel (146) established one of the first classifications of quartz CL colors in sandstones with: (a) "violet" or blue luminescent quartz derived from igneous and high-grade metamorphic rocks ($t > 573$ °C) having undergone a relatively fast cooling (the spectra show two major peaks 450 and 620 nm), (b) "brown" or orange luminescent quartz from low-grade metamorphic rocks ($t < 573$ °C) or slow cooled high-grade metamorphic rocks (one major peak around 620 nm and a minor near 450 nm) and (c) non-luminescent quartz, hydrothermal or authigenic in origin ($t < 300$ °C). In fact, the absence of luminescence in some quartz is only apparent as high sensitivity CL microscopes with improved detection limits enable the detection of faint and short-lived CL emissions, e.g., short-lived bottle-green or blue colors, alternating with obscure bands are very common in authigenic quartz overgrowths according to Zinkernagel (146) and Ramseyer et al. (97).

Fuchtbauer et al. (28) and Matter and Ramseyer (78) improved the previous classification by describing six classes of luminescent quartz. More recently Ramseyer et al. (97) reported brown colors revealing lattice defects induced by twinning, mechanical deformation, particle bombardment or very rapid growth, bottle green and blue colors revealing the presence of interstitial cations and yellow and red colors revealing the presence of trace elements in oxidizing solutions and the presence of Fe^{3+} respectively.

As previously discussed, the origin of CL colors in quartz is still quite obscure and far from being solved; many more accurate analytical data have to be collected and,in the meantime, applications to geosciences will have to proceed with caution.

Feldspars: As quartz, the feldspars are widely distributed; the family includes two series, i.e., the alkali feldspars ($KAlSi_3O_8$-$NaAlSi_3O_8$) and the plagioclases ($NaAlSi_3O_8$-$CaAl_2Si_2O_8$), both of them exhibiting CL emissions with various colors ranging from blue to green, greenish-yellow and red as reported in Marshall (75). Unlike quartz, the activators responsible are much better known as Mariano et al. (72) synthesized doped plagioclases and found the following colors: blue for Eu^{2+} and Cu^{2+} (420 nm), blue for Ti^{4+} (460 nm), yellow-green for Fe^{2+} (550 nm) and Mn^{2+} (570) and red for Fe^{3+} (700 nm). In addition, Smith and Stenstrom (124), Görz et al. (30) and Sippel (122) reported in all feldspars, with the exception of adularia and sanidine, a polarisation of the CL emission, its intensity changing with the orientation of the crystal. Authigenic feldspars do not exhibit luminescence and no quenching element has yet been reported.

The applications of CL are basically the same as for the previous minerals: distinguishing in rock samples between the different species, both in time and space. In particular for the case of fine grained rocks, orthoclase can easily be distinguished from plagioclases. Typical crystallizing conditions can be inferred too: Mariano (69) reported a brilliant red CL emission (Fe^{3+}) in feldspars forming in strongly alkaline environments such as in peralkaline magmas or in rocks submitted to an alkali metasomatism. Hearn (36) used CL microscopy analysis to determine the mass fraction of authigenic and detrital feldspar in mineral separates.

Concentrations of unusual elements can also be detected in feldspars by CL as reported by de St. Jonne and Smith (20): albite crystals from rare metal deposits associated with peralkaline syenites and granites at Thor Lake, Canada, have a gallium-enriched margin (up to 4000 ppm) displaying a bright blue cathodoluminescence. A very similar spectrum was obtained with a Ga-doped plagioclase.

Rare-earth element bearing minerals: (RE) elements are very interesting to study because none of them enters a mineral structure alone, but are always associated with others in various proportions depending on the geochemical environment; they give more or less complex CL spectra but, fortunately, peak identification is facilitated in most cases owing to the availability of synthetic doped compounds. (RE) elements are also excellent CL activators of sharp line emissions which are largely used in the laser industry, phosphors for cathode-ray tube, screen and fluorescent lamps.

(RE) elements are classically divided into "light RE" (LRE) or the "cerium group", from lanthanum ($Z = 57$) to europium ($Z = 63$), and "heavy RE" (HRE) or the "yttrium group", from gadolinium ($Z = 64$) to lutecium ($Z = 71$). More than 170 (RE)-

bearing mineral species are recorded but there are also many minerals where these elements are not essential but can occasionally (and sometimes very frequently) enter as minor amounts or traces. The most studied of these minerals are anhydrite, apatite, calcite, fluorite, strontianite, scheelite and zircon.

The main interest of CL microscopy and spectroscopy applied to (RE)-bearing minerals is probably its role as a useful and non-destructive indicator of the crystallizing conditions. For example, in apatites, Roeder et al. (108) suggest the use of the relative Sm^{3+} and Dy^{3+} peak heights in the CL emission spectra to distinguish between apatites with dominant (HRE), crystallized in acid environment (granite pegmatites and granites) from those originating from more alkaline environment (carbonatites and genetically related rocks) and tending to be enriched in (LRE). Theoretically, redox conditions could be inferred comparing the intensity of the Eu^{2+} broad-band emission (blue part of the spectrum) with the Eu^{3+} narrow bands as have shown Mariano and Ring (73) and Roeder et al. (108) in glasses doped with europium and prepared at a series of oxygen fugacities. However, this kind of information must be used with caution as Palilla and O'Reilly (94) pointed out the preference of Eu^{2+} for some structural positions in the host mineral: for example, the fact that Eu^{3+} is strongly dominant over Eu^{2+} in the apatite structure cannot be used to evaluate the redox potential of the original solution as this structure seems to favor the incorporation of Eu^{3+} relative to Eu^{2+}.

Cathodoluminescence as prospecting guide in exploration

Some minerals exhibiting CL emission can be used as a guide to trace ore deposits even if the exact nature of the activators remains unknown. Of course the observed colors are not of general value throughout world and must be only considered in a given regional context.

Hagni (33) mentioned sillimanite (Al_2SiO_5) crystals associated with the Benson iron deposits of New-York State. In the mineralized district, sillimanite displays a dull bluish white CL sharply contrasting with the usual bright red color observed elsewhere in the Adirondack Mountains. Another example concerns dolomite found in East Tennessee carbonate sediments: CL reveals strong zonings in gangue crystals associated with zinc deposits, indicating changes in the solution composition. In dolomite from the host rock, CL is more uniform or non-existent. When observed, such zonings can indicate the proximity to mineralization.

In porphyry-copper deposits, as well as in molybdenum porphyries affected by several episodes of alteration, secondary orthoclase found in the potassic alteration zone shows a strong blue CL emission, apparently activated by Ti^{4+}, and contrasting with the white colour of primary feldspars (69). Of course CL is not a panacea and a good petrographer, trained in alteration patterns and only using morphological clues, is usually able to make the distinction between the generations of feldspars without the help of CL !

CL can also be used for uranium exploration in sedimentary formations such as the Precambrian Sandstones from Canada or the Jurassic Sandstones from the Colorado Plateau. Morton (85), Marshall (75), Owen (93) and, more recently, Meunier et al. (82), reported CL rims affecting quartz grains from such deposits, due to radiation damage. Meunier et al. (82) even observed three concentric rims corresponding to the most energetic alpha particles in the U decay series. As these rims are still visible in the quartz grains even if the uranium has been displaced by further leaching, they can be useful for hidden uranium deposit exploration.

Identification of minerals

Identification in thin sections of accessory or rare mineral species is not always easy and frequently needs the help of X-ray diffraction and microprobe analysis. CL properties were successfully used by Mariano (71) to distinguish zircon ($ZrSiO_4$) from xenotime (YPO_4), both common as accessory minerals in the Thor Lake granite syenite complex. These minerals show similar optical and morphological properties but xenotime CL spectrum does not show here the so-called intrinsic band always present in zircon. Additional examples are given by Mariano (71) concerning bertrandite ($Be_4Si_2O_7(OH)_2$), agrellite ($NaCa_2Si_4O_{10}F$), isokite ($CaMg(PO_4)F$), all of them giving (RE) characteristic CL peaks that help in their recognition. Very recently, Mariano and Roeder (74) reported that the CL emission spectra of wehlerite ($NaCa_2(Zr,Nb)Si_2O_7(O,OH,F)_2$) from different localities are basically the same (light greenish blue), but different from the spectra of chemically and structurally related minerals such as niocalite ($Ca_4NbSi_2O_{10}(O,F)$) and hiortdahlite ($(Ca,Na)_3ZrSi_2O_7(O,OH,F)_2$), both exhibiting CL emission spectra of (RE) luminescence-activating ions.

Summary

CL emission is an efficient method for spatially resolved analysis of point defects in crystals. CL emission microscopy was first applied to easily characterize the degree of purity of materials used in modern technologies. Because the physical and chemical defects are a signature of the crystal growth conditions CL emission is also a signature of the genetic conditions. CL microscopy was naturally used in the field of mineralogy and petrology for revealing growth zoning or for identifying minerals from different

sequences of crystallization but having similar chemical composition which could not be easily distinguished by means of optical microscopy. Consequently, many efforts have been devoted to the development of more or less sophisticated devices for CL microscopy.

For mineralogical and petrological applications, cold cathode electron gun attachments to optical microscopes are now available making easy CL microscopy combined with optical microscopy on a routine basis. CL collectors based on spherical or semi-ellipsoidal mirrors are used to improve the light collection efficiency for CL microscopy with SEM or EPMA techniques.

The dissipation of the incident electron energy leads to the production of several forms of energy within the target. The observed CL emission is the sum of several luminescence emissions induced by each of the available energies. The emissions induced by electrons, X-ray photons, heat, and electrical fields developed within the solid exhibit small shifts and small intensity changes of their characteristic emission bands. These changes in the luminous photon distribution as a function of the participating energies lead to small changes in the color of the resulting observed CL emission. The reliability in distinguishing several populations of crystal based on color CL imaging has been greatly improved by CL spectroscopy. CL spectrometers using prism or grating monochromators and modern detectors have a high detection efficiency for CL spectroscopy by means of SEM or EPMA techniques. The recent use of intensified photodiode arrays as detectors are very promising for future applications to CL spectroscopy. These detectors, combined with a multichanel analyzer, lead to a simultaneous analysis mode of the spectral emission distribution and are suitable for studying weak and short-lived CL emissions.

The available modern technologies allow the use of CL emission analysis to complement other spectroscopies for spatially resolved studies of point defects in crystals. CL spectroscopy complements optical absorption measurements for the study of the recombination centers while thermoluminescence complements EPR spectroscopy for studying the electron traps usually associated with the luminescent centers.

CL emission studies can be carried out with two major objectives. By analogy with X-ray spectrometry with the EPMA, the first direction in the use of CL is an analytical application to the identification of trace elements in minerals. The energy of CL lines or bands expresses the difference in energy between the levels located within the band gap involved in the CL emission mechanisms. The problem consists in relating the photon energy distribution, i.e., the energy levels in the energy diagram with the nature of the luminescent centers whether intrinsic (lattice defect) or extrinsic (impurities) in origin. The problem is very complex because there is no unique relation between the color of the CL emission and the nature of the impurities within the minerals. The second direction in the use of CL emissions, consists in by-passing the identification of the nature of the point defects and using the CL signal as a signature of the genetic conditions of the minerals.

Both types of applications have been carried out with success. **However there is still a need for a better understanding of the mechanisms of generation and emission of the CL photons to get a reliable relationship between the CL emission and the microscopic (point defects) or macroscopic (geological phenomena) properties of the minerals**.

In minerals, the CL emission resulting from lattice defects and presence of impurities, reflects the dielectric property of the crystal. The relationship between the CL emission and the impurities is complex and the emission is more often considered as a signature of the genetic conditions. In absence of a unique theoretical framework, some conclusions drawn from CL studies have been sometimes considered too hasty and speculative leading to a distrust in CL applications.

The CL emission bands may be intrinsic or extrinsic in origin depending upon the nature of the point defects in the crystal. The former are associated with impurities (luminescent ions or recombination centers), the latter resulting from lattice defects originally existing **or induced by the electron bombardment**. Several mechanisms may be responsible for the CL property changes during electron irradiation. Two possible mechanisms in insulating crystals can take place simultaneously or sequentialy.

The first probable mechanism involves the filling of already existing defects. The second mechanism corresponds to the creation of new defects induced by the incident ionizing energy. According to the first mechanism, the filling of defects with electrons e.g. oxygen vacancies in silicates, fluor vacancies in fluorites... leads to the development of "pseudo atoms" able to partly absorb the generated luminous photons. A decrease in the CL intensity as a function of electron dose may also result from thermal quenching, i.e., an increase of the ion-radiative transition probabilities with respect to the probabilities of radiative process. Although less frequent, a second possible mechanism leading to CL property changes is an increase of the hole populations. Such an effect can be observed in natural and synthetic silicates and may arise in CL induced by electrons whose energies are of the same order of magnitude than those of particles of radioactive origin.

Whatever is the mechanism responsible for CL changes with electron dose, a steady-state is rapidly obtained indicating a saturation effect resulting from competitive processes: (a) the filling of pre-

existing electron traps is counterbalanced by charge recombinations or (b) creation and annealing of defects, are counterbalanced.

For future developments, quantitative expression of the observed CL color derived from spectral analysis will greatly reinforce the use of CL color imaging for comparisons between specimens from several origins. However, an accurate knowledge of all factors involved in the generation, emission and detection processes is needed for a reliable use of CL emission as a signature of a mineral with respects to its geological environment. For each mineral of interest, a rigorous approach should include two steps. The first step aims to identify the defects associated with the energy levels involved in the radiative transitions. For this purpose, detailed studies of the fine structure and emission bands of cathodo- photo- and thermoluminescence **spectra observed as a function of the specimen temperature** must be combined with sensitive analytical techniques (EPMA, SIMS, EPR...). The second step aims to prepare synthetic materials under controlled conditions and to compare their luminescence properties with those of the natural crystals.

Provided that a rigorous experimental procedure has been established, CL microscopy and spectroscopy should be recognized as a reliable method for the detection and the localization of defects. Besides, its interest for the microcharacterization of mineral materials, CL will also contribute to a better understanding and prediction of the behavior of insulating materials exposed to ionizing particles.

Acknowledgements

The authors would like to thank Dr. R. Caruba (Université de Nice, France), Dr. A.M. Lejus (Ecole Nationale Superieure de Chimie de Paris, France) for providing the synthetic doped zircons and the rare-earth oxide single crystals, and Dr. Zarka (Université P. et M. Curie, Paris, France) for examining our quartz specimen by X-ray topography.

References

(I) Alonso PJ, Halliburton LE, Kohnke EE, Bossoli RB (1983). X-ray induced luminescence in crystalline SiO_2. J. Appl. Phys., **54**, (9), 5369-5375.

(2) Amieux P (1982). La cathodo-luminescence : Méthode d'étude sédimentologique des carbonates. (Cathodoluminescence : a method for studying carbonaceous sediments) Bull. Centre. Rech. Explor.-Prod. Elf Aquitaine, **6**, 437-483.

(3) Angus JG, Berveridge D, Barrie Raynor J (1984). Dolomite thermometry by electron spin resonance (ESR). Chemical Geology, **43**, 331-346.

(4) Barker CE, (1986). Bibliography on cathodoluminescence petrography. Process Mineralogy VI.RD Hagni (ed) the Metallurgical Society of AIME, 159-190.

(5) Blasse G, Brill A (1970). Luminescences caractéristiques. Philips Technical Review, **31**, n° 10, 13-47.

(6) Bröcker W, Pferfferkorn GE (1978). Bibliography on cathodoluminescence. Scanning Electron Microsc., I ; 333-351.

(7) Bröcker W, Pfefferkorn GE (1980). Bibliography on cathodoluminescence, Part II. Scanning Electron Microsc., I ; 298-302.

(8) Buschbeck F, Hörl EM (1978). Electronic adding-up and storing of SEM color images. Scanning Electron Microsc., I ; 835-839.

(9) Carpenter AB, Oglesby TW (1976) . A model for the formation of luminescently zoned calcite cements and its implications. Geol. Soc. of America. Abstracts with Programs, **8**, 469-470.

(10) Caruba R (1979). Etude experimentale de la cristallochimie, de la morphologie, de la stabilité et de la genèse du zircon et des zircono-silicates en vue d'applications pétrogénétiques (Experimental study of crystallo-chemistry and morphology of zircons for petrological application). Thesis, University of Nice, France, 1-139.

(11) Caruba R, Baumer A, Hartman P (1988). Crystal growth of synthetic zircon round natural seeds. J. Crystal Growth, **88**, 297-302.

(12) Castaing R (1951) . Application des sondes électroniques à une méthode d'analyse ponctuelle chimique et cristallographique. (Electron beam based techniques for spatially resolved chemical and crystallographical analyses). Thèse, Université de Paris, France.

(13) Cazaux J (1986). Electrostatics of insulators charged by incident electron beams. J. Microsc. Spectrosc. Electron., **11**, 215-228.

(14) Cervelle B, Malezieux JM (1977). Expression quantitative de la couleur liée à la réflectance diffuse de quelques roches et minéraux. (Quantitative expression of the color of some rocks and minerals based on reflectance measurments). Bull. Soc. Fr. Mineral. Cristallogr., **100**, 185-191 .

(15) Chin AK (1982). A simple, high collection efficiency cathodoluminescence imaging technique: Application to GaSb and CdTe. Scanning Electron. Microsc., III ; 1069-1075.

(16) Coy-Yll R (1969). Quelques aspects de la cathodoluminescence des minéraux (Some aspects of CL in minerals). Chem geol., **5**, 243-254.

(17) Curie D (1963). Luminescence in crystals (translated by GFJ Garlick). Methuen and Co Ltd, London, England, 1-332.

(18) Czernuszka JT, Page TF (1985). Cathodoluminescence: A microstructural technique for exploring phase distributions and deformation structures in zirconia ceramics. J. Am. Ceram. Soc., **68**, n° 8, C196-Cl99.

(19) Dennen WH., Shields R (1956). Yttria in zircon. Amer. Min., **41**, 655-656.

(20) De St Jonne L, Smith D G W (1988). Cathodoluminescent gallium enriched feldspars from the Thor Lake rare metal deposits, Northwest Territories. Canad. Miner., **26**, 301-308.

(21) Dexter DL, Schulman JH, (1954). Theory of concentration quenching in inorganic phosphors. J. Chem. Physics., **22**, 1063-1070.

(22) Duraud JP, Jollet F, Langevin Y, Dooryhee E (1988). Radiation effects in SiO_2 under electronic excitation. Nuclear Inst. and Meth. in Phys. Res., **B32**, 348-357.

(23) El Ali (1989). Etude des roches carbonatées de réservoirs d'hydrocarbures par résonance paramagnétique électronique et cathodoluminescence (EPR and CL applied to the study of carbonaceous rocks). Thesis, Université de Paris, France.

(24) Fielding PE (1970). The distribution of uranium, rare-earth and color centers in a crystal of natural zircon. Am. Miner., **55**, 428-440.

(25) Fischer AG (1966). Electroluminescence in II.VI compounds. *In* : Luminescence in Inorganic Solids, P. Goldberg (ed), Academic Press, 541-559.

(26) Fisher AJ, Hayes W, Stoneham AM (1989). Theoretical studies of the blue luminescence in α quartz. J. Chem. Soc., Faraday Trans. 2, **85** (5), 467-469.

(27) Frank JR, Carpenter AB, Oglesby TW (1982). Cathodoluminescence and composition of calcite cement in the Taum Sauk limestone (upper Cambrian), south-east Missouri. J. Sedim Petrol., **52**, 631-638.

(28) Fuchtbauer Von H, Leggewie R, Gockeln C, Heinemann C, Schroder P (1982). Methoden der quarzuntersuchung, angewandt auf mesozoische und pleistozane sandsteine und sande. Neues Jahr. Geol. Paloeontol., **4**, 193-210.

(29) Goni J, Remond G (1969). Localization and distribution of impurities in blende by cathodoluminescence. Miner. Mag. **37**, N°. **86**, 153-155.

(30) Görz HN, Bhalla RJR, White E (1970). Detailed cathodoluminescence characterisation of comon silicates. Penn. State Univ., Materials Research Lab., Special Publication, **70-101,** 62-70.

(31) Grant PR, White SH (1978). Cathodoluminescence and microstructure of quartz; overgrowths on quartz. Scanning Electron. Microsc., I; 786-794.

(32) Guzzi M, Martini M, Mattaini M, Pio F, Spinolo G (1987). Luminescence of fused silica: observation of the O_2^- emission band. Physical Review B, **35**, n° 17, 9407-9409.

(33) Hagni RD (1985). Cathodoluminesence microscopy applied to mineral exploration and beneficiation. Applied Mineralogy. WC Park, DM Hausen, RD Hagni (eds). The Metallurgical Society of AIME, New-York, 41-66.

(34) Halden NM, Hawthorne FC, Campbell JL, Teesdale WJ (1991). Chemical characterization of oscillatory zoning and overgrowths in zircon using low-energy micro-PIXE. Annual meeting of the Geological Association of Canada and the Mineralogical Association of Canada, May 27-29, Toronto, Canada. Abstracts, **16**, A49.

(35) Hautefeuille P, Perrey A (1898). Sur la production de zircon (About the production of zircon). C.R. Acad. Sci., Paris, **107**, 1000-1001.

(36) Hearn PR Jr. (1987). A quantitative technique for determining the mass fractions of authigenic and detrital K-feldspar in mineral separates. Scanning Microscopy, **1**, N°. 3, 1039-1043.

(37) Henry DJ, Toney JB (1987). Combined cathodoluminescence/backscatter electron imaging and trace element analysis with the electron microprobe: applications to geological materials. Microbeam Analysis, RH Geiss, (ed), San Francisco Press, San Francisco, CA, USA, 339-342.

(38) Hoffman JF, Long JVP (1984). Unusual sector zoning in Lewisian zircons. Miner. Mag., **48**, 513-517.

(39) Holt DB (1974). Quantitative scanning electron microscope studies of cathodoluminescence in adamantine semiconductors. *In*: Quantitative Scanning Electron Microscopy, DB Holt, MD Muir, PR Grant and IM Boswarva (eds), Academic Press, 335-388.

(40) Holt DB (1992). New directions in SEM CL microcharacterization. Scanning Microscopy **6** (1), 1-21 (this issue).

(41) Holt DB, Datta S (1980). The cathodoluminescence mode as an analytical technique: It's development and prospects. Scanning Electron Microsc., 1980; I : 259-278.

(42) Holt DB, Saba FM (1985). The cathodoluminescence mode of the scanning electron microscope: A powerful microcharacterization technique. Scanning Electron Microsc., 1985; III: 1023-1045.

(43) Hörl EM, Roschger P (1980). CL SEM investigations of biological material at liquid helium and liquid nitrogen temperatures. Scanning Electron Microsc., 1980; I: 285-292.

(44) Iacconi P, Caruba R (1980). Trapping and emission centres in X-irradiated zircon. (III) : Influence of trivalent rare-earth impurities. Phys. Stat. Sol.(a), **62**, 589-596.

(45) Iacconi P, Caruba R (1984). Trapping and emission centres in X-irradiated natural zircon. Characterization by thermluminescence. Phys. Chem. Minerals, **11**, 195-203.

(46) Iacconi P, Deville A, Gaillard B (1980). Trapping and emission centres in X-irradiated zircon. (II): Contribution of the SiO_4^{4-} groups. Phys. Stat. Sol.(a), **59**, 639-646.

(47) Ishikawa A, Uchikawa Y, Maruse S (1972). Contrast of the cathodoluminescent image in SEM. Proc. of the 6th International Conference on X-ray Optics and Microanalysis, G Shinoda, K Kohra, K and T Ichinokawa, (eds), University of Tokyo Press, 597-601.

(48) Itoh N, Tanimura K (1990). Formation of interstitial-vacancy pairs by electronic excitation in pure ionic crystal. J. Phys. Chem Solids, **51**, n° 7, 717-735.

(49) Itoh C, Tanimura K, Ithoh N (1988). Optical studies of self-trapped excitons in SiO_2. J. Phys. C : Solid State Phys, **21**, 4693-4702.

(50) James NP, Klappa CF (1983). Petrogenesis of earlier Cambrian reef limestones, Labrador, Canada. J. Sedim. Petrol., **53**, 1051-1096.

(51) Jones D, Landon DO (1983). A diode array spectrograph and associated optics for cathodoluminescence measurements in a scanning electron microscope. Microbeam Analysis, R Gooley, (ed), San Fransisco Press, San Francisco, CA, USA, 151-152

(52) Kirsh Y, Townsend PD (1987). Electron and hole centres produced in zircon by irradiation at room temperature. J. Phys. C : Solid State Phys., **20**, 967-980.

(53) Kristianpoller N (1983). Effects of ultra-violet irradiation on quartz. PACT 9, Ed. du Conseil de l'Europe. Strasbourg, France, 153-162.

(54) Kyser DF (1972). Experimental determination of mass absorption coefficients for soft X-rays. Proc. 6th International Conference on X-ray Optics and Microanalysis, G Shinoda, K Kohra and T Ichinokawa (eds), University of Tokyo Press, 147-156.

(55) Kyser DF, Wittry DB (1964). Cathodoluminescence in gallium arsenide. *In*: the Electron Microprobe, TD Mc Kinley, KFJ Heinrich and DB Wittry (eds), John Wiley and Sons, 691-714.

(56) Larach S (1968). Cathode-ray excited emission spectroscopic analysis for trace rare-earths. Part II : Determination of europium. Anal. Chim. Acta, **42**, 407-413.

(57) Larach S, Shrader RE, Kauffunger RA (1970). Cathode-ray excited emission spectroscopic analysis of trace rare-earths. Part IV: Determination of thulium in zinc sulfide. Anal. Chim. Acta, **51**, 393-398.

(58) Le Gressus C, Vigouroux JP, Duraud JP, Boiziau C, Geller J (1984). Charge neutralization on insulators by electron bombardment. Scanning Electron Microsc., 1984; I : 41-48.

(59) Lejus AM, Collongues R (1980). Lanthanide oxides, structural anisotropy, physical and mechanical properties. Current Topics in Materials Science, E Kaldi (ed), North-Holland Publishing Co., **4**, 481-577.

(60) Le Nindre YM, Farjanel G, Giot D, Remond G (1991). Techniques modernes en pétrographie sédimentaire : Utilisation des propriétés de luminescence des minéraux et de l'analyse d'image. (Modern techniques in sedimentary petrography: Use of luminescence emission and image analysis). Manuels et Méthodes, Edition du BRGM, Orléans, France, in press.

(61) Le Poole JB, Bok AB, Boogerd WJ (1968). An electron luminescence microscope. Geologie en Minjbouw, **47**, 443-450.

(62) Leverenz HW (1950) . An introduction to luminescence of solids. John Wiley and Sons, New York, 1-569.

(63) Löhnert K, Hastenrath M, Kubalek E (1979). Spatially resolved cathodoluminescence studies of GaP LED's in the scanning electron microscope using optical multichannel analysis. Scanning Electron Microsc., 1979; I: 229-233.

(64) Long JVP, Agrell SO (1965). The cathodoluminescence of minerals in thin section. Miner. Mag., **34**, n° 268, 318-326.

(65) Luff BJ, Townsend PD (1990). Cathodoluminescence of synthetic quartz. J. Phys. Condens. Matter, **2**, 8089-8097.

(66) Lumsden DN, Lloyd RV (1984). Mn (II) partitioning between calcium and magnesium sites in studies of dolomite origin. Geochim. and Cosmochim. Acta, **48**, 1861-1865.

(67) Mc Keever SWS (1984). Thermoluminescence in quartz and silica. Radiation Protection Dosimetry, **8**, n° 1, 81-98.

(68) Marfunin AS (1979). Spectroscopy, luminescence and radiation centers in minerals. (Translated by VV Schiffer). Springer-Verlag, Berlin Heidelberg New-York, 1-347.

(69) Mariano AN (1978). The application of cathodoluminescence for carbonatite exploration and characterization. *In*: Proceedings of the 1st, International Symposium on Carbonatites, Pocos de Caldas, Minas Gerais, Brasil, 1976. CJ Braga (ed), Brasil Departamento Nacional da Producao Mineral, Brasilia.

(70) Mariano AN (1988). Some further geological applications of cathodoluminescence. *In*: Cathodoluminescence of Geological Materials, Marshall DJ, Unwin Hyman (ed), London.

(71) Mariano. AN (1989). *In*: Geochemistry and mineralogy of rare-earth elements. BR Lipin, GA McKay (eds). Reviews in Mineralogy, Mineralogical Society of America, **21**.

(72) Mariano AN, Ito J, Ring PJ (1973). Cathodoluminescence of plagioclase feldspars. Geological Society of America, Abstracts with program, **5**, 726.

(73) Mariano AN, Ring PJ (1975). Europium activated cathodoluminescence in minerals. Geochim. Cosmochim. Acta, **39**, 649-660.

(74) Mariano AN, Roeder PL (1989). Wohlerite: chemical composition, cathodo-luminescence and environement of crystallization. Canad. Miner, **27**, 709-720.

(75) Marshall DJ (1988). Cathodo-luminescence of Geological Materials. Unwin Hyman, (ed) London.

*(76) Marshall DJ (1992). The present design status of optical microscope attachments for CL studies. Scanning Microscopy (in press).

(77) Mason RA, Mariano AN (1990). Cathodoluminescence activation in manganese-bearing and rare earth-bearing synthetic calcites. Chemical Geology, **88**, 191-206.

(78) Matter A, Ramseyer K (1985). Cathodoluminescence microscopy as a tool for provenance studies of sandstones. *In*: NATO ASI series GG Zuffra (ed), Reidel Publ. Co, Boston, **148**, 191-211.

(79) Mattler J, Ceva T (1961). *In*: Luminescence in Crystals, D. Curie (translated by G F J Garlick), Methuen and Co Ltd, 244.

(80) Medlin WL (1963). Emission centers in thermoluminescent calcite, dolomite, magnesite, aragonite and anhydrite. J. of the Optical Society of America, **53**, N°.11, 1276-1285.

(81) Medlin WL (1964) . Trapping centers in thermoluminescent calcite. Physical Review, **135**, n°6A, 1770-1779.

(82) Meunier JD, Sellier E, Pagel M (1990). Radiation-damage rims in quartz from uranium-bearing sandstones. J. Sedim. Petrol, **60**, 53-58.

(83) Miller J, Clarkson ENK (1980). The post-ecdysial development of the cuticle and the eye of the Devonian trilobite Phacops ana milleri Stewart 1927. Philos. Trans., **288**, 461-480.

(84) Monod-Herzen G (1966). Luminescence; l'électron et la lumière, matière et photoluminescence (Luminescence: electron and light, solid and photoluminescence). Dunod, Paris.

(85) Morton RD (1978). Cathodoluminescence applied to uranium exploration. Nuclide Spectra, **11**, 1.

(86) Muir MD, Grant PR (1974). Cathodo-luminescence. *In* Quantitative Scanning Electron Microscopy. DB Holt, MD Muir, PR Grant, IM Bosworva. (eds), Academic Press, 287-334.

(87) Myhajlenko S, Davidson SM, Hamilton B (1983). *In:* Cathodoluminescence Microscopy of Inorganic Solids, BG Yacobi, DB Holt, (eds), Plenum Press, 1990, p. 87.

(88) Nassau K, Prescott BE (1975). A reinterpretation of smoky quartz. Phys. Stat. Sol.(a), **29**, 659-663.

(89) Nicholas JV (1967). Origin of the luminescence in natural zircon. Nature, **215**, 1476.

(90) Nickel E (1978). The present status of cathode luminescence as a tool in sedimentology. Minerals Science and Engineering, **10**, 73-100.

(91) Ohnenstetter D, Cesbron F, Remond G, Claude JM, Caruba R (1991). Cathodoluminescence of natural zircon: evidence for the existence of two populations. C.R. Acad. Sci., Paris, t. 313, serie II, 641-647.

(92) Ohuchi F, Holloway PH (1982). Contribution of electron stimulated desorption to electron beam domage in oxides. Scanning Electron Microsc., 1982; IV: 1453-1463.

(93) Owen MR (1988). Radiation-damage halos in quartz. Geology, **16**, 529-532.

(94) Palilla FC, O'Reilly BE (1968). Alkaline earth halophosphate phosphors activated by divalent europium. J. Electrochem. Soc., **115**, 1076-1081.

(95) Pfefferkorn G, Bröker W, Hastenrath M, (1980). The cathodoluminescence method in the scanning electron microscope. Scanning Electron Microsc. 1980; I : 251-258.

(96) Powell RC, Venikovas GE, Lin XI, Tyminski JK (1986). Thermal effects on the optical spectra of Al_2O_3 : Ti^{3+}. J. Chem. Phys., **84** (2), 662-665.

(97) Ramseyer K, Baumann J, Matter A, Mullis J (1988). Cathodoluminescence colours of α quartz. Miner. Mag., **52**, 669-677.

(98) Ramseyer K, Fischer J, Matter A, Eberhardt P, Geiss J (1989). A cathodoluminescence microscope for low intensity luminescence. J. Sedimentary Petrology, 619-622.

(99) Ramseyer K, Mullis J (1990). Factors influencing short-lived blue cathodoluminescence of α-quartz. Am. Miner., **75**, 791-800.

(100) Reimer (1985). *In*: Cathodoluminescence Microscopy of Inorganic Solids, BG Yacobi, DB Holt (eds), Plenum Press, 1990, 55-88.

(101) Remond G (1973). Exemples d'identification et de localisation des éléments en traces dans des minéraux luminescents (cassitérites) à l'aide de l'analyseur ionique. (Trace element analysis in luminescent minerals with the ion microprobe). Bull. Soc. fr. Mineral. Cristallogr., **96**, 183-198.

(102) Remond G (1977). Applications of cathodoluminescence in mineralogy. Journal of Luminescence, **15**, n° 2, 121-155.

(103) Remond G, Holloway PH, Hovland CT, Olson RR (1982). Bulk and surface silver diffusion related to tarnishing of sulfides. Scanning Electron Microsc., 1982; III : 995-1011.

(104) Remond G, Joseph E, Jeanrot P (1972). Evaluation de la correction d'absorption dans l'analyse quantitative des silicates (Absorption correction in quantitative analysis of silicates). Proc. 6th International Conference on X-ray Optics and Microanalysis, G Shinoda, K Kohra and T Ichinokawa (eds), University of Tokyo Press, 203-210.

(105) Remond G, Kimoto S, Okuzumi H (1970). Use of the SEM in cathodoluminescence observations in natural specimens. Scanning Electron Microsc., 1970: 33-40

(106) Remond G, Kimoto S, Okuzumi H (1972). Applications du microscope électronique à balayage à l'étude de la cathodoluminescence de quelques minéraux : Limites de résolution et de sensibilité (Applications of the SEM to the study of CL in minerals: Limits of resolution and sensitivity). Proc. 6th International Conference on X-Ray Optics and Microanalysis. G Shinoda, K Kohra, T Ichinokawa (eds), University of Tokyo Press, 611-617.

(107) Remond G, Le Gressus C, Okuzumi H (1979). Electron beam effects observed in cathodoluminescence and Auger electron spectroscopy in natural minerals: Evidence for ionic diffusion. Scanning Electron Microsc., 1979; I : 237-244.

(108) Roeder PL, Mac Arthur D, Ma Xin-Pei, Palmer GL, Mariano AN (1987). Cathodo-

luminescence and microprobe study of rare-earth elements in apatite. Amer. Min., **72**, 801-811.

(109) Ruppert LF (1987). Applications of cathodoluminescence of quartz and feldspar to sedimentary petrology. Scanning Microscopy, **1**, 63-72.

(110) Ruppert LF, Cecil CB, Stanton RW (1985). Authigenic quartz in the Upper Freeport coal bed, west-central Pennsylvania. J. Sedim. Petrol., **55**, 334-339.

(111) Saparin GV, Obyden SK (1988). Colour display of video information in scanning electron microscopy: Principles and applications to physics, geology, soil science, biology and medicine. Scanning, **10**, 87-106.

(112) Schindler P, Ghose S (1970). Electron paramagnetic resonance of Mn^{++} in dolomite and magnasite and Mn^{++} distribution in dolomite. Amer. Min., **55**, 889-896.

(113) Schvoerer M, Guibert P, Piponnier D, Bechtel F (1986). Cathodoluminescence des matériaux archéologiques (Cathodoluminescence of archeological materials). PACT 15, Ed. du Conseil de l'Europe, Strasbourg, France, 93-110.

(114) Semo J (1974). Spectroscopie optique en cathodoluminescence au microscope électronique à balayage (CL spectroscopy with the SEM). Revue de Physique Appliquée, **9**, 355-359.

(115) Semo J (1975). Etude et réalisation d'un spectroscope pour cathodoluminescence en microscopie électronique a balayage, et applications aux semi-conducteurs à large bande interdite (Development of a CL spectrometer for SEM technique: Applications to large band gap semiconductors). Thesis, Université de Paris VI, France.

(116) Shionoya S (1966). Luminescence of lattices of the ZnS type, *In*: Luminescence in Inorganic Solids, P. Goldberg (ed.), Pergamon Press, 206-286.

(117) Sibley DF, Blatt H (1976). Intergranular pressure solution and cementation of the Tuscarora orthoquartzite J. Sedim. Petrol., **46**, 881-896.

(118) Siegel GH (1973/1974). Ultraviolet spectra of silicate glasses: A review of some experimental evidence. J. Non-cryst. Solids, **13**, 372-398.

(119) Siegel GH, Marrone MJ (1981). Photoluminescence in as-drawn and irradiated silica optical fibers: An assessment of the role of nonbridging oxygen defect centres. J. Non-Cryst. Solids, **45**, 235-247.

(120) Sippel RF (1965). Simple device for luminescence petrography. Review of Scientific Instruments, **36**, **1**, 556-558.

(121) Sippel RF (1968). Sandstone petrology, evidence from luminescence petrography. J. Sedim. Petrol., **38**, 530-554.

(122) Sippel RF (1971). Luminescence petrography of the Apollo 12 rocks and comparative features in terrestrial rocks and meteorites. *In:* Proc. of the Second Lunar Conference. Vol.I, AA. Levinson, (ed), Cambridge, Mass, MIT, 247-263.

(123) Sippel RF, Glover ED (1965). Structures in carbonate rocks made visible by luminescence petrography. Science, **150**, 1283-1287.

(124) Smith JV, Stenstrom RC (1965). Electron-excited luminescence as a petrologic tool. J. of Geology, **73**, 627-635.

(125) Sommer SE (1972). Cathodoluminescence of carbonates 1: Characterization of cathodoluminescence from carbonate solid solutions. Chemical Geology, **9**, 257-273.

(126) Sommer SE, (1972). Cathodoluminescence of carbonates 2: Geologic applications. Chemical Geology, **9**, 275-284.

(127) Sprunt ES, Dengler LA, Sloan D (1978). Effects of matamorphism on quartz cathodoluminescence. Geology, **6**, 305-308.

(128) Steele IM (1992). Digital CL imaging of minerals. Scanning Microscopy (in press).

(129) Stoecklein W, Gobel R (1991). Applications of CL in forensic paint analysis. Scanning Microscopy, to be published.

(130) Tanimura K, Itoh C, Itoh N (1988). Transient optical absorption and luminescence induced by band to band excitation in amorphous SiO_2. J. Phys. C : Solid State Phys., **21**, 1869-1876.

(131) ten Have T, Heijnen WJ (1985). Cathodoluminescence activation and zonation in carbonate rocks: An experimental approach. Geologie en Mijnbouw, **64**, 297-310.

(132) Trigg AD (1985). A high efficiency cathodoluminescence system and its application to optical materials. Scanning Electron Microsc., 1985; III : 1011-1022.

(133) Van Gool (1961). Fluorescence centers in ZnS. Philips Res. Respt. Suppl. 3, 1-119.

(134) Van Uitert LG, (1966). Luminescence of Insulating Solids for Optical Masers. *In*: Luminescence of Inorganic Solids, P. Goldberg (ed), Pergamon Press, 465-539.

(135) Vigouroux JP, Duraud JP, Le Moel A, Le Gressus C, Griscom DL (1985). Electron trapping in amorphous SiO_2 studied by charge built-up under electron bombardment. J. of Applied Physics, **57**, 5139-5144.

(136) Vigouroux JP, Duraud JP, Le Gressus C, Petite G, Agostini P, Boiziau C (1985). Study by scanning electron microscopy, and electron spectroscopy of the cascade of electron multiplication in an insulator submitted to an electrical field. Scanning Electron Microscopy, 1985; I : 179-182.

(137) Warwick CA (1986). *In*: Cathodoluminescence Microscopy of Inorganic Solids, Yacobi BG, Holt DB, Plenum Press, 1990, p. 84.

(138) Warwick CA (1987). Recent advances in scanning electron microscope cathodoluminescence assessment of GaAs and InP. Scanning Microscopy, **1**, 51-61.

(139) Wilson M, Ogden R, Holt DB (1980). Slow contamination and fast surface state effects in SEM studies in Si phototransistors. J. Mater. Sci., **15**, 2321-2324.

*(140) Wright P (1992). An improved CL spectral analysis system.Scanning Microscopy (in press).

(141) Wright WD (1964). The measurement of colour. Hilger and Watts Ltd, London, 1-291.

*(142) Wright P, Kearsley A (1992). Digital colour CL imaging and spectral analysis. Scanning Microscopy (in press).

(143) Yacobi BG, Herrington CR (1986). Cathodoluminescence attachment to electron probe instrument. J. of Electron Microscopy Technique, **3**, 343-346.

(144) Yacobi BG, Holt DB (1990). Cathodoluminescence microscopy of inorganic solids, Plenum Press, New-York-London, 1-292.

(145) Yamamoto N, Spence ICH, Fathy D (1984). *In*: Cathodoluminescence Microscopy of Inorganic Solids, BG Yacobi, DB Holt (eds), Plenum Press, 1990, 264-266.

(146) Zinkernagel U (1978). Cathodoluminescence of quartz and its application to sandstone petrology. Contribution to sedimentology, n°8, Stuttgart: E. Schweizerhartsche Verlagsbuchhandlung, 1-69.

Discussion with reviewers

DB Holt: How widespread is the excitation of CL at a distance from the point of beam impact? Is it unique to ZnS or even only to some particular type of sphalerite? Is there any possibility of testing the interior field hypothesis by discharging the field in some way? For example can the effect be altered by applying a conductive surface coating or making contact with a mechanical probe, or by applying, e.g., a magnetic field to cause the charge to follow different trajectories?

Authors: The emission of CL far from the incident beam spot has been observed in several natural ZnS crystals but we are not able to correlate this phenomenon with the presence of a specific impurity in the crystal. The same effect is frequently observed in Al_2O_3 crystals we use as reference materials for quantitative analysis by means of X-ray spectrometry with the EPMA.

We also have shown the existence of bulk charging by studying crystalline quartz by means of energy dispersive X-ray spectrometry. Quartz specimens were analyzed using a standardless based approach. According to this approach the X-ray intensities measured at the surface of the specimens were compared to **theoretically** calculated reference intensities using a fundamental parameter data base. No surface charging effect was observed when the **uncoated** quartz was irradiated by a 3 keV electron beam. However X-ray data processing did not lead to calculated values consistent with the stoichiometric concentrations. Detailed examination of the X-ray spectra showed that the intensity of the continuous emission became negligible at energies lower than that of the primary beam energy. The energy difference between the incident energy and the highest measured X-ray photon energy was about 500 eV. Assuming that the effective energy within the target is reduced by 500 eV with respect to the incident energy led to calculated concentrations consistent with the theoretical values. Similar conclusions were drawn when increasing the primary beam energy from 5 to 15 keV at the surface of **carbon coated** quartz specimens. The presence of the conductive surface film prevented surface charging. However the cut-off energy of the X-ray emission spectra still existed indicating that electrical charging occurred within the bulk of the specimens leading in turn to a modification of the electron distribution as a function of depth with respect to that calculated when neglecting charging effects.

Surface coating will avoid surface charging without cancelling bulk charging. To study the depth distribution of charges in an insulating material we will create a sub-surface conductive area by ion implantation and analyze the X-ray emission by varying the incident energy. As suggested, CL emission changes will be studied by making contact with a mechanical probe and applying a magnetic field to modify the electrical field distribution around the beam spot.

D. Marshall: Are there examples where coactivation or sensitization have been found to be applicable to CL emission or are they restricted to PhL emission?

Authors: As mentioned in text, a second activator may act as a coactivator or a sensitizer according to its role in the formation of a luminescence center (coactivator) creating with the principal activator a donor-acceptor pair or serving as an energy transfer system (sensitizer). Consequently, a coactivator is related to the energy levels involved in the luminescence emission, while a sensitizer is related to the excitation mechanism of the center.

An example of luminescence resulting from the presence of activators and co-activators is given in Fig. 25 for the case of ZnS crystals.

The sensitization effect leads to the enhancement of the luminescence emission of an activator by the presence of a sensitizer ion. When absorbing the incident energy, the sensitizer may emit luminescence or may partly transfer the excitation energy to a neighbouring activator. The well-known example of sensitized emission is that reported in 1947 by Schulman for Mn activated calcites (Schulman JH, Evans LW, Ginther RH, Murata KJ.: The sensitized luminescence of manganese-activated calcite. J. of Appl. Phys., 1947, **18**, 732-739). The Mn-

activated calcites exhibit CL emission, but photoluminescence (PhL) by UV excitation is only produced when Mn is accompanied by an other impurity, such as Pb. The transfer of the excitation energy from the sensitizer to the activator may occur either without electron charge displacement, e.g., non-radiative resonance or light reabsorption, or with charge transfer, e.g., hole or exciton migration. Both mechanisms involved in the excitation energy transfer are independent of the nature of the incident energy and the sensitization effect will take place in both CL and PhL emissions.

D. Marshall: Please comment on the effects of the current (and power) density used for the quartz example as contrasted with the values used by Ramsayer et al. (90).

Authors: A beam current density of 0.4 $\mu A/mm^2$ was used by Ramseyer et al. (97) studying CL colors of α quartz. This value is about thousand times lower than the beam current density we used for studying CL emission changes in quartz (Fig. 22) and zircon (Fig. 33) as a function of irradiation time. Ramseyer et al. (97) showed that the intensity of the short-lived luminescence in quartz decreased before to reach a plateau after about 40 s of electron bombardment. In our experiments, the interval of time between two spectra was 20 s. In Fig. 22 and Fig. 25 the electron irradiation time leading to the CL intensity changes is in the same order of magnitude than that reported by Ramseyer et al. (97)while the beam densities differ by a factor of $\approx 10^3$. Consequently, we are not observing the same electronic beam damages than those shown by Ramseyer et al. (97).

D. Holt: We have done a little work in cooperation with the British National Physical Laboratory on Al_2O_3 and found that we could obtain characteristic spectra for rare-earth dopants despite the near impossibility of obtaining truly chromium-free alumina starting material. It is planned to continue this effort. Are there plans to synthetize other materials of mineralogical interest with known dopant contents?

Authors: Quartz and zircon are at present time the principal minerals we are studying by CL, PhL and TL. Doped and synthetic crystals will be prepared. Luminescence studies are a federative research topic and the authors are now working on the project to constitute an european laboratory network for interdisciplinary research program in this field.

Additional comments: Since this paper was written, many papers dealing with CL applications have been published. Most of these studies are related with carbonates:

Machel HG, Mason RA, Mariano AN, Mucci A (1991). Causes and emission of luminescence in calcite and dolomite. *In* Luminescence Microscopy: Qualitative and Quantitative Applications. CE Barker and OC Kopp (eds), Society for Sedimentary Geology, SEPM Short Course, **25**, 9-25

Barbin V, Ramseyer K, Burns SJ, Decrouez D, Maier JL, Chamay J (1991). Cathodoluminescence signature of white marble artefacts. Mat. Res. Soc. Symp. Proc., **185**, 299-308.

Barbin V, Ramseyer K, Debenay JP, Schein E, Roux M, Decrouez D (1991). Cathodoluminescence of recent biogenic carbonates: an environmental and ontogenetic fingerprint. Geol. Mag., **128**, n° 1, 19-26.

*** Editor's Note**: For preprints of references (76), (140) and (142) readers may contact the authors at the following addresses:

(76) Dr Donald J. Marshall, M A A S, Inc., 225 Stedman St. - # 35, Lowell, MA 01851

(140, 142) Dr Paul J. Wright, Oxford Instruments Ltd., Eynsham, Oxford OX8 1TL, U.K.